

**UNIVERSITÄT
BAYREUTH**

**Activation and inhibition of Sirt6 by
small molecules**

DISSERTATION

zur Erlangung des akademischen Grades eines
Doktors der Naturwissenschaften (Dr. rer. nat.)
an der Fakultät für Biologie, Chemie und Geowissenschaften
der Universität Bayreuth

vorgelegt von
M.Sc. Biochemiker

Weijie You

aus Zhangping, People's Republic of China
Bayreuth, Dezember 2018

This doctoral thesis was prepared at the department of Biochemistry at the University of Bayreuth from January 2014 until December 2018 and was supervised by Prof. Dr. Clemens Steegborn.

This is a full reprint of the dissertation submitted to obtain the academic degree of Doctor of Natural Sciences (Dr. rer. nat.) and approved by the Faculty of Biology, Chemistry and Geosciences of the University of Bayreuth.

Date of submission: 07.12.2018

Date of defence: 02.07.2019

Acting dean: Prof. Dr. Stefan Peiffer

Doctoral committee:

Prof. Dr. Clemens Steegborn	(reviewer)
Prof. Dr. Birte Höcker	(reviewer)
Prof. Dr. Stephan Schwarzinger	(chairman)
Prof. Dr. Rainer Schobert	
(Prof. Dr.)

(additional reviewer: Prof. Dr. Wolfgang Sippl)

Acknowledgements

This thesis is dedicated to my wife Yan Li and my daughter Chang You for their constant support and love.

I would like to express my most sincere appreciation to my supervisor Prof. Dr. Clemens Steegborn for being the role to provide me with the professional discussions and serve as a guide for the research objectives during the period of my doctorate study.

I would also like to show my gratitude to our collaborators, Prof. Dr. Mike Schutkowski, Prof. Antonello Mai and Prof. Katrin Faye Chua, for their excellent work in bringing great outcomes. I also want to offer my heartfelt thanks to Dr. Christian Kambach for his kind introduction, help and discussion throughout the research; and to my colleague Ms. Sandra Riemer for the help and support for the project.

I appreciate the help from Dr. Michael Weyand and Dr. Sebastien Moniot for the problem-solving discussion about crystallography. My thanks also go out to Dr. Andrea Di Fonzo for the excellent support on Mass spectrometry experiments. I sincerely thank the secretaries Ms. Renate Crowe and Ms. Gabriele Kassler for helping me to fit into a good German life in Bayreuth. Specific thanks to my former colleagues Dr. Benjamin Sünkel and Dr. Martin Pannek for their role in making work fun. I also want to thank our technical assistants, Mr. Norbert Grillenbeck, Ms. Susanne Schäfer, Ms. Lisa Meisel, Ms. Sabrina Wischt and Ms. Edith Guthmann, for their support at work. I am very thankful to all the members of AG Steegborn group, AG Höcker group and AG Möglich group, in particular to Mr. Sooruban Shanmugaratnam, Ms. Ramona Adolph, Mr. Julian Pfahler, Ms. Holly Towell and Mr. Jonathan Quast, for their help during my work and also for their effort to create a friendly work environment.

Table of contents

List of abbreviations.....	1
Summary	2
Zusammenfassung.....	4
1 Introduction.....	6
1.1 Aging is associated with metabolism	6
1.2 Sirtuins in Biology	8
1.2.1 Roles of Sirtuin in longevity	8
1.2.2 The mammalian Sirtuins	8
1.2.3 Sirtuin structure and catalytic mechanism.....	11
1.3 Pharmacological modulation of Sirtuins	14
1.3.1 Sirtuin activators.....	14
1.3.2 Sirtuin inhibitors.....	16
2 Aims of this Study	19
2.1 Identify and characterize Sirt6 activating compounds.....	19
2.2 Biochemical and structural studies of quercetin-based compounds on Sirtuins.....	19
2.3 Identify the mechanism of Sirtuin 6 inhibition by Trichostatin A.....	19
2.4 Engineer protein sequence of Sirt7 to facilitate crystallization.....	19
3 Results and discussion	20
3.1 Structural Basis of Sirtuin 6 Activation by Synthetic Small Molecules.....	20
3.1.1 UBCS compounds enhance Sirt6 deacetylase activity.....	20
3.1.2 Sirt6's specific long acyl channel is identified as the activator binding site	22
3.2 Structural basis for Sirtuin6 activation and inhibition by quercetin and its derivatives	28
3.2.1 Quercetin enhances Sirt6 deacetylase activity	28
3.2.2 Quercetin-based compounds show different effects on Sirt6 deacetylation	31
3.2.3 Isoquercetin acts as a Sirt6 activator and exhibits higher isoform specificity ...	33

3.3	Structural basis of Sirtuin 6 inhibition by [the hydroxamate] trichostatin A	37
3.3.1	Crystal Structure of Sirt6 in complex with trichostatin A.....	37
3.3.2	Implication to develop class selective inhibitor based on TSA for HDACs	39
3.4	Identification of a subdomain of Sirt7 for crystallization.....	41
4	References	43
5	List of publications.....	48
5.1	Publication 1	48
5.2	Publication 2	74
5.3	Publication 3	82
6	(Eidesstattliche) Versicherungen und Erklärungen	115

List of abbreviations

2'-OAAADPr	2'-O-acetyl-ADP-ribose
AceCS2	acetyl-CoA synthetase 2
AMPK	AMP-activated protein kinase
ATP	adenosine-triphosphate
CPS1	carbamoyl phosphate synthetase
CR	Calorie restriction
DDAs	DNA-damaging agents
DHP	1,4-dihydropyridine
ECS	extended C-site
ERCs	extrachromosomal rDNA circles
FFAs	free fatty acids
FITC	Fluorescein isothiocyanate
G6PDH	glucose-6-phosphate dehydrogenase
GAPDH	glyceraldehyde 3-phosphate dehydrogenase
GDH	Glutamate dehydrogenase
GIIS	glucose-induced insulin secretion
HDACs	histone deacetylases
Hif1a	Hypoxia Inducible Transcription factor 1a
hMSC	human mesenchimal stem cells
HPLC	high-performance liquid chromatography
ICD2	isocitrate dehydrogenase 2
IR	ionizing radiation
LCAD	long-chain acyl-CoA dehydrogenase
MCD	malonyl CoA decarboxylase
MST	microscale thermophoresis
NAD ⁺	nicotinamide adenine dinucleotide
NAM	nicotinamide
NF-κB	nuclear factor-kappaB
PD	Parkinson's disease
PDH	pyruvate dehydrogenase
PTMs	post-translational modifications
rDNA	ribosomal DNA
ROS	reactive oxygen species
SAM	S-adenosylmethionine
SIR2	silent information regulator 2
SOD	superoxide dismutase
STACs	Sirtuin-activating compounds
TNFα	tumor necrosis factor-α
TSA	Trichostatin A

Summary

Mammals have 7 Sirtuin isoforms (SIRT1–7) localized in different subcellular compartments and with different functions. Sirt6 is a heterochromatin-associated protein that serves in the regulation of telomere maintenance, DNA repair and gene expression. A Sirt6 knockout causes aging-associated degeneration in mice. Conversely, Sirt6 overexpression has been reported to extend lifespan in male mice. Thus, activators of Sirt6 are considered to be attractive therapeutics to treat cancer and age-related diseases. Sirtuin-activating compounds (STACs) were initially described to activate Sirt1, and bind to the Sirt1's unique N-terminal segment (SBD domain). In contrast, progress towards the development of activators which modulate the activity of other Sirtuin isoforms that lack the Sirt1's SBD domain has been significantly taken up speed only recently.

The pyrrolo[1,2-a]quinoxaline-derived compound UBCS038 were previously characterized as a very weak Sirt6 activator. We screened a panel of pyrrolo[1,2-a]quinoxaline-derived derivatives and identified several compounds as more potent activators for Sirt6-dependent deacetylation of peptide substrates, histone proteins and complete nucleosomes. Furthermore, these compounds showed no effect on Sirt1, 2 and 3, but promoted the desuccinylase activity of Sirt5. Solving the complex structures by using X ray crystallography revealed that these compounds as the first synthetic Sirt6 activators bind to the Sirt6 specific acyl channel branching from the catalytic core and activate Sirt6 deacetylation by an allosteric mechanism, which can explain their different effects against acyl substrates. Moreover, structure-activity relationship analyses indicate that the presence of a nitrogen atom in the meta position of the pyridine group is crucial for ligand affinity or Sirt6 activation. Our data reveal promising acyl-selective Sirt6 activators and offer clues for the development of Sirt6 drug-like compounds as molecular tools and potential therapeutics.

Next, we utilized a robust mass spectrometry-based assay to determine the effect of quercetin on Sirtuins. We confirmed the weak activation effect of quercetin for Sirt6 and found out that quercetin can inhibit other Sirtuin isoforms. We solved crystal structures of a Sirt6/quercetin complex and a Sirt2/quercetin complex to reveal two mutually exclusive binding modes that lead to the dual effects of quercetin among Sirtuins. Based on the structural information, we have identified a novel quercetin derivative, namely isoquercetin, able to activate Sirt6 with improved selectivity. We then determined the crystal structure of Sirt6 and isoquercetin to better understand its activation mechanism. Moreover, we also confirmed the effects of quercetin derivatives catechin gallate (the first potent Sirt6 inhibitor) and cyaniding (the most robust Sirt6 activator) in our mass spectrometry assay and further determined the crystal

structures of Sirt6 in complex with these two compounds. Our results demonstrate that the substitution in the C ring of quercetin can significantly alter the effect of compounds from activation to inhibition, and reveal molecular features essential for further drug development. Trichostatin A (TSA) inhibits classical HDACs by chelating the zinc ion in the active site, but in Sirtuins the zinc ion does not play a catalytic role and its binding site is remote from the catalytic site. Surprisingly, TSA is also identified to show promising efficacy towards Sirt6, while demonstrates no appreciable inhibitory effect on Sirt1-3 or Sirt5. We obtained the Sirt6/TSA complex structure by soaking experiment. We found that TSA binds into the C pocket of the NAD⁺ binding site and inserts into Sirt6's specific acyl binding channel, which thus explains its relative specificity for Sirtuin isoforms. Binding studies further revealed that TSA binds to Sirt6 in a noncompetitive manner with respect to ADP-ribose (fragment of NAD⁺) or substrate, suggesting that TSA might acts as sirtuin inhibitor via binding to the C pocket upon the dissociation of NAM group and prevent product release by stabilizing the intermediate complex. Our data provides insight into the TSA binding site and the inhibition mechanism to support the development of Sirt6-selective inhibitors.

Zusammenfassung

In Säugetieren existieren 7 Sirtuin Isoformen (SIRT1-7), die in verschiedenen Zellkompartimenten lokalisiert sind und verschiedene Funktionen ausüben. Sirt6 ist ein mit Heterochromatin assoziiertes Protein, welches in der Regulation der Erhaltung von Telomer-Strukturen, DNA-Reparatur, und Genexpression involviert ist. Ein Sirt6 Knockout in Mäusen führt zu beschleunigtem, altersbedingtem Verfall. Im Gegensatz dazu führt die Überexpression von Sirt6 zur Verlängerung der Lebensspanne männlicher Mäuse. Daher werden Sirt6-Aktivatoren als attraktive potentielle Therapeutika für Krebs und alterungsbedingte Krankheiten angesehen. Synthetische Sirtuin-Aktivatoren (*Sirtuin-activating compounds*, STACs) wurden ursprünglich für Sirt1 beschrieben und binden an eine Sirt1-spezifische Domäne N-terminal von der katalytischen Domäne (SBD, für *STAC-binding domain*). Die Entwicklung von Aktivatoren anderer Sirtuin-Isoformen, welche die einzigartige Sirt1 SBD nicht besitzen, hat sich erst kürzlich beschleunigt.

Die von Pyrrolo[1,2-a]Chinoxalin abgeleitete Substanz UBCS038 ist als schwacher Sirt6-Aktivator beschrieben worden. Im Zuge dieser Arbeit wurden verschiedene Pyrrolo[1,2-a]Chinoxalin Derivate synthetisiert und es konnten verschiedene Substanzen, welche die Deacetylierungsaktivität von Sirt6 gegenüber Peptid-Substraten, Histonproteinen und Nucleosomen stimulieren, identifiziert werden. Darüber hinaus zeigten diese Substanzen keinen Effekt auf Sirt1, 2, und 3, förderten jedoch die Desuccinylase-Aktivität von Sirt5. Strukturelle Studien zeigten, dass diese Substanzen – die ersten charakterisierten Sirt6-Aktivatoren – in dem Sirt6-spezifischen Acylkanal binden, der vom katalytischen Zentrum ausgeht und die Sirt6 Deacetylierung durch einen allosterischen Mechanismus aktiviert. Dies erklärt auch die verschiedenen Effekte auf Acylsubstrate. Weiterhin zeigen die Analysen der Struktur-Wirkungsbeziehung, dass die Präsenz eines Stickstoffatoms in meta-Stellung zum Pyridin-Rest essentiell für die hochaffine Bindung sowie Sirt6 Aktivierung ist. Unsere Daten weisen auf vielversprechende acylselektive Sirt6 Aktivatoren hin und liefern Hinweise zur Entwicklung von Wirkstoffkandidaten, die als molekulare Werkzeuge und potentielle Therapeutika dienen können.

Des Weiteren verwendeten wir einen auf massenspektrometrischer Analyse beruhender Assay, um die Wirkung von Quercetin auf Sirtuine zu untersuchen. Wir konnten bestätigen, dass Quercetin Sirt6-aktiviert, aber andere Sirtuinisofome inhibiert. Unsere Kristallstrukturen von Sirt6 und Sirt2 im Komplex mit Quercetin zeigen, dass die Substanz in zwei nicht miteinander zu vereinbarenden Bindungsmodi an Sirt6 bzw. Sirt2 bindet und diese die unterschiedlichen Wirkungen von Quercetin auf verschiedene Sirtuinisofome bedingen. Auf Basis dieser Kristallstrukturen haben wir ein Quercetin-Derivat, nämlich Isoquercetin, definiert, welches eine erhöhte Selektivität gegenüber Sirt6 zeigt. Um den Mechanismus, der zur Aktivierung führt, zu verstehen, haben wir die Kristallstruktur des Sirt6/Isoquercetin-Komplexes gelöst. Außerdem bestätigten wir die Effekte der Quercetinderivate Catechin-Gallat (der erste potenter Inhibitor) und Cyanidin (der stärkste Sirt6-Aktivator) auf Sirt6 mit unserem Massenspektrometrieassay und lösten die Kristallstrukturen von Sirt6 in Komplex mit diesen

Zusammenfassung

Verbindungen. Unsere Ergebnisse zeigen, dass der Austausch im C-Ring von Quercetin signifikant den Effekt der Substanz von Aktivierung zu Hemmung hin verändern kann und schaffen die molekulare Grundlage für die weitere Medikamentenentwicklung.

Trichostatin A (TSA) inhibiert klassische HDACs, indem es das Zink-Ion im katalytischen Zentrum komplexieren. In Sirtuinen hingegen spielt das Zink-Ion keine katalytische Rolle und die Zinkbindestelle befindet sich nicht in der Nähe des katalytischen Zentrums. Überraschenderweise zeigt TSA dennoch eine vielversprechende Wirkung auf Sirt6, aber besitzt für Sirt1-3 bzw. Sirt5 keinen inhibitorischen Effekt. Wir konnten die Komplexstruktur von Sirt6 mit TSA lösen und fanden heraus, dass TSA in der C-Tasche der NAD⁺-Bindestelle bindet und sich in den Sirt6 spezifischen Kanal einfügt. Dies erklärt die Isoformspezifität. Bindungsexperimente ergaben ferner, dass TSA in einer nichtkompetitiven Weise zu ADP-ribose (Fragment von NAD⁺) oder einem Substrat an Sirt6 bindet. Dies legt nahe, dass die inhibitorische Wirkung von TSA durch Bindung in der C-Tasche nach Dissoziation der NAM-Gruppe erfolgt und durch die Stabilisierung des Intermediatkomplexes die Freisetzung des Produktes verhindert wird. Unsere Daten beleuchten die molekulare Struktur der TSA-Bindetasche und den Inhibitionsmechanismus. Beides trägt zur Entwicklung Sirt6 spezifischer Inhibitoren bei.

1 Introduction

1.1 Aging is associated with metabolism

Aging is characterized by a time-dependent loss of physiological integrity at the organismal level. There is a general perception that human life expectancy has increased and the effects of aging as measured by appearance have diminished compared to the 1960s¹. These observations have led to the question what are the cellular and molecular mechanisms that help to slow down the effect of aging and how to define the cause of aging at the cellular level². Early theories were derived from simple model organisms like yeast, worms, and flies^{3, 4}. Many genes that affect lifespan in model organisms have been identified and have been shown to extend both maximum and average lifespans in lower organisms. Research on mammals has also experienced unprecedented progress in the past few decades; many pathways governing the aging processes have been identified in aging, dysfunctional cells. This work eventually led to the definition of several candidate hallmarks of ageing, such as genomic instability⁵⁻⁸, telomere attrition⁹⁻¹², epigenetic alterations¹³, loss of proteostasis¹⁴, deregulated nutrient sensing¹⁵⁻¹⁷, mitochondrial dysfunction¹⁸, cellular senescence¹⁹⁻²¹, stem cell exhaustion²², and altered intercellular communication (Figure 1)^{23, 24}.

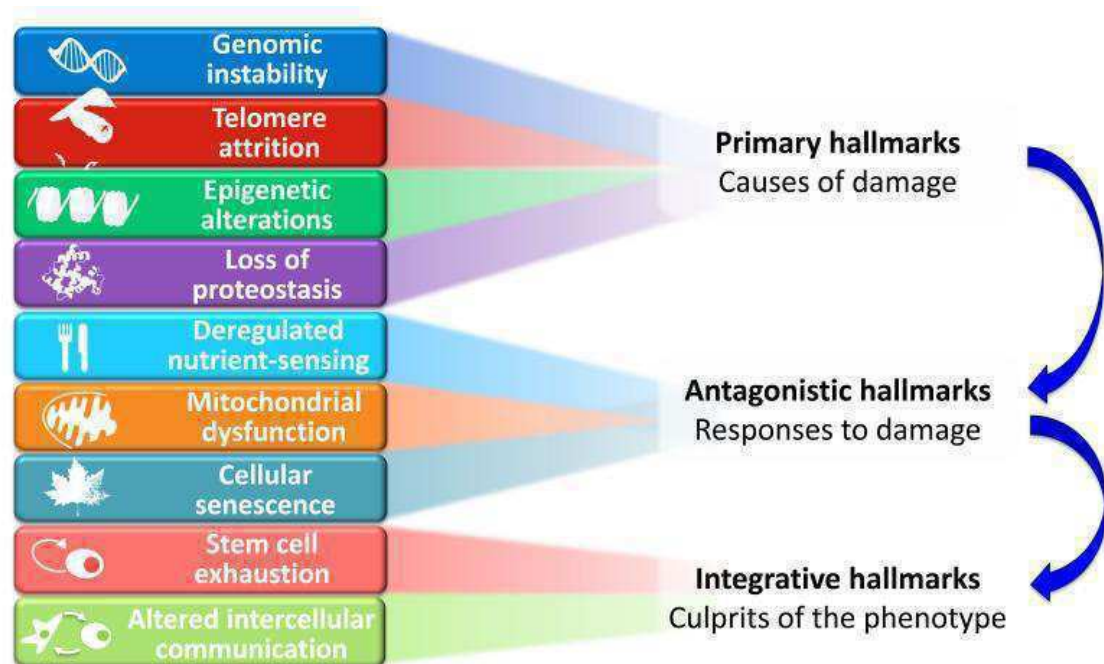


Figure 1: Aging has been defined as the time dependent deterioration of physiological integrity and several primary causes of aging have been designated as its hallmarks (Figure taken from López-Otín et al., 2013²⁵ with permission of Cell Press).

Metabolism has been associated with aging since 80 years ago. Calorie restriction (CR) without malnutrition has been shown to delay senescence and extend the lifespan in rats²⁶. An

1.2 Sirtuins in Biology

1.2.1 Roles of Sirtuin in longevity

Sir2 is an NAD⁺-dependent deacetylase, and the silent information regulator (SIR) proteins were found to regulate gene expression and increase the replicative lifespan of yeast cells almost 20 years ago³⁸. It has been demonstrated that the formation of transcriptional silencing in yeast requires the NAD⁺ dependent deacetylase activity of SIR2³⁹. During SIR2-mediated gene silencing, SIR2 was identified to deacetylate histones to provide high-affinity binding sites for SIR3 and SIR4, which in turn enables assembly of additional SIR2 protein and facilitates the spreading of silencing complexes along the chromosome^{40, 41}. SIR2-mediated lifespan extension in yeast can be affected by enzymatically inactive SIR2 mutants and the NAD⁺ concentration, whose level is strongly correlated with the cellular stress response and nutrient limitation⁴². These findings offer the intriguing possibility that SIR2 related proteins could act as metabolic sensors that respond to nutrient input and are affected by the NAD⁺/NADH ratio to alter diverse physiological processes with an impact on metabolism and aging. Sirtuins thereby act as a link between metabolic rate and aging.

1.2.2 The mammalian Sirtuins

The SIR2 homologs found in mammals are termed Sirtuins (derived from "SIR-2-ins"). There are seven Sirtuin isoforms in mammals, and they can be divided into four classes based on their phylogenetic relationship^{43, 44}. Mammalian sirtuins (Sirt1-7) differ in their subcellular localization and in their substrate specificity (Figure 3)⁴⁵. Similar to yeast SIR2, the mammalian Sirtuins SIRT1, SIRT6 and SIRT7 are predominately found in the nucleus but differ in their subnuclear distributions⁴⁶⁻⁴⁸. Sirt2 primarily localizes in the cytoplasm^{49, 50}, Sirt3-5 are characterized as mitochondrial Sirtuins⁵¹. However, Sirt1 & Sirt2 can shuttle between cytoplasm and nucleus in response to physiological stimuli. Sirt1-3 are much more catalytically active deacetylases than Sirt4-7, but there is growing evidence that mammalian Sirtuins are able to remove other lysine acyl moieties. For example, Sirt5, has been found to be a more efficient desuccinylase, demalonylase and deglutarylase than deacetylase^{52,53}. Consistently, knocking out Sirt5 in mice leads to elevated levels of lysine malonylation, succinylation and glutarylation on diverse mitochondrial proteins⁵⁴. Furthermore, Sirt6 was found to exhibit 300-fold better efficiency for the hydrolysis of long chain fatty acyl groups from protein lysines than that of deacetylation *in vitro*⁵⁵. However, several studies revealed that Sirt6 primarily acts as histone deacetylase *in vivo*^{56, 57}. In addition, both Sirt4 and Sirt6 have been reported to possess low mono-ADP-ribosylation activity⁵⁸⁻⁶⁰, and recently Sirt4 has

been identified to show specific activity against hydroxymethylglutarylation⁶¹. Little is known about the deacylation specificity of Sirt7. The growing list of substrate acyl group chemistries has led to Sirtuins being considered as protein deacylases rather than deacetylases.

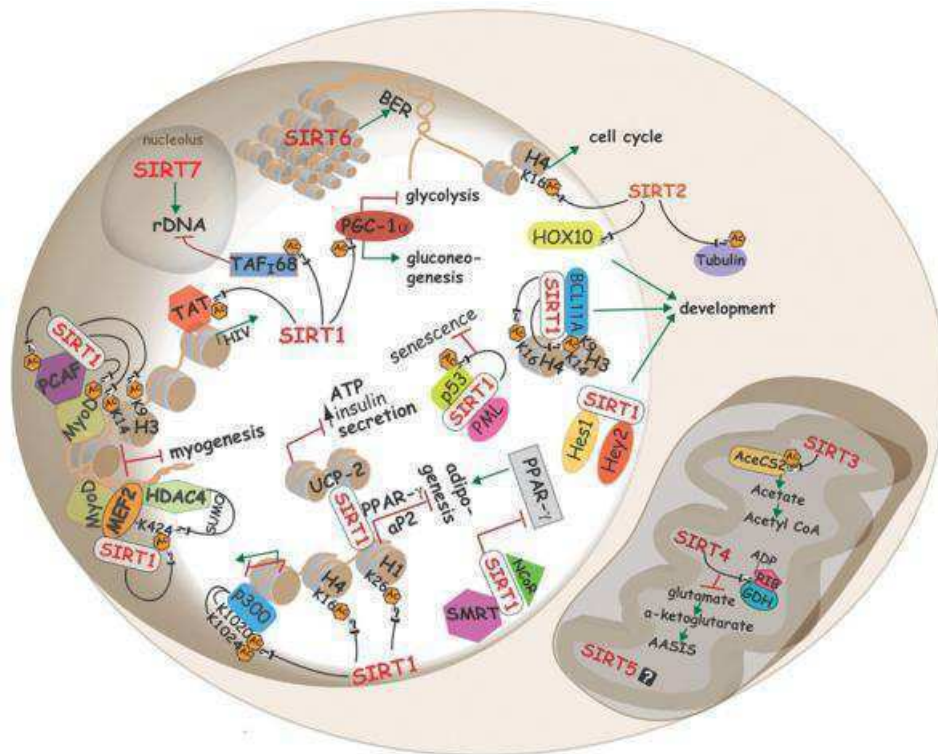


Figure 3: Mammals have 7 Sirtuin isoforms that localize in different subcellular compartments and regulate different cellular functions (Figure taken from Michan et al., 2007⁴⁸ with permission of Portland Press).

Of the seven mammalian Sirtuin isoforms, Sirt1 is the best characterized family member. Sirt1 was first described to modulate chromatin structure through histone deacetylation. It has also been implicated in deacetylation of non-histone targets involved in cell survival, DNA repair, stress response, inflammation, apoptosis and energy metabolism^{62, 63}. Sirt2 is shown to deacetylate α -tubulin to regulate microtubule dynamics⁴⁹. Sirt3-5 target a large variety of metabolic enzymes to mediate energy production, metabolism, apoptosis and stress response^{64, 14}.

Sirt6 was demonstrated to associate with heterochromatin and regulate chromatin structure to promote proper chromatin function in numerous physiological processes, including telomere maintenance and DNA repair (Figure 4)^{56, 57}. SIRT6 deficiency in mice and cells was reported to result in the most striking phenotype among the seven mammalian sirtuins⁶⁵⁻⁶⁷. SIRT6-knockout mice are born with a low birth weight and suffer from a severe age-related degenerative phenotype that includes metabolic defects, loss of subcutaneous fat, chronic inflammation, and lymphopenia. Overall, these physiological defects result in a severely

reduced lifespan of about one month⁵⁹. Sirt6 knockout cells exhibit genomic instability and increased sensitivity to DNA-damaging agents (DDAs) such as ionizing radiation (IR) and ROS. These observations indicate that there is defect in DNA repair and suggest a hypothesis that Sirt6 is able to promote DNA repair^{59, 68}. Together, these studies suggest that Sirt6 deficiency affects multiple cellular phenotypes with an impact on organismal health and aging. The studies in vitro showed that Sirt6 favors to remove long chain fatty acyl groups from protein lysines over acetyl group, and Sirt6 can promote secretion of tumor necrosis factor- α (TNF α) through lysine demyristoylation⁵⁵. However, in vivo studies revealed that Sirt6 function is majorly associated with its deacetylase activity of lysines 9 and 56 on histone H3^{56, 57}.

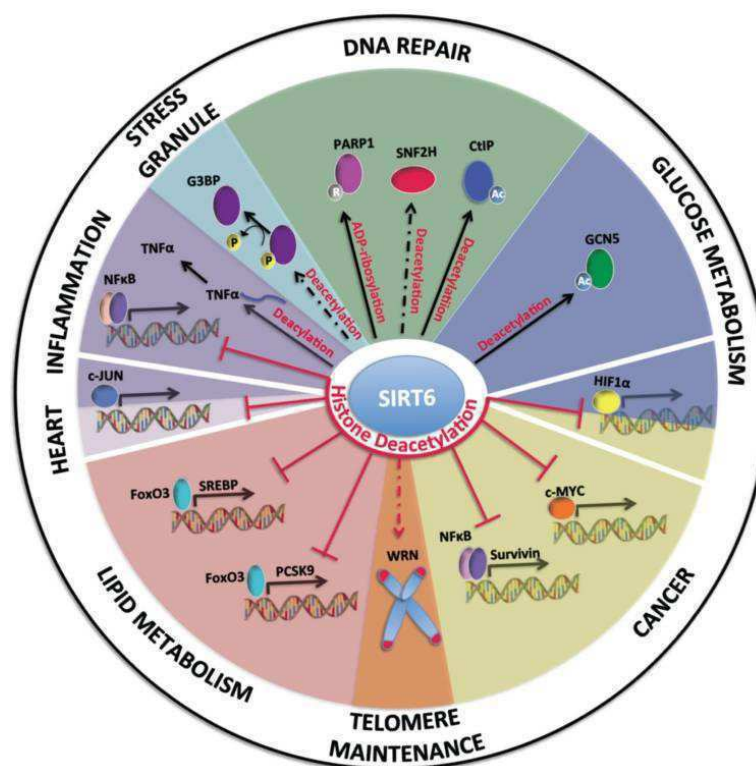


Figure 4: Sirt6 associates with heterochromatin to regulate numerous cellular functions (Figure taken from Kugel et al., 2014⁶⁹ with permission of Cell Press).

Sirt6 can regulate transcription silencing of target genes by deacetylating specific histone lysine residues in their promoter region^{67, 70-72}. There is ample evidence for this functionality. First, nuclear factor-kappaB (NF- κ B) is a nuclear transcription factor that affects multiple biological processes in inflammation, proliferation and aging. NF- κ B activation contributes to the development of aging-associated diseases; earlier studies indicate that Sirt6 functions to suppress the transcriptional activity of nuclear NF- κ B by deacetylating histone H3 at position K9 in its promoter region to alter the expression of a subset of NF- κ B target genes⁷¹. Second, Hypoxia Inducible Transcription factor 1a (Hif1a) is a transcription factor that mediates the

cellular adaptation to the nutritional environment and regulates the expression of glycolytic enzymes^{72, 73}. SIRT6 was found to bind to Hif1a and deacetylate histone H3 at position K9 in the promoter region of Hif1a target genes to regulate nutrient response⁶⁷. Additionally, Sirt6 was reported to suppress gluconeogenesis by activating the acetyltransferase GCN5 and thereby indirectly regulate the activity of PGC-1 α (a transcription factor of gluconeogenic genes)⁷⁴. Knocking out Sirt6 was shown to abolish glucose homeostasis and upregulate glucose level and gluconeogenesis in muscle and fat tissues⁵⁹. Like Sirt1, Sirt6 has been linked to longevity; its expression level decreases during aging in dermal fibroblasts, and overexpression of Sirt6 can extend the lifespan in male mice by ~15%⁷⁵. Thus Sirt6 serves important roles in the control of metabolism and longevity.

Sirt7 is a nuclear sirtuin and is involved in the regulation of ribosome biogenesis by promoting RNA polymerase I (Pol I)-dependent transcription of ribosomal DNA (rDNA)^{64, 76}. Sirt7 is shown to interact with transcription factors and deacetylate the Pol I subunit PAF53 to enhance the interaction between Pol I and DNA, which in turn enhance pre-rRNA synthesis⁷⁷. Moreover, rDNA transcription can be depressed during mitosis when Sirt7 is phosphorylated and resumes after mitosis due to the dephosphorylation of Sirt7⁷⁸. In addition, Sirt7 also contributes to the process of pre-rRNA maturation⁷⁹. Notably, Sirt7 expression is correlated with cell proliferation and tumorigenesis. Sirt7 was ascribed to deacetylate histone H3 at position K18 to repress transcription of tumor suppressor genes, which in turn promotes tumorigenesis including hepatic, breast and thyroid cancer. In contrast, SIRT7 depletion was shown to inhibit cell proliferation and oncogenic transformation⁸⁰. Recently, several studies have highlighted the function of Sirt7 in the regulation of metabolic homeostasis. SIRT7 was shown to restore metabolic homeostasis indirectly by deacetylating GABP β 1, a master regulator of nuclear-encoded mitochondrial genes, to activate the mitochondrial biogenesis⁸¹. Other reports on Sirt7 function include its role in the repression of ER stress (response to the accumulation of unfolded proteins) through its interaction with Myc to silence gene transcription related to ribosome biogenesis, the negative regulation of Hif1a and Hif2a activity, and the impact on lipid metabolism⁸². Even though Sirt7's in vivo function is majorly related to the deacetylase activity, but it only displays very weak deacetylase activity in vitro, as described for Sirt6.

1.2.3 Sirtuin structure and catalytic mechanism

Despite their different intracellular distribution and substrate specificity, all Sirtuins share a conserved catalytic core with yeast Sir2^{43, 83}. The conserved catalytic domain encompasses about 275 amino acids and is flanked by N- and C- terminal extensions, which differ in

sequence and length among isoforms (Figure 5A). The extensions offer a way to regulate subcellular localization, enzymatic activity and the interaction with regulator proteins^{51, 84}. High-resolution crystal structures of apo or (co)substrate-bound forms of several Sirtuins have been published and contribute to our understanding of their catalytic mechanism. The overall structure of the Sirtuin catalytic core is conserved. It consists of two domains, a large α/β Rossmann-fold domain for NAD⁺ binding and a small, structurally diverse domain containing a zinc-binding motif and a four-helix bundle absent in Sirt6⁸³. The zinc ion is located far away from the enzyme catalytic site, but seems to play a structural role, since any mutation in the zinc-binding motif lowering the zinc affinity was shown to destabilize the structure and therefore indicates a catalytic function. Unlike for other protein deacetylase, the zinc ion does not participate directly in catalysis to assist the hydrolysis reaction⁸⁵. The two domains are connected by several loops that form an active site cleft in which both the acylated lysine and NAD⁺ bind (Figure 5B). The catalytic site is flexible and conformational changes occur upon Sirtuin binding to substrate protein or the cofactor. The NAD⁺ binding site contains three sub-pockets, where the adenosine moiety of NAD⁺ binds to pocket A, the diphosphoribose group binds to pocket B and the nicotinamide group binds to pocket C⁸⁶. NAD⁺ binding causes a conformational change of the so-called “cofactor binding loop”, the largest linking loop within the cleft between two domains, whose conformation is highly flexible in the absence of NAD⁺. It gets more ordered upon cofactor binding⁸³. The acylated substrate binds to the cleft, forming a β -staple interaction between substrate main chain and β -sheets from both domains. The acylated lysine inserts into a narrow hydrophobic tunnel within the cleft, reorganizing the linking loops between the two domains and facilitating the formation of a more closed conformation^{83, 87}. Additionally, the crystal structure of Sirt5 with a bound succinyl peptide reveals that the Tyr102 and Arg105 residues within the catalytic site of Sirt5 recognize the acyl group carrying a negatively-charged carboxylate⁵² (Figure 5C). Furthermore, the complex structure of Sirt6/myristoyl-peptide/ADPr revealed a Sirt6-specific acyl channel to accommodate the long-chain fatty acyl group⁵⁵ (Figure 5D). Notably, Sirt 1-3 were also identified to have long-chain deacylation activity *in vitro*, such as demyristoylation activity⁸⁸. The crystal structures of Sirt2 and Sirt3 in complex with myristoylated peptides revealed that the myristoyl group occupies the cleft between two domains and demonstrates diverse orientation for Sirt2 and Sirt3 to avoid the clash with nearby helix bundle^{89, 90}. Although Sirt 1-3 displayed higher K_m values with the myristoylated peptides than those of the acetylated peptides, the K_{cat}/K_m for Sirt 1-3 demyristoylation is similar to that of their deacetylation⁸⁸. Compared to Sirt 1-3, Sirt6 has a wider space for the myristoyl group due to the reduction of

cofactor-binding loop and neighboring helix bundle, and the K_{cat}/K_m value from Sirt6's demyristoylation to its deacetylation increase more than 300 fold⁵⁵.

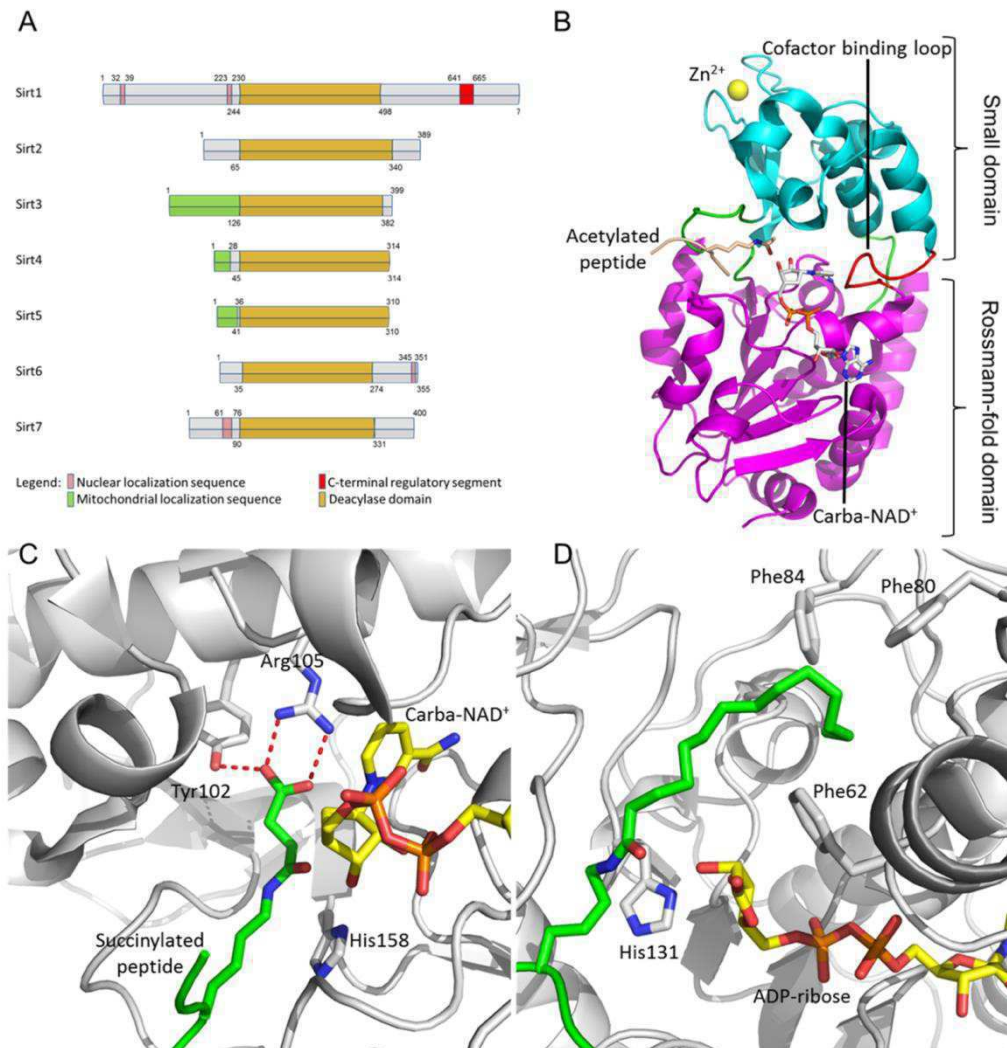


Figure 5: Mammalian Sirtuins share a conserved catalytic core, but display different acyl group preference. (A) Primary sequence alignment of mammalian Sirtuins. (B) The complex structure of Sirt3/ AceCS2 peptide /carba-NAD⁺ (PDB ID 4FVT). The Rossmann-fold domain (magenta), small domain (cyan) and the connecting loops (green) between the domains are shown in cartoon. The cofactor binding loop is highlighted in red. Carba-NAD⁺ (gray) and the acetyl-lysine of AceCS2 peptide in the active site are represented in sticks. (C) Close view of the succinyl-lysine peptide binding site in Sirt5's active site. The ternary complex structure of Sirt5/ IDH2 peptide /carba-NAD⁺ (PDB ID 4G1C) is shown in gray cartoon, carba-NAD⁺ (gray), the succinyl-lysine of IDH2 peptide (green) and the important residues for recognizing the specific acyl group are labeled in sticks, and polar interactions are indicated by dashed red lines. (D) Close view of Sirt6's specific long chain acyl group binding channel. The ternary complex structure of Sirt6/H3K9 peptide /ADP-ribose (PDB ID

3ZG6) is shown in gray cartoon, ADP-ribose (gray), the myristoyl-lysine of H3K9 peptide (green) and the important residues for recognizing the specific acyl group are labeled in sticks. The catalytic mechanism of Sirtuins has been proposed to occur in two steps (Figure 6). In the presence of substrate and NAD⁺, the co-substrate binding loop becomes ordered and the catalytic site undergoes a major conformational change to a productive conformation, which comprises the rotation of the ribose sugar of NAD⁺ towards acylated lysine and the shift of acylated lysine carbonyl oxygen in close proximity to NAD⁺. The reaction begins with the replacement of nicotinamide (NAM) from NAD⁺ by the acyl oxygen and forms a 1'-O-alkylamidate intermediate between acylated lysine and the ADP-ribose moiety, then the catalytic histidine activates the 2'-hydroxyl group of the NAD⁺ ribose and induces the nucleophilic attack on O-alkylamidate carbon to form a bicyclic intermediate, subsequently, a water molecule reacts with this bicyclic intermediate to complete the reaction and yield deacylated substrate and 2'-O-acetyl-ADP-ribose (2'-OAADPr)^{43, 91}. Thus Sirtuins act as metabolic sensors to link NAD⁺ consumption with protein deacetylation.

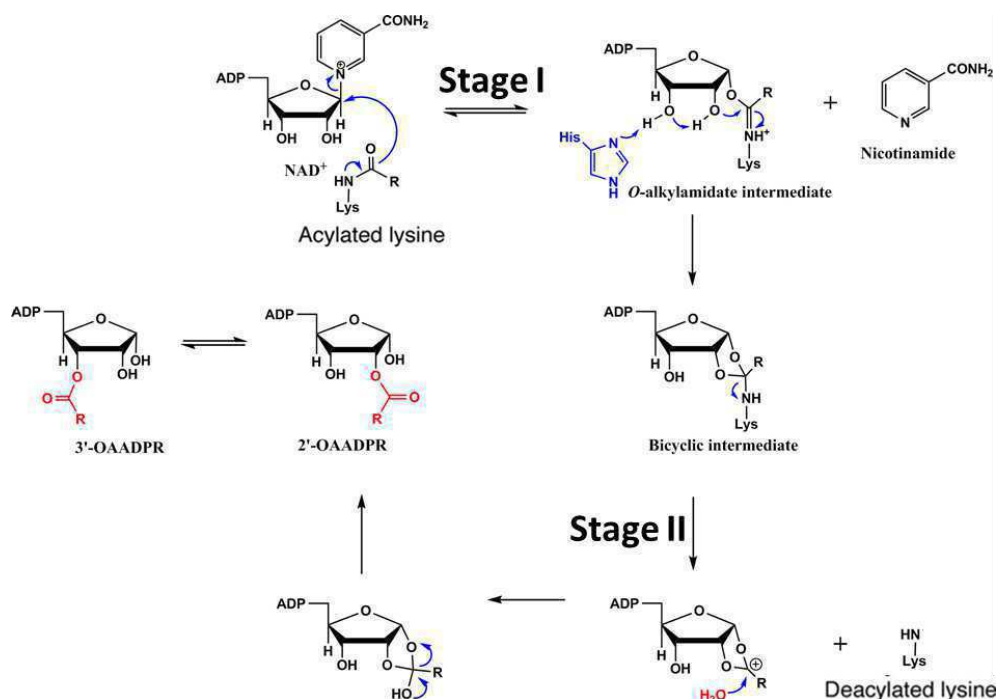


Figure 6: Sirtuin deacetylation mechanism (Figure taken from Yu et al., 2016⁹² with permission of PLOS ONE).

1.3 Pharmacological modulation of Sirtuins

1.3.1 Sirtuin activators

Sirtuin-activating compounds (STACs) were first reported for Sirt1 (Figure 7A). The plant polyphenol resveratrol was identified as the first Sirtuin activator in a natural compound screen, and it has been shown to extend lifespan in yeast and metazoans as well as to promote

human cell survival in a Sirtuin dependent manner³⁷. Biochemical studies identified that the N terminal sequence of Sirt1 is required for resveratrol mediated activation and the relevant region was hence called STAC-binding domain (SBD)^{93,94}. Moreover, Sirt1 was described as the primary resveratrol target *in vivo*, supported by the finding that inactive Sirt1 mutants do not show the effects of resveratrol in primary cells⁹³. However, resveratrol has only moderate potency against Sirt1. It also demonstrates off-target effects on other proteins and displays poor bioavailability, which makes it less suitable for pharmaceutical application⁹⁵. Therefore, high through-put screens were performed to identify further, more potent Sirt1 activators. Notably, new activators with different chemotypes were identified to activate Sirt1 through a common allosteric mechanism with resveratrol, and they showed EC_{1.5} values for activating Sirt1 nearly 1000 fold lower⁹³. Biochemical and crystallographic studies reveal that synthetic STACs as well as resveratrol increase Sirt1 activity through binding to the SBD domain and rotate the domain on the top of the active site to stabilize the close conformation and enhance the binding of the substrate (Figure 7B, C). Although more detailed mechanistic information of how sirtuins can be activated still is lacking, the effects of synthetic STACs as Sirt1 activators are currently being evaluated in clinical trials for anti-inflammatory drugs and the management of metabolic diseases³⁷.

Promising activators for the other Sirtuin isoforms, that lack Sirt1's N-terminal activator binding domain, have been described only recently. 1,4-dihydropyridine (DHP)-derived compounds, and in particular the derivatives carrying a benzyl group at the N1 position were found to show activating effects on Sirt1, 2 and 3 in the Fluor-de-Lys assay. They induced a dose-dependent increment of mitochondrial density in murine C2C12 myoblasts, and reduce senescence in primary human mesenchymal stem cells (hMSC). However, the effect of these compounds was determined using the FdL assay and needs to be confirmed with physiological substrates⁹⁶. Additionally, Honokiol has been demonstrated to enhance Sirt3 expression and promote Sirt3 activity *in vivo*, but showed rather weak potency and non-specific effects⁹⁷. Moreover, activators using well-established assays on physiological substrates were described for Sirt6. For example, certain free fatty acids and endogenous fatty acid ethanolamides were reported to behave as dose-dependent activators of Sirt6-dependent deacetylation. They displayed competitive inhibition of Sirt6-dependent demyristoylation when on physiological peptide substrates, indicating that free fatty acids may occupy the binding site of myristoylated peptide in the enzyme's long acyl binding channel⁸⁸. Nevertheless, these compounds enhanced Sirt6 deacetylation activity only at very high concentrations (several hundred micromolar) and the interaction details are unknown.

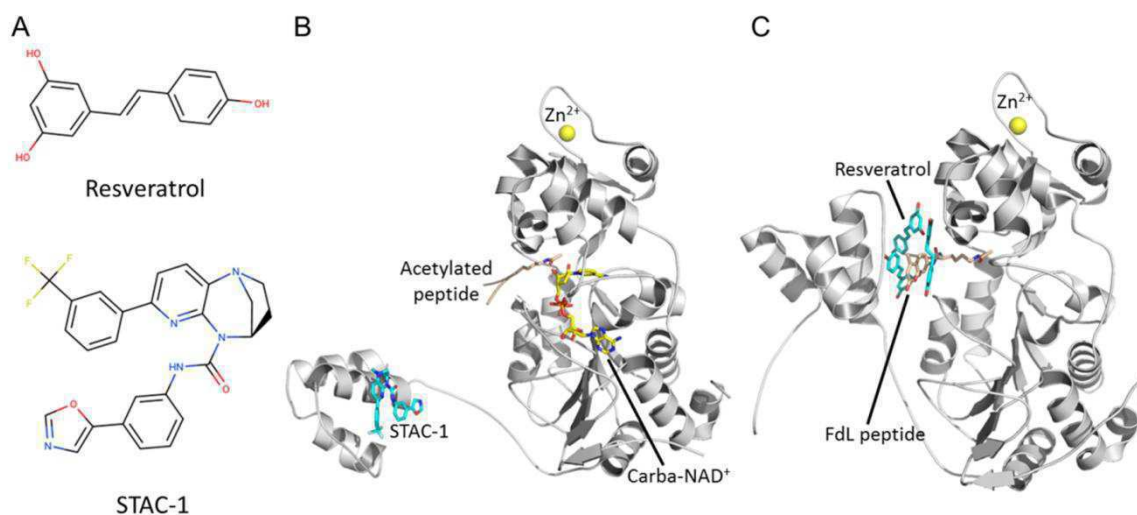


Figure 7: Sirtuin activators work by improving the binding affinity of the substrate. A) Chemical structures of Sirtuin activators. B) The ternary complex structure of human Sirt1/carba-NAD⁺/ STAC-1 (PDB ID 4ZZJ) is shown in gray cartoon. The carba-NAD⁺ (yellow) and activator (cyan) are labeled in sticks. C) The ternary complex structure of human Sirt1/FdL peptide/ resveratrol (PDB ID 5BTR) is shown in gray cartoon. The FdL peptide (yellow) and activator (cyan) are presented as sticks.

1.3.2 Sirtuin inhibitors

Sirtuins have been shown to affect diverse physiological processes linked to aging and cancer, and therefore are considered potential molecular targets for the development of small molecule modulators to treat various age-related diseases and cancer. Several compounds have been identified to inhibit Sirtuins, but the binding sites and molecular mechanisms for many of these compounds still remain unknown. Many of them also show unfavorable properties for drug development such as low potency and poor specificity^{84, 98}. Among the seven Sirtuin isoforms, mainly inhibitors of Sirt1 and 2 have been studied with regard to their promising therapeutic potential for neurodegenerative disorders. The isoform-specific areas in the C-pocket surrounding region have also exploited to generate highly selective Sirtuin inhibitors. The extended C-sites can be classified into three parts, namely ECS I-III (Figure 8).⁸⁴. For example, Ex-527 occupies the ECS I and shows higher potency against Sirt1 than Sirt2 and Sirt3^{99, 100}. ELT-11c occupies the ECS II and is characterized as the most potent inhibitor of Sirt1, Sirt2 and Sirt3 with IC₅₀ values in the nanomolar range¹⁰¹. 4'-bromo-resveratrol occupies the ECS III and is inhibitor for Sirt1 and Sirt3¹⁰². More recently, novel deacetylation functions for Sirt 4-7 have been identified^{52, 103} and enables the discovery of isoform selective chemical modulators. For example, Sirt5 was found to display more efficient demalonylase, desuccinylase and deglutarylase activities than its deacetylase

activity^{52,53}. As controls, other Sirtuins do not deacylate the peptides containing malonyl, succinyl and glutaryl lysine. In addition, the thioacetyl-lysine peptides by substitution of the acyl oxygen with sulfur have been developed as mechanism-based inhibitors for Sirt 1-3 by forming a stalled S-alkylamidate intermediate¹⁰⁴. Therefore, thioacetyl-lysine peptides with chemical modifications at the N- and C-termini were exploited for the design of Sirt5's specific inhibitors. A thiosuccinyl-lysine H3K9 peptide was found to display significant inhibition potency against Sirt5's desuccinylase activity with an IC₅₀ value of 5 μ M, and to show no appreciable effect on Sirt1-3 at 100 μ M¹⁰⁵. Conversely, a thioacetyl-lysine H3K9 peptide was potent on Sirt1-3 but did not inhibit Sirt5. Even more recently, one set of thioglutaryl-lysine peptide derivatives have been identified as the most potent Sirt5's specific inhibitors¹⁰⁶.

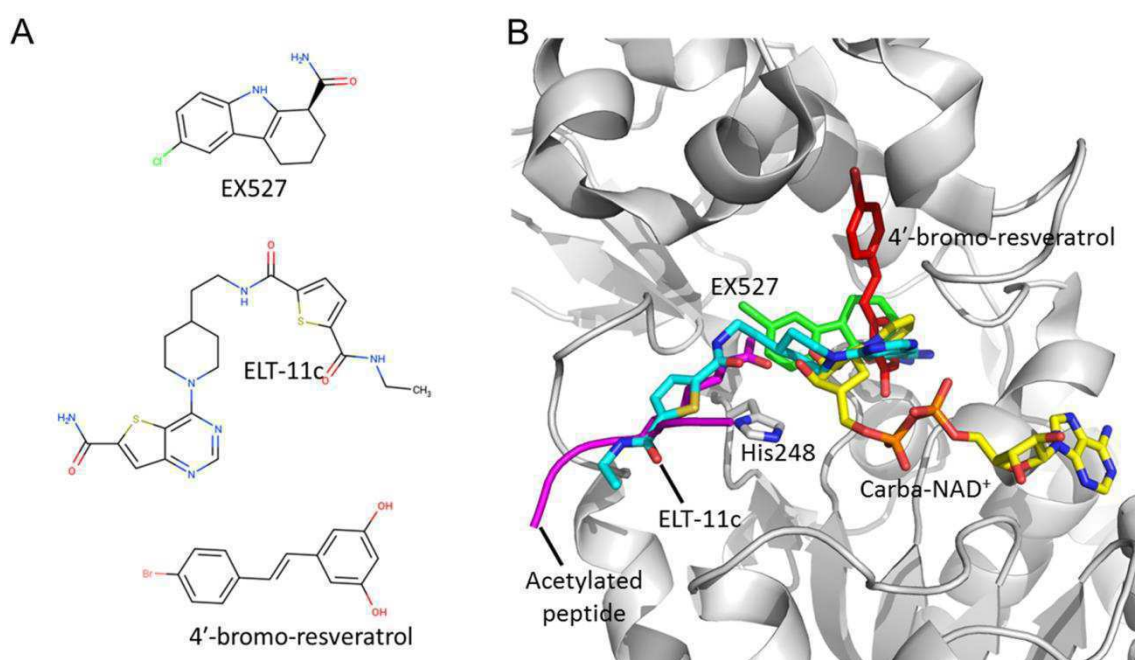


Figure 8: Structural information of Sirtuin inhibition by small molecules. A) Chemical structures of Sirtuin inhibitors. B) Structural overlay of the Sirt3/FdL peptide/ carba-NAD⁺ (gray cartoon, PDB ID 4FVT) with Sirt3/ELT-11c (PDB ID 4JSR), Sirt3/EX527 (PDB ID 4BVH) and Sirt3/bromo-resveratrol (PDB ID 4C7B). The carba-NAD⁺ (yellow) and acetylated peptide (magenta) are shown in sticks format.

Accumulating data suggest that inhibition of Sirt6 activity can be used within therapeutic approaches for some cancers, notably in the treatment of pancreatic cancer. However, as yet only few Sirt6 modulators with unfavourable characteristics are available, including poor efficacy, low solubility and bioavailability^{107, 108}. Nicotinamide (NAM) acts as a pan inhibitor for Sirtuins because of its ability to rebind to the enzyme in the presence of product

intermediate and reform NAD⁺ by undergoing nicotinamide exchange in a non-competitive fashion¹⁰⁹. In addition, Salicylate derivatives have been identified to inhibit Sirt6 with modest potency and isoform selectivity^{107,110}. The catechin derivatives catechin gallate and gallic acid gallate were identified to be the most potent Sirt6 inhibitors able to reduce Sirt6-dependent deacetylation in the single-digit micromolar range¹¹¹. However they show wide effects on a broad variety of cellular targets¹¹². TSA is an antifungal antibiotic and has been found to be a potent and selective inhibitor of Class I and II mammalian histone deacetylases (HDACs) with IC₅₀ values in the low nanomolar range¹¹³. Treating mammalian cells with TSA could halt the cell cycle in G1 and G2 phase, induce cell differentiation and repress progression of tumor cells in vitro¹¹⁴. TSA analogue Vorinostat has been approved by FDA for the treatment of cancer¹¹⁵. Recently, TSA has been demonstrated to exert isoform-specific inhibition of Sirt6-dependent deacetylation by competing with the substrate rather than serve as a Zn²⁺ ion chelator¹¹⁶. However, the molecular mechanism of Sirt6 inhibition by TSA still awaits clarification. Although these compounds are not suitable as pharmacological inhibitor for Sirt6, understanding their binding interaction detail and the mode of inhibition can support the rational development of more suitable compounds.

2 Aims of this Study

2.1 Identify and characterize Sirt6 activating compounds

Schlicker et al have identified a novel compound scaffold namely UBCS038/CSC38 as a Sirt6 modulator from a virtual screen employing the FdL assay¹¹⁷. The goal of this project was to characterize the activator binding site and elucidate the activation mechanism, and to identify more potent derivatives design UBCS038 derivatives with better potency and provide structural insights into Sirtuin 6 activation by small molecules.

2.2 Biochemical and structural studies of quercetin-based compounds on Sirtuins

It was demonstrated that quercetin can activate the deacetylase activity of Sirtuins and some of the quercetin derivatives were shown to potently inhibit Sirt6 instead of activation, but the molecular mechanism is not well clarified.^{32, 118}. The aim of this project was to clarify the effect of quercetin-based compounds on Sirtuins and identify the compound binding site and modulation mechanism.

2.3 Identify the mechanism of Sirtuin 6 inhibition by Trichostatin A

In this study, we aimed to determining the crystal structure of the Sirt6/TSA complex to identify the inhibitor binding site and understand the inhibition mechanism to improve Sirt6 inhibitor, which maybe also helpful for the development of Sirt6 activator.

2.4 Engineer protein sequence of Sirt7 to facilitate crystallization

Sirtuins have been identified to show different selectivity against acyl substrates⁵², which is dictated by the structural feature in the catalytic domain, but the crystal structure of the catalytic core of Sirt7 remains unknown. Thus, we want to reveal the catalytic mechanism of Sirt7 by biochemical and structural studies. Therefore we need to establish recombinant production of Sirt7 to obtain the required amounts of pure protein.

3 Results and discussion

3.1 Structural Basis of Sirtuin 6 Activation by Synthetic Small Molecules

3.1.1 UBCS compounds enhance Sirt6 deacetylase activity

To verify the previously reported weak Sirt6 activating effect of UBCS038 in the error-prone FdL assay, we set out to identify a more potent compound by testing UBCS038 derivatives. Our collaborator generated a series of UBCS038 derivatives with a common feature of Pyrrolo-quinoxaline ring (Fig. 9A) and we tested all the 14 compounds in a coupled enzymatic assay. Several compounds showed activating effects on Sirt6 deacetylase activity, including UBCS039, UBCS058, UBCS059, UBCS060, UBCS061 and UBCS068, and the strongest effect was measured for UBCS039 (Fig. 9B). Titration with UBCS039 showed a concentration dependent activation with a maximum stimulation around 2-fold (Fig. 9C). The EC₅₀ value of UBCS039 was around 40 μM, and we didn't observe any effect of this compound on the assay's downstream enzymes in control reactions. We also assessed the effect of UBCS039 in a mass spectrometry-based deacylation assay with an acetylated human Histone H3 Aly9 peptide substrate, and we found that the deacetylase activity of Sirt6 increased around 3.5-fold in the presence of 100μM UBCS039 (Fig. 9D). These results demonstrated that UBCS039 is able to directly stimulate Sirt6 deacetylase activity. In addition, we found that UBCS039 shows no measurable effects on Sirt6's demyristoylation activity in the coupled enzymatic assay (Fig. 9E). To determine whether UBCS039 can stimulate other Sirtuin isoforms, we also tested the compound against Sirt1, 2, and 3 with acetylated substrate peptide, and Sirt5 with succinylated substrate peptide. Our results revealed that UBCS039 exerts selective activation for Sirt6's deacetylation activity and display no effects on the other Sirt1-3 deacetylase activities, but it can also promote the physiologically dominant function of Sirt5 (Fig. 9F). To identify whether the pyrrolo[1,2-a]quinoxaline compounds have any effect to stimulate Sirt6-dependent deacetylation activity upon physiological substrates, our collaborators performed western blot to analyze the effect of compounds on full-length histone proteins and complete HeLa nucleosomes. UBCS038 and UBCS039 at 100μM were found to significantly promote the deacetylation rate of H3K18Ac of both native substrates by Sirt6. The weak in vitro activator UBCS060 showed no effect on Sirt6-dependent H3K18ac deacetylation, and UBCS068 was observed to display variability in assays, likely owing to the lower solubility of this compound in the buffer solution. Our data demonstrate that the pyrrolo[1,2-a]quinoxaline-derived compounds can stimulate Sirt6-dependent deacetylation towards peptide substrates and native substrates (Fig. 9G).

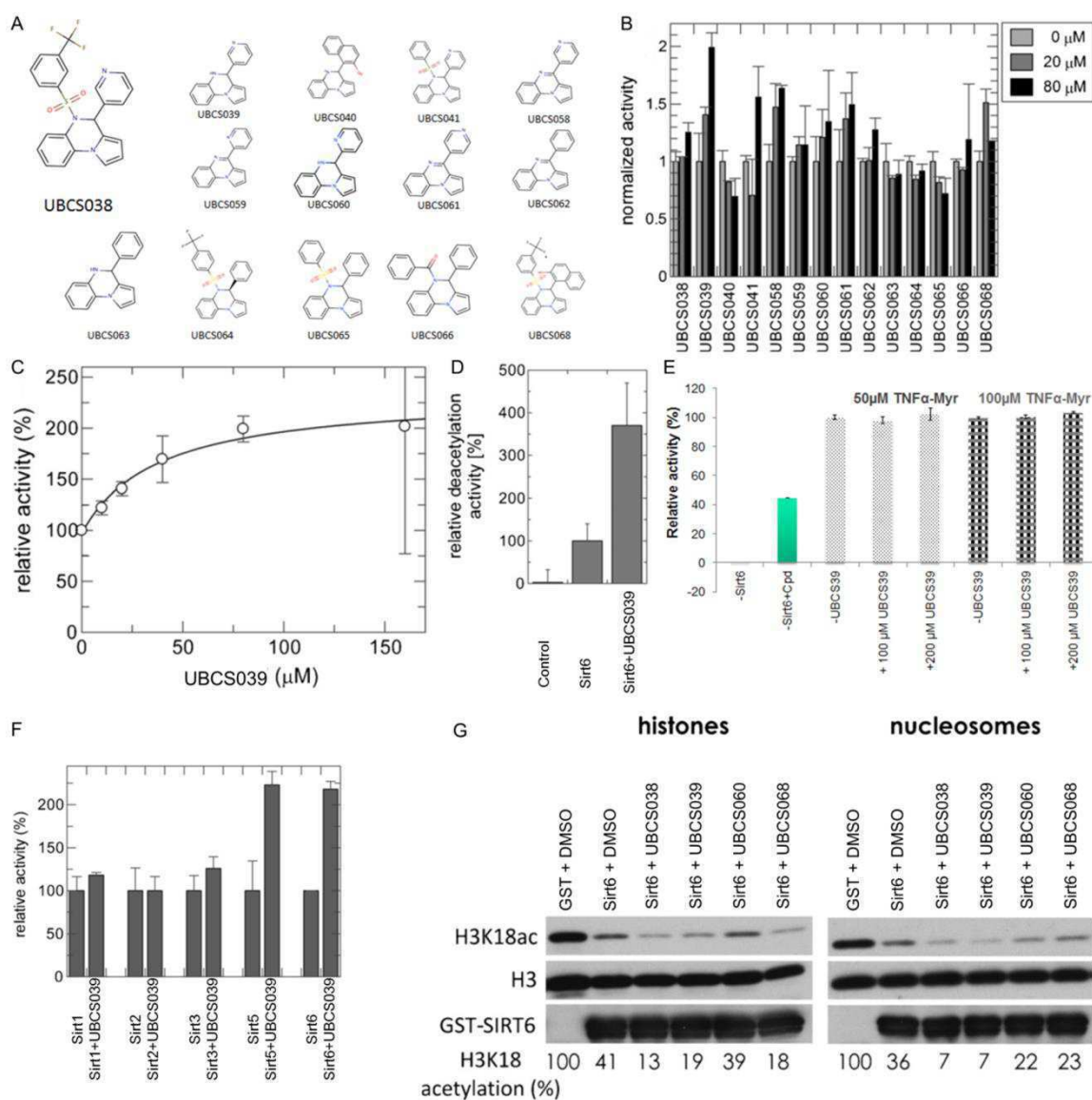


Figure 9: UBCS compounds activate Sirt6-dependent deacetylation of peptide substrates and native substrates. A) Chemical structures of the compound library based on UBCS038. B) A panel of UBCS038 derivatives was tested for effects on Sirt6 deacetylase activity in the coupled enzymatic assay at concentrations of 20 and 80 μM. C) Titration of UBCS039 yields a concentration-dependent Sirt6 activation. D) The effect of UBCS039 on Sirt6-dependent deacetylation of an acetylated human Histone H3 Aly9 peptide substrate analyzed by a mass spectrometry-based assay. E) The effect of UBCS039 on Sirt6's demyristoylation activity. F) Selectivity of UBCS039 (100 μM) was tested against human Sirt1-3 and 6 with an acetylated peptide substrate, and Sirt5 with a succinylated peptide substrate. G) Western blot analysis of the effects of compounds (100μM) on the Sirt6-dependent deacetylation of native histone H3 lysine 18 from a histone protein preparation (left) and HeLa nucleosomes (right).

3.1.2 Sirt6's specific long acyl channel is identified as the activator binding site

To analyze activator binding, we measured the interaction between Sirt6 and UBCS039 by microscale thermophoresis (MST). As concentration dependent fluorescence quenching was observed with some compounds in label-free MST, subsequent thermophoresis measurements were done with FITC-labeled Sirt6. The dissociation constant of apo Sirt6 with UBCS039 was determined to be $44 \pm 12 \mu\text{M}$, which is of the same order of magnitude as its EC50 value. The value of the dissociation constant is not significantly altered in the presence of 2 mM acetylated peptide substrate, which has a K_m around 200 μM , or 1 mM ADP-ribose, an NAD⁺ derived moiety with a K_d of 38 μM , indicating that the interaction between Sirt6 and activator is independent from the binding of the peptide substrate or ADP-ribose. However, there is an order of magnitude drop of the binding affinity for UBCS039 in the presence of 100 μM myristoylated peptide substrate ($K_d=3.4 \pm 0.9 \mu\text{M}$), implicating Sirt6's specific long acyl channel as activator binding site (Fig. 10A). We further demonstrated that the binding affinities of UBCS058 ($K_d \sim 236 \pm 49 \mu\text{M}$) and UBCS068 ($K_d \sim 467 \pm 135 \mu\text{M}$) are much weaker than for UBCS039, which is consistent with their less potent Sirt6 activation. Moreover, UBCS060 ($K_d \sim 740 \pm 391 \mu\text{M}$) shows even weaker binding to Sirt6, consistently with its further decreased activation of Sirt6 on peptide substrates and native substrates (Fig. 10B). These results indicated that UBCS compounds bind to Sirt6 in a ligand independent manner and display a binding behavior that is competitive with myristoylated peptide.

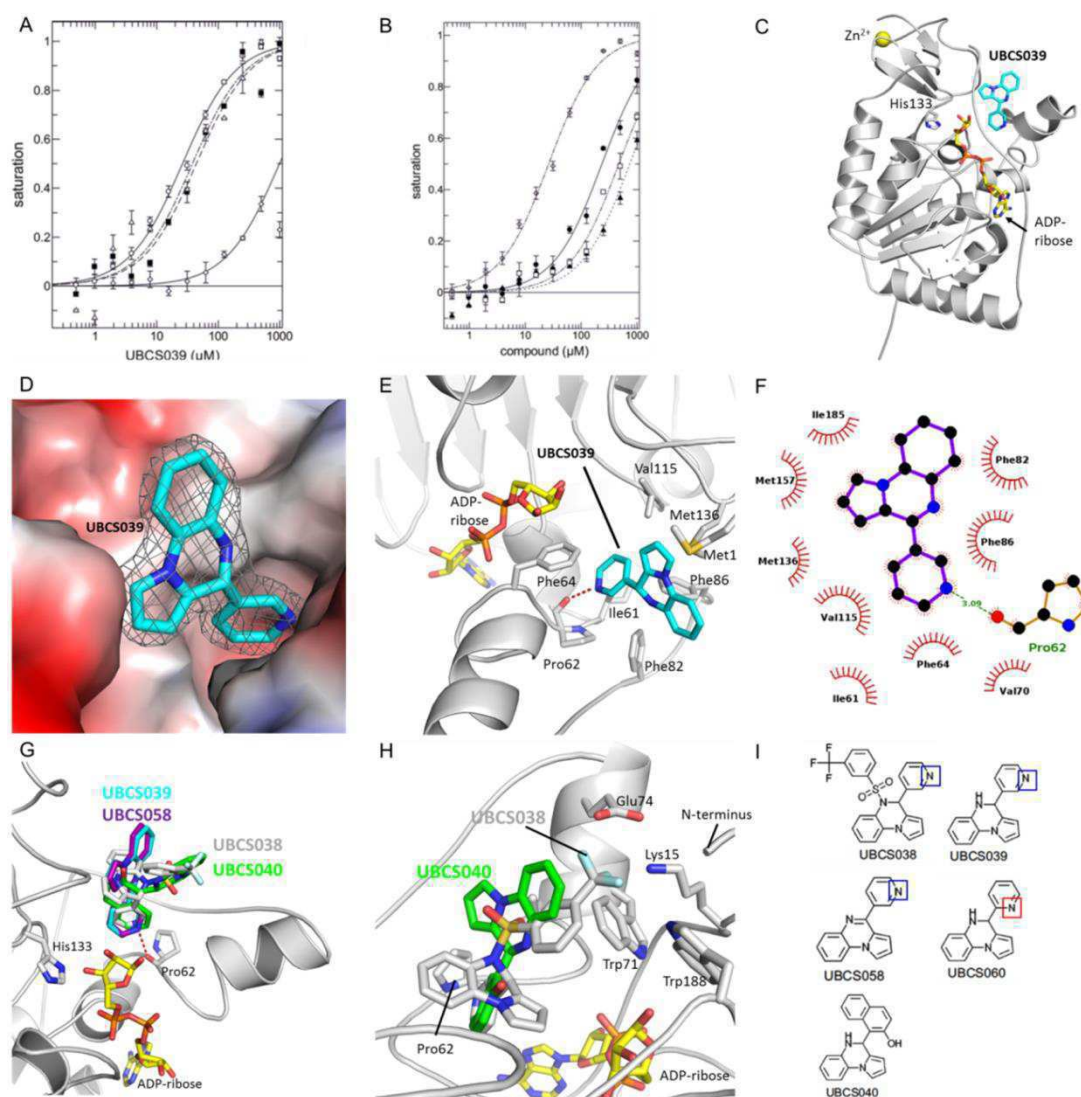


Figure 10: Crystal structure of the ternary complex of human Sirt6 with ADP-ribose and UBSC compounds. A) Binding of UBSC039 to apo-Sirt6 (■, K_d 44 ± 12 μ M), in the presence of 2mM H3K9ac peptide substrate (○, K_d 26 ± 3 μ M), 1mM ADP-ribose (△, K_d 38 ± 16 μ M), or 100 μ M TNF α -Myr peptide (◇, $K_d > 400$ μ M). B) Binding of UBSC compounds to Sirt6 in the presence of 2mM H3K9ac peptide: UBSC039 (◇, K_d $\sim 44 \pm 12$ μ M), UBSC058 (●, K_d $\sim 236 \pm 49$ μ M), UBSC068 (□, K_d $\sim 467 \pm 135$ μ M) and UBSC060 (▲, K_d $\sim 740 \pm 391$ μ M). C) Overall view of the ternary complex structure with human Sirt6 (cartoon presentation), ADP-ribose (yellow sticks), and UBSC039 (cyan sticks). His133 at the active site is represented in sticks. D) Closer view of the Sirt6 activator complex. The surface of Sirt6 is colored according to electrostatic potential, and UBSC039 (cyan sticks) is covered with 2Fo-Fc density contoured at 1σ . E) Interactions between UBSC039 and human Sirt6, red dash line represents polar contact and the potential hydrogen bond. F) LigPlot of human Sirt6 and UBSC039 interactions. G) Structural overlay of Sirt6 complexes with UBSC038 (gray), UBSC058 (purple), UBSC040 (green), and UBSC039 (cyan). H) Interactions between UBSC038 and human Sirt6, red dash line represents polar contact and the potential hydrogen bond. I) Chemical structures of UBSC038, UBSC039, UBSC058, UBSC060, and UBSC040.

UBCS039 (cyan), UBCS040 (green) and UBCS058 (magenta). H) Close view of the structures overlay of Sirt6 complexes with UBCS038 (gray) and UBCS040 (green), showing their interaction with the surface patch around Trp71/188. I) Chemical structures of activator derivatives, blue or red squares highlight the different positions of the nitrogen atom in the pyridine C-group.

Since binding of an activator to Sirt6 appears to be independent of substrate and ligand binding, we crystallized Sirt6 in complex with ADP-ribose and then soaked the crystals with 100 mM activator between 7 and 10 days to obtain Sirt6/activator complex structures. We solved the crystal structure of a ternary complex of Sirt6 with ADP-ribose and UBCS039 at a resolution of 1.87 Å with R_{work} and R_{free} values of 19.6 % and 22.5 %, respectively. One UBCS039 molecule binds per protein molecule with well-defined electron density (Fig. 10C, D). The activator was identified to occupy a hydrophobic pocket and is exposed to the solvent through the exit channel of Sirt6's catalytic core, which is distinct from the ADP-ribose binding site. The 3-pyridyl C-group of UBCS039 was found to insert into the hydrophobic pocket and form a polar contact, and likely hydrogen bond if protonated, with the peptide backbone oxygen of Pro62 through the nitrogen of its pyridine. In addition, the pyrrolo[1,2-a]quinoxaline group of UBCS039 is located between Phe64/82/86 and Ile185 via hydrophobic interactions, and comes into close contacts with Met136/157 to possibly form methionine–aromatic ring interactions (Fig. 10E, F).

We also obtained the ternary complex structures of Sirt6/ADPr with UBCS038, UBCS040 and UBCS058 at a resolution range of 1.97–2.10 Å by using the same procedure as described for UBCS039. The compounds occupy the same binding site as UBCS039 with well-defined electron density coverage. The pyrrolo[1,2-a]quinoxaline group of these compounds share the hydrophobic interaction with Sirt6 at the active site exit, albeit with different orientation in the tricyclic plane, likely due to the nature of the substitutions at the N5 (N-group) and C4 (C-group) positions. These derivatives suggest that the 6-ring in the center of the tricyclic system in either saturated (UBCS038, UBCS039) or unsaturated format (UBCS058) presents a limited surface for interaction with protein. The binding of activators and their function are thus for the most part governed by substitutions at the N5 (N-group) and C4 (C-group) positions. Comparison with the complex structure of Sirt6/ADP-ribose/UBCS039 reveals that in spite of the different orientation of the tricyclic plane, the 3-pyridyl C-group of UBCS038 and UBCS058 are found to bind in the same position inside the catalytic core as observed for that of UBCS039 (Fig. 10G). This similarity suggests that this pyridine C-group in the

activators might play an important role for binding and function. This “C-group pocket” is composed of hydrophobic residues including Ile61, Pro62, Phe64/82/86, Val70, and Val115. Moreover, the potential hydrogen bond between the nitrogen atom at meta position of the pyridine ring and the peptide backbone oxygen of Pro62 seems important for high affinity and robust Sirt6 activation. When the pyridine nitrogen is shifted from meta to ortho position like in UBCS060, it will lose its ability to interact with the backbone oxygen of Pro62, explaining the lower Sirt6 binding affinity and potency of compound UBCS060 (Fig. 10I).

The dominant effect of the pyridine C-group on binding to Sirt6 is highlighted by the complex structure of Sirt6 and UBCS038. The 3-(trifluoromethyl-) phenylsulfonyl moiety at the N5 position of UBCS038 points towards the Sirt6 surface and forms interactions with a patch of residues near the entrance of the substrate binding channel, encompassing Trp71/188, Lys15, and Glu74. This interaction is enabled by a quinoxaline ring rotation by approximately 60 degrees around the axis of the pyridine C-group following a slight translation. The pyridine C-group is allowed to be placed into the same position as that of UBCS039 due to this switch (Fig. 10G). In comparison with the activator UBCS038, the distal ring of the hydroxynaphthyl moiety of the inactive compound UBCS040 is found to bind in the same position. This causes a huge rotation of the quinoxaline ring due to the limited interaction surface, which places the quinoxaline ring into the same position as that of the N5 substituent of UBCS038 but does not lead to activation (Fig. 10H). Thus the pyridine group at the C4 position provides the dominant contribution for the protein-activator interaction, while the quinoxaline ring and the N5 substituent also contributing to the binding albeit with weaker and less specific interactions. Therefore the quinoxaline ring and the substitutions at the N-group are considered to be prime candidates for further development aiming to improve compound performance, including solubility and potency.

Comparison of the Sirt6/UBCS039 structure with the previously published Sirt6/myristoyl-peptide structure (PDB ID 3ZG6) demonstrates that the UBCS compounds occupy a common region in the distal part of Sirt6’s specific catalytic pocket, which accommodates the long chain fatty acyl group of substrates (Fig. 11A). This location fits to the observation that the compounds specifically activate Sirt6’s deacetylation activity without affecting its demyristoylation activity. However, the compounds do not behave as strong competitive inhibitors toward myristoylated peptide substrates, likely due to their weak binding affinity in comparison to myristoyl peptides, as well as their limited solubility. On the other hand, in the presence of 100 μ M myristoylated peptide substrate, the binding affinity of UBCS039 to Sirt6

decreases by more than one order of magnitude when compared to its value in the presence of acetylated peptide substrate. Our results thus demonstrate that our activators compete with the distal end of substrate myristoylation and thus differentially modulate Sirt6-mediated deacetylation and demyristoylation. Moreover, comparing Sirt6/UBCS039 structure with other published Sirtuin – activator complex structures revealed that the UBCS compound binding site within the Sirt6-specific acyl channel is not found in other Sirtuin isoforms, since it is covered by the cofactor binding loop and neighboring helix bundles in other Sirtuin isoforms like Sirt1 and Sirt5. These features are reduced to a short loop and single helix in Sirt6. Conversely, the activator binding site in other Sirtuin isoforms would be inaccessible in Sirt6, since it is covered by Sirt6's N-terminus (Fig. 11B).

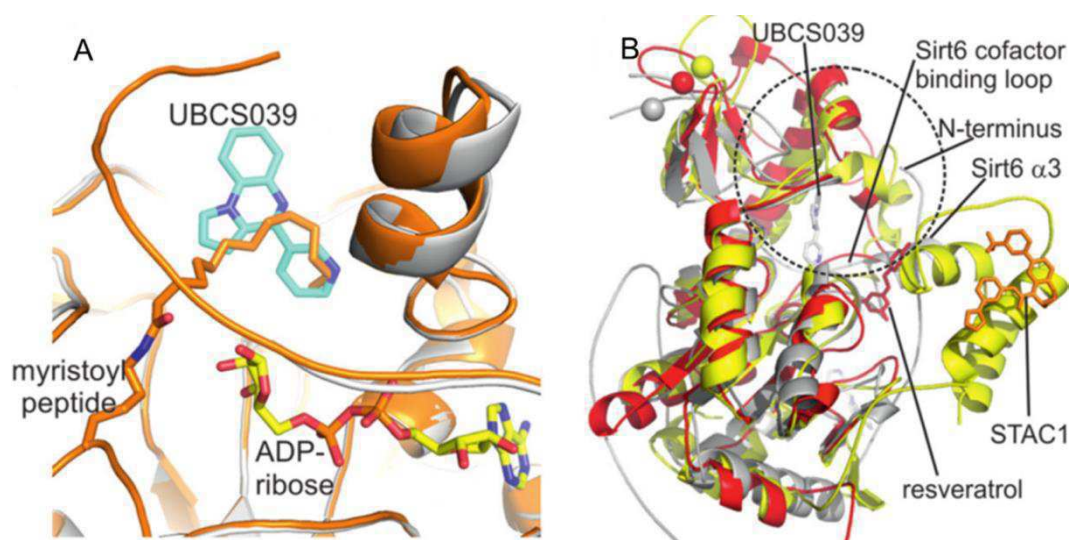


Figure 11: The mechanism of substrate and Sirtuin isoform selection for Sirt6 activators.

A) Structural overlay of the Sirt6/UBCS039 complex (gray cartoon/cyan sticks) with the Sirt6/myristoyl peptide complex (orange; PDB ID 3ZG6). B) Structural overlay of the Sirt6/activator complex (gray color) with Sirt1/ STAC1 (yellow color; PDB ID 4ZZI) and Sirt5/resveratrol (red color; PDB ID 4HDA). Dotted circle: Cofactor binding loop and neighboring helix bundle.

Compared to the well-defined Sirt1 activators, the need to identify small molecule activators for other Sirtuin isoforms to treat aging-related disease is apparent. Our results identify isoform specific Sirt6 deacetylation activators with moderate potency, and reveal a novel activator binding pocket in Sirt6's acyl binding channel, which is covered by the cofactor binding loop and neighboring helix bundle in other Sirtuin isoforms. The compounds only increase Sirt6's deacetylation activity and compete with Sirt6's deacetylation activity. Moreover, the compounds do not display apparent activation on Sirt1, Sirt2 and Sirt3, but

Results and discussion

promote the Sirt5-dependent deacetylase activity. In addition, comparison of Sirt6 apo and complex structures reveals no significant conformational changes, suggesting the compounds to mediate activation through mechanisms distinct from Sirt1 and Sirt5 modulation. Further investigation is needed to establish the activation mechanism of UBCS compounds. However, we present here for the first time synthetic small molecule Sirt6 activators and provide information to develop Sirt6 activators with higher potency and specificity for therapeutic applications.

compared to DMSO vehicle negative control. Data are representative of 3 independent experiments. Relative acetylation on the indicated sites was determined by normalization to total H3 and control samples.

To exclude assay artefacts, we therefore analyzed the effect of quercetin with a previously developed mass spectrometry-based assay by measuring the rate of deacetylated peptide formation from the substrate peptide H3K9Ac. The titration of quercetin and its analogue luteolin yield a concentration-dependent activation of Sirt6-mediated deacetylation with a higher than 2-fold maximum stimulation (Fig. 12D). The EC₅₀ values of both compounds were around 1 millimolar, and we did not observe any evidence for the inhibition at lower concentrations described in previous reports. Thus, we speculate that the GST tag of Sirt6 used in the previous study might cause the inhibition of Sirt6 in the presence of quercetin at low concentrations, due to the tight interaction between GST and quercetin. We further examined the effect of quercetin on Sirt6's physiological substrates, including nucleosomes purified from HeLa cells and chicken. Quercetin was shown to activate the Sirt6-dependent deacetylation of H3K18Ac on nucleosomes and promote the deacetylation of H3K9Ac and H3K18Ac on free histones (Fig. 12E).

To investigate the interaction between quercetin and Sirt6, we solved their complex structure by soaking experiments. The crystal structure of the Sirt6 catalytic domain in complex with quercetin was determined at a resolution of 1.84 Å. We identified the quercetin binding site in a hydrophobic pocket, mostly overlapping with the UBCS039 binding site (Fig. 13A, B). The two hydroxyl groups of quercetin's catechol moiety form hydrogen bonds with the backbone oxygen of Pro62, and also make multiple water-mediated interactions with the distal backbone atoms, especially from residues Ala53, Val15 and Ile61, as well as with the side chain of Asp116 (Fig. 13B). The binding mode resembles the binding of the UBCS039 pyridin and is thus likely that the catechol group functions as an anchor to bind at the bottom of the Sirt6 substrate binding channel. This binding mode appears to be a very important interaction pattern for Sirt6 modulators. In addition, the chromen-4-one group of quercetin forms hydrophobic interactions with Phe64/82/86 and Val70/115, and contacts Met136/157 through a methionine–aromatic ring interaction.

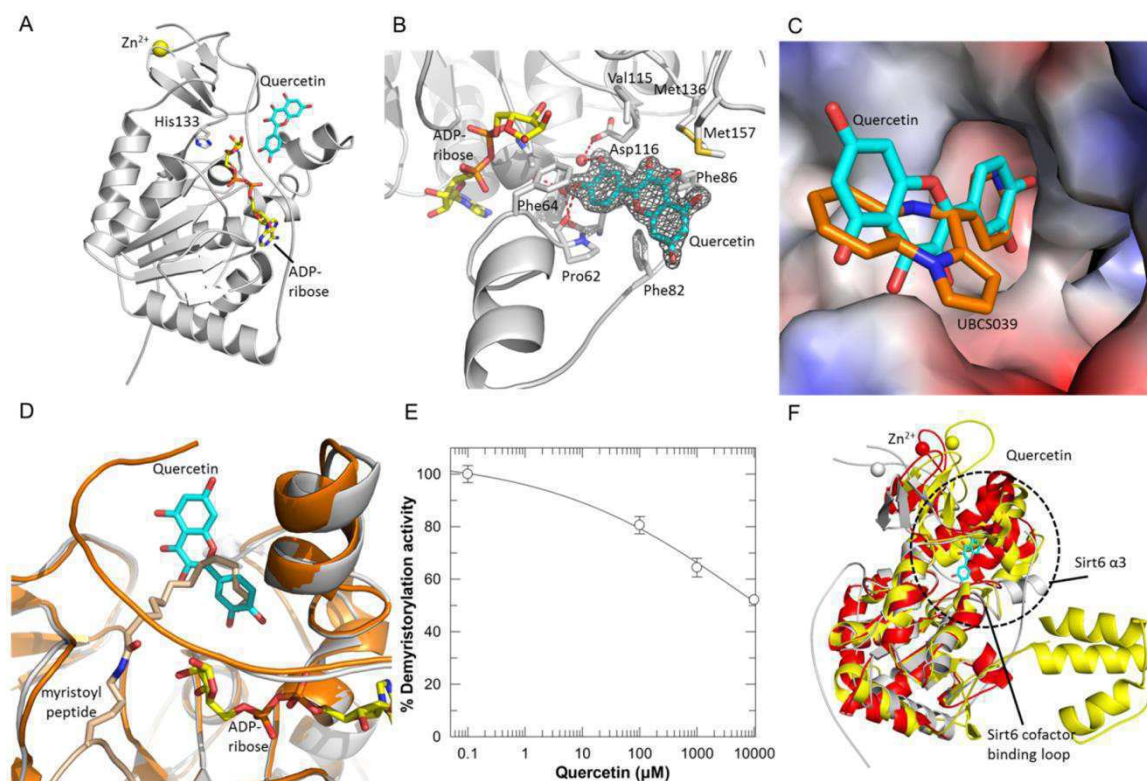


Figure 13: crystal structure of a Sirt6/quercetin complex. A) Overall structure of human Sirt6 (cartoon presentation), ADP-ribose (yellow sticks), and quercetin (cyan sticks), His133 at the active site is represented in sticks. B) Interactions between quercetin and human Sirt6, red dash lines represent the hydrogen bonds; atoms of quercetin are covered with 2Fo-Fc density contoured at 1σ . C) Protein surface of the Sirt6/quercetin complex colored according to the electrostatic potential. The ligand is shown as cyan sticks and overlaid with UBCS039 (orange sticks). D) Structures overlay of Sirt6/ADPr/quercetin complex (gray cartoon, cyan ligand) with Sirt6/ADPr/myristoyl-peptide complex (orange cartoon, wheat peptide, PDB code 3ZG6). E) A quercetin titration shows dose-dependent inhibition of Sirt6 demyristoylation. Data are shown as means \pm SD ($n = 3$). F) Structural overlay of sirt6/ADPr/quercetin with Sirt1/ STAC1 (yellow color; PDB ID 4ZZI) and Sirt5/resveratrol (red color; PDB ID 4HDA). Dotted circle: Cofactor binding loop and neighboring helix bundle.

A comparison between the Sirt6/quercetin complex and the Sirt6/UBCS039 complex structure described above indicates that the chromen-4-one group possesses a different plane orientation from the strong activator UBCS039 (Fig. 13C). This might lead to difference in potency against Sirt6. Moreover, structural alignment of the Sirt6/quercetin complex with the Sirt6/myristoyl-peptide complex reveals that quercetin also occupies the region accommodating the distal end of the myristoyl group of the substrate (Fig. 13D), indicating

that quercetin might inhibit the demyristoylase activity of SIRT6. We therefore analyzed the effect of quercetin on Sirt6 dependent hydrolysis of long chain fatty acyls in mass spectrometry-based assay by measuring the rate of myristoyl-TNF α substrate peptide deacylation. Titration of quercetin was found to inhibit Sirt6 dependent demyristoylation in a dose-dependent manner (Fig. 13E). Thus our data demonstrated that quercetin is able to stimulate Sirt6 dependent deacetylase activity and also inhibit the demyristoylase activity of SIRT6, likely using a mechanism related to that of UBCS039-mediated stimulation. Moreover, quercetin occupies the Sirt6-specific acyl channel, which is not present in the other Sirtuin isoforms (Fig. 13F). Our results thus implicate that this Sirt6 - quercetin interaction mode should be isoform-specific.

3.2.2 Quercetin-based compounds show different effects on Sirt6 deacetylation

Other flavonoids have been reported to alter SIRT6 activity. However, their effects vary depending on structure and chemical properties. For example, members of the flavanol family, lacking the keto group at position 4 of the C ring and the double bond occurring between carbons 2 and 3 of the C ring, were reported to inhibit Sirt6 deacetylase activity. Especially catechin gallate (CG) and gallic catechin gallate were identified as the most potent Sirt6 inhibitors with IC₅₀ values of 2.5 μ M and 5.4 μ M respectively¹¹¹. On the other hand, cyanidin was reported to be the most potent activator of Sirt6 with a maximal activation up to 55-fold, albeit with a moderate potency with an EC₅₀ value of 460 μ M¹¹¹. To understand the mechanism, we analysed the effect of these compounds in our mass spectrometry-based deacetylation assay. Titration of CG yielded a dose-inhibition curve with a much lower potency (IC₅₀ 80 \pm 15 μ M, Fig. 14A) compared to a previous report (IC₅₀ 2.5 \pm 0.1 μ M). In addition, we observed a dose-dependent activation of Sirt6 by treatment with cyanidin at a low compound concentration, from 9.76 to 78.12 μ M (Fig. 14G). However, we failed to detect stimulation at high compound concentrations likely due to heavy compound precipitation, which might cause protein and peptide aggregation.

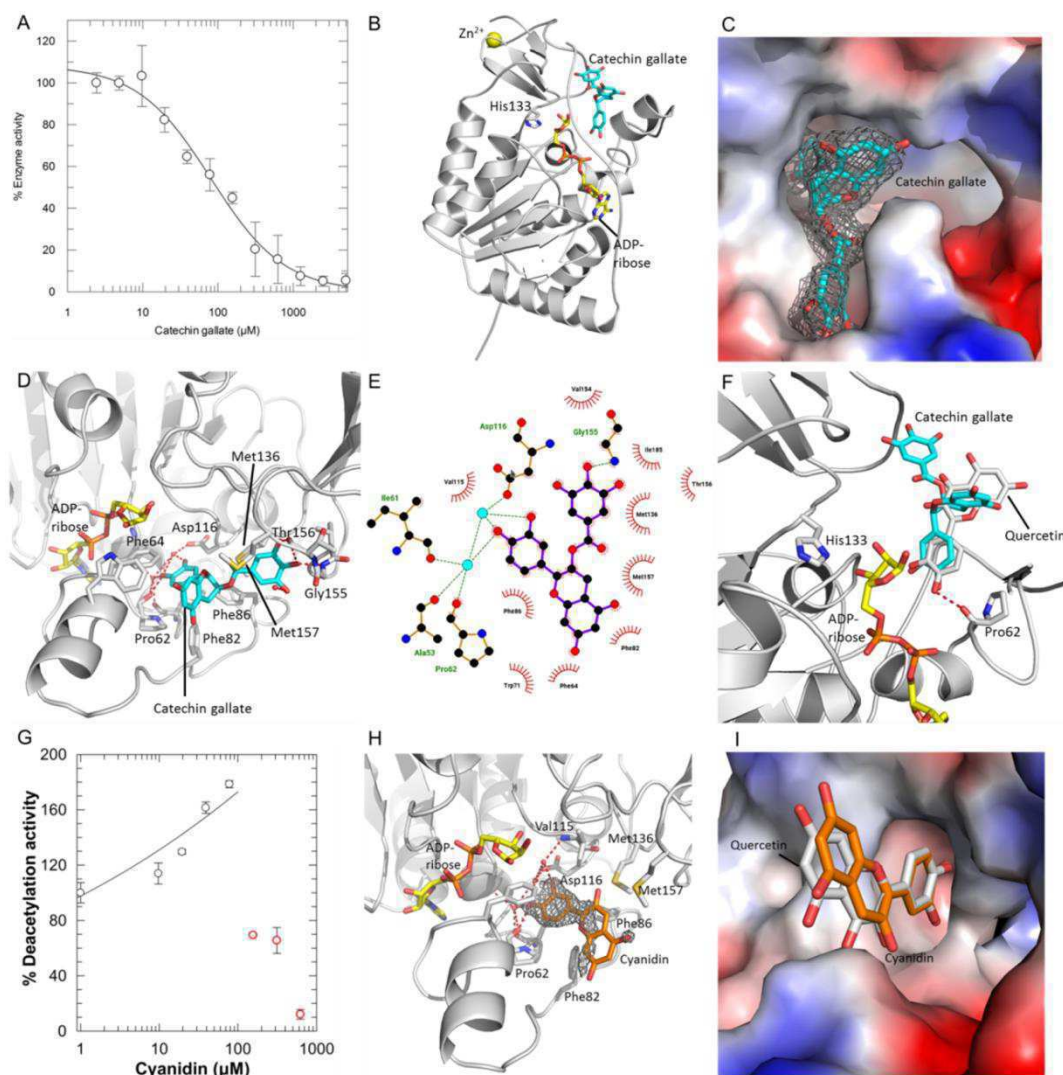


Figure 14: Quercetin derivatives can modulate Sirt6 activity with different functions.

A) Dose-dependent effects of CG on Sirt6-mediated deacetylation activity. B) Overall structure of human Sirt6 (cartoon presentation), ADP-ribose (yellow sticks), and CG (cyan sticks), His133 at the active site is represented as sticks. C) Protein surface of the Sirt6/CG complex colored according to electrostatic potential; atoms of CG are embedded in 2Fo-Fc density contoured at 1σ . D) Interaction of CG with Sirt6. Interacting residues are represented as sticks, and polar interactions are indicated by dashed red lines. E) LigPlot of the Sirt6 and CG interaction. F) Overlay of Sirt6 complexes with CG (cyan) and quercetin (gray), respectively. ADP-ribose (yellow) and His133 at the active site is represented in sticks. G) Dose-dependent effects of cyanidin on Sirt6 deacetylation activity, red spots indicate high concentrations. H) Interactions between cyanidin and Sirt6. Residues that interact with cyaniding are represented as sticks and polar interactions are indicated by dashed red lines. 2Fo-Fc electron density for the ligand is contoured at 1σ . I) Protein surface of the Sirt6/cyanidin complex colored according to electrostatic potential. The ligand is shown as cyan sticks and superposed with quercetin (gray sticks).

To investigate the mechanisms of inhibition and activation, we obtained the ligand complex structures of Sirt6 with CG and cyaniding by soaking crystals of Sirt6/ADPr with the compounds overnight. The Sirt6/ADPr/CG ternary complex structures was determined at a resolution of 2.01 Å and revealed that one catechin gallate binds to each protein molecule with clearly defined electron density (Fig. 14B, C). CG was found to occupy the quercetin binding site at the end of the Sirt6-specific acyl binding channel, using the same binding space for its catechol moieties as quercetin, but with a rotation of the chromen-4-one scaffold with respect to the non-planar C ring and the additional trihydroxy benzoyl moiety on the carbon 3 of the C ring (Fig. 14D, E, F). Catechin gallate does not occupy the acetyl substrate binding site, but its catechol moiety partly overlaps with the NAM group of NAD⁺ in the C-pocket. Therefore, CG could be assumed to perform inhibition in competition with NAD⁺. However, structural comparison of the Sirt6 complex with inhibitor and activator reveals that the catechol moiety of both compound types binds to the identical site, overlapping the binding site of the NAM moiety. Thus, we suggest that quercetin-based compounds bind to Sirt6 after nicotinamide release as similar to EX-527, and the variability in effects of quercetin-based compounds maybe due to the orientation of the chromene group or the substitution of a gallate group. The ternary complex structures of Sirt6/ADPr/ cyanidin was determined at a resolution of 2.1 Å. Cyanidin was found to occupy the same binding site as quercetin (Fig. 14I), indicating a similar mechanism on activation, however, the compound only displayed good electron density coverage for its catechol moiety while the chromen-4-one group had poor density coverage, suggesting the presence of alternative conformations likely due to the lack of a keto group at the position 4 of the C ring (Fig. 14H). However, the mechanism of quercetin-based compounds requires further analysis.

3.2.3 Isoquercetin acts as a Sirt6 activator and exhibits higher isoform specificity

As quercetin and related polyphenols have been reported to affect the activity of other Sirtuin isoforms, we further tested it against human Sirt1-3 with acetylated substrate and Sirt5 with succinylated substrate. Notably, quercetin was found to inhibit all Sirtuins except Sirt6; for example, it caused the loss of deacetylase activity of Sirt2 to more than 80% upon treatment with 1250 μM quercetin (Fig. 15A). To understand why quercetin behaves differently in different Sirtuin isoforms, we obtained the crystal structure of a Sirt2/quercetin complex by soaking Sirt2/ADPr crystals with 100 mM quercetin for three days. Together with Sandra, the structure was determined at a resolution of 2.23 Å, and revealed that a quercetin molecule binds at the symmetry-based dimer interface near the entrance to the active site (Fig. 15B), and exhibits distinct interaction with two symmetrical subunits. Quercetin is found to form π-

π stacking with Tyr-114 and Phe-235, and forms hydrophobic contacts with Glu-116 and Glu-120 from one subunit (Fig. 15C, D). It only exhibits a few contacts with the other monomer in a different rotated orientation. In comparison to the Sirt2 substrate complex structure, quercetin was found to occupy the volume accommodating the distal C-terminal residues of the substrate and thus sterically hinders its binding (Fig. 15E). To confirm the mechanism of inhibition, we next tested the competitive effect of quercetin in our mass spectrometry assay with concentrations of acetylated α -tubulin peptide in the range from 100 to 400 μ M, and for each peptide concentration we tested quercetin at two different concentrations 312.5 and 1250 μ M. Our data revealed that quercetin induced Sirt2 deacetylation inhibition can be reduced by adding more acetylated α -tubulin peptide (Fig. 15F), consistent with the structural observation that quercetin binds to the active site entrance and blocks substrate binding. Moreover, overlays with the structures of other Sirtuin isoforms illustrate that this quercetin binding site is at the accessible surface area for some Sirtuin isoforms including Sirt1, Sirt3 and Sirt5 (Fig. 15G), indicating that quercetin might use the same mechanism to regulate those Sirtuin isoforms. However, this quercetin binding site is inaccessible to Sirt6, since it is blocked by the N-terminal region of Sirt6 (Fig. 15H).

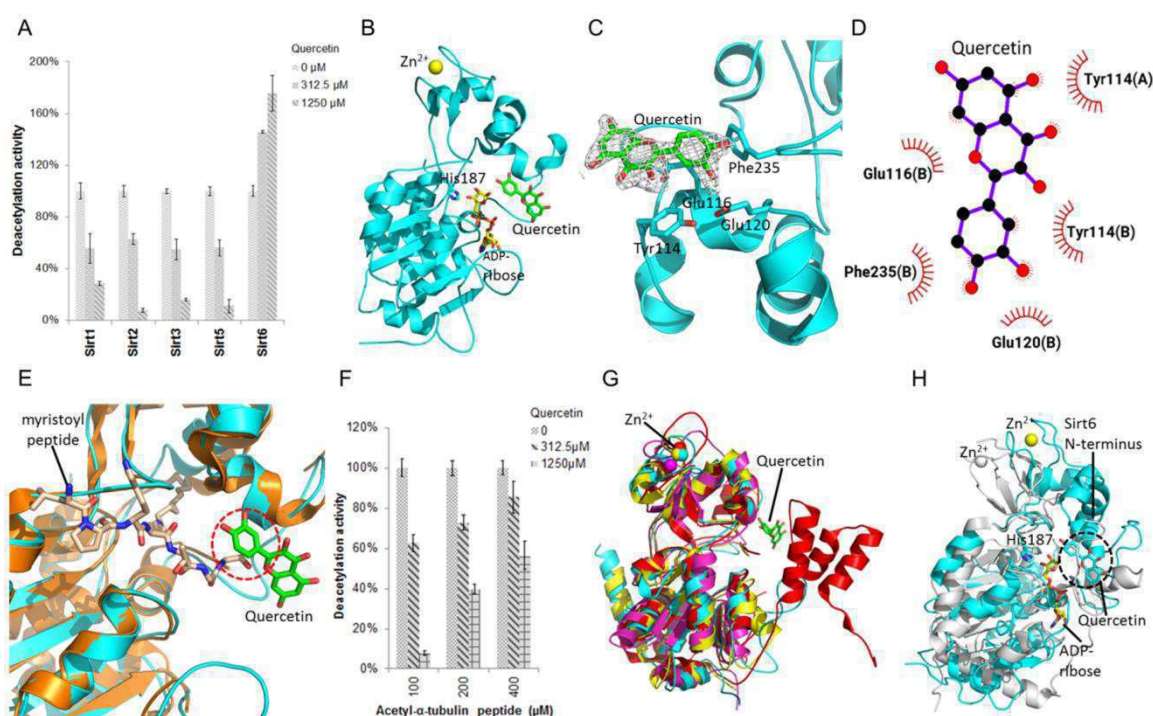


Figure 15: The effect of quercetin on Sirtuins and the complex structure of Sirt2 with quercetin. A) Quercetin effects on deacetylation by Sirtuin isoforms. B) Overall structure of human Sirt2 (cartoon presentation), ADP-ribose (yellow sticks), and quercetin (green sticks), His187 at the active site are represented as sticks. C) Close view of the Sirt2/quercetin complex. Residues interacting with quercetin are represented as sticks and quercetin (green

Results and discussion

sticks) is covered with 2Fo-Fc density contoured at 1σ . D) LigPlot of Sirt2 and quercetin interaction. E) Structures overlay of Sirt2/quercetin complex (cyan cartoon, green ligand) with Sirt2/myristoyl-peptide complex (gold cartoon, wheat peptide in sticks, PDB code 4Y6O). Dotted circle: steric clash between substrate C-terminal and quercetin. F) Effects of quercetin on Sirt2 deacetylase activity against various substrate concentrations. G) Structural overlay of the Sirt2/quercetin complex (cyan cartoon, cyan ligand) with Sirt1 (red;PDB ID 5BTR), Sirt3(yellow;PDB ID 4HD8) and Sirt5 (magentas;PDB ID 4HDA). H) Structural overlay of the Sirt2/quercetin complex (cyan cartoon, green ligand) with Sirt6/quercetin complex (gray cartoon and ligand). Dotted circle: steric clash between Sirt6 N-terminus and quercetin.

To support the development of highly selective Sirt6 modulators, we investigated the effect of quercetin derivatives. We found that isoquercetin retains the activating effect on Sirt6-dependent deacetylase activity with a maximum stimulation of more than 2-fold, but did not significantly modulate Sirt1-3 deacetylase or Sirt5 dependent desuccinylase activity (Fig. 16A, B). Since isoquercetin showed improved selectivity for Sirt6, we tried to determine the complex structure of Sirt6/isoquercetin to obtain insights into the underlying molecular mechanism. An attempt to soak crystals with isoquercetin as described for quercetin initially failed. Lateron, we recognized that a PEG molecule occupied the active site with close proximity to the hydroxyl group at ring C of quercetin, which might prevent isoquercetin from binding to the Sirt6 specific acyl channel due to the weak potency of the compound and the high PEG concentration in the soaking condition. So we optimized the soaking condition by substituting PEG with ethylene glycol to obtain a crystal of the Sirt6/isoquercetin complex. The ternary complex structure of Sirt6/ADPr/isoquercetin was determined at a resolution of 1.8 Å. We found that the quercetin group of isoquercetin binds to Sirt6 in the same manner as quercetin (Fig. 16C, D) and the additional sugar moiety of isoquercetin inserts into the Sirt6 specific acyl channel with an overlap with the PEG molecule bound there (Fig. 16E). The electron density for the additional sugar moiety of isoquercetin is present but it is weaker than that for the quercetin group, likely due to its inherent flexibility, and it does not contribute to protein-ligand interactions. We further investigated the mechanism of isoquercetin for improved selectivity by placing the Sirt6/ADPr/isoquercetin complex structure on top of the Sirt2/ADPr/quercetin complex structure, and found that the sugar moiety of isoquercetin would form a steric clash with Tyr-114 of Sirt2 to improve selectivity for Sirt6 (Fig. 16F). Our results reveal that the sugar moiety can act as selector, which enables the ligand to bind into the Sirt6 specific acyl channel and negatively affects the interaction with other Sirtuin

isoforms. This indicates the C-ring hydroxyl group of quercetin as a potential site for modifications to enhance selectivity among Sirtuins.

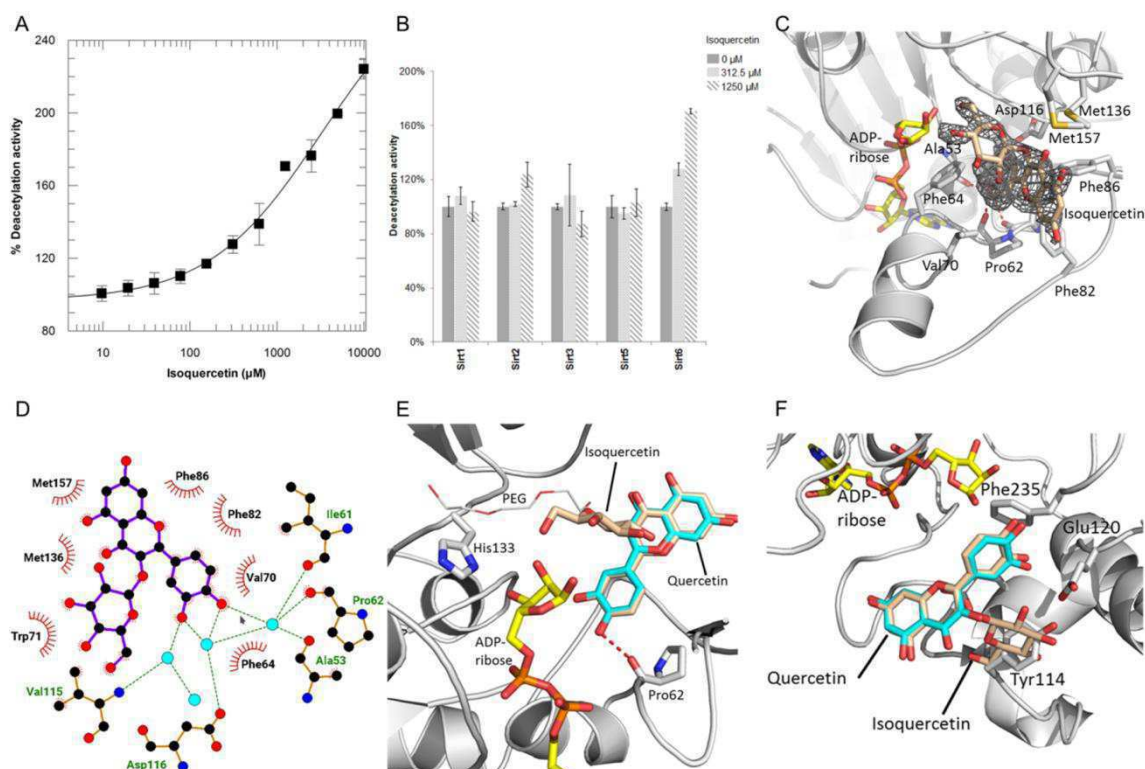


Figure 16: The effect of isoquercetin on Sirtuins and the complex crystal structure of Sirt6 and isoquercetin. A) Dose-dependent effects of isoquercetin on Sirt6 deacetylation activity. B) Effect of isoquercetin on Sirtuin isoforms. C) Close view of the Sirt6 and isoquercetin complex, interacting residues are labeled and isoquercetin (wheat sticks) is covered with 2Fo-Fc density contoured at 1σ . D) LigPlot of Sirt6 and isoquercetin interaction. E) Overlay of Sirt6/ADPr/isoquercetin complex (wheat ligand) with Sirt6/quercetin complex (cyan ligand), and the white line indicates the PEG molecule in the Sirt6/quercetin complex. F) Place isoquercetin (wheat ligand) on top of quercetin (cyan ligand) in the Sirt2/ADPr/quercetin complex structure (gray cartoon, side chains involved in quercetin interactions are displayed in gray sticks)

3.3 Structural basis of Sirtuin 6 inhibition by [the hydroxamate] trichostatin A

3.3.1 Crystal Structure of Sirt6 in complex with trichostatin A

We first studied the impact of Sirt6 substrate (acetyl peptide) and coligand (NAD^+) on the Sirt6-TSA interaction in a binding assay using label-free MST. Our results revealed that the interactions between Sirt6 and TSA was enhanced in the presence of ADP-ribose (a fragment of NAD^+), indicating that the complex of Sirt6-TSA can be stabilized by the nucleotide bound conformational state. Binding of TSA was not significantly altered by adding substrate peptide (Fig. 17B). We therefore determined the ternary complex structure of Sirt6/TSA/ADP-ribose through soaking crystals of Sirt6/ADP-ribose complex with 10 mM compound overnight. Our complex structure revealed that TSA inserts into a hydrophobic pocket at the bottom of Sirt6 substrate binding channel, and the phenyl group is exposed to the solvent through the exit of the Sirt6's catalytic core (Fig. 17C). The hydroxamate group binds in the C pocket, interacts with conserved residues there like the carboxamide part of nicotinamide, but apparently with improved affinity. The hydroxamate nitrogen of TSA forms a hydrogen bond with the side chain of a conserved residue in the C pocket (Asp116), and makes multiple water-mediated hydrogen bonds with the backbone oxygen of Ala53, Ile61 and Pro62, whereas the hydroxamate carbonyl oxygen interacts with the backbone amide of Val115 and Asp116. Moreover, the hydroxamate hydroxyl group is buried at the deep end of the C pocket, and forms additional hydrogen bonds with the side chain of residues Asp116, Asn114 and Ser56. It would be expected to greatly increase the relative binding affinity in comparison to the effect of the carboxamide of NAM (Fig. 17D, E, F). Additional TSA-Sirt6 interactions include the van der Waals contacts of the aliphatic linker of TSA and the diaminomethylphenyl moiety within the acyl channel of Sirt6, and it is likely to contribute to improving the binding affinity. The aliphatic chain of TSA is observed with well-defined electron density coverage, and forms interactions with Phe64/80/86, Ile61, and Val70/115 in a largely hydrophobic cavity, which can accommodate the pyridine ring of nicotinamide. The phenyl ring of TSA is positioned away from the C pocket of the NAD^+ binding site, and interacts with Val70 and Trp71. However, this moiety has poor density coverage, which is likely due to its flexibility (Fig. 17D).

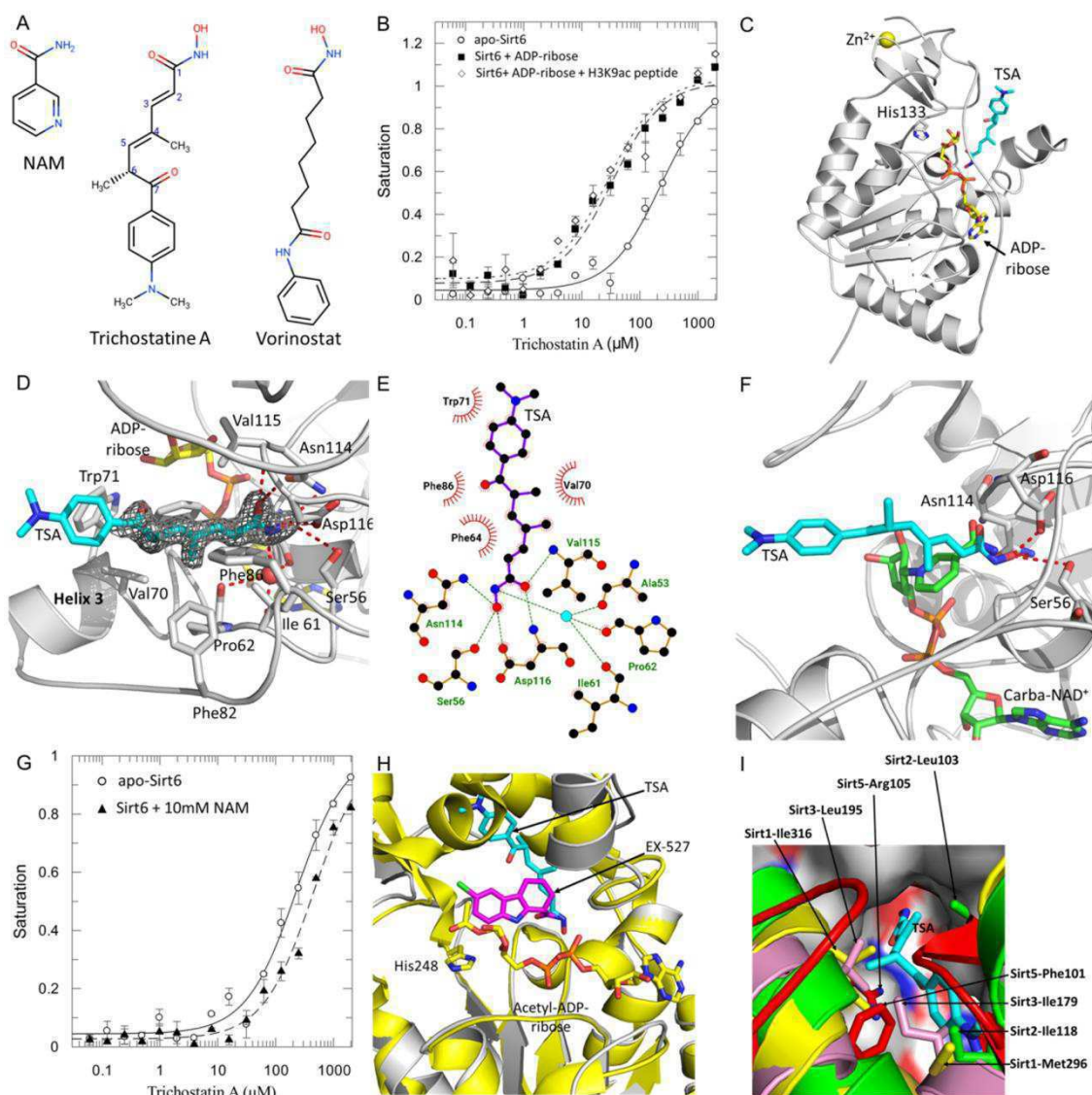


Figure 17: Crystal structure of a Sirt6/TSA complex. A) Structures of NAM, TSA and SAHA. B) Binding of TSA to apo-Sirt6 (\circ , K_d $227 \pm 35 \mu\text{M}$), in the presence of 1mM ADP-ribose (\blacksquare , K_d $32.9 \pm 5.9 \mu\text{M}$), and in the presence of 1mM ADP-ribose and 1mM acetylated H3K9ac peptide substrate (\diamond , K_d $28.9 \pm 8.2 \mu\text{M}$). C) Overall structure of human Sirt6 (cartoon presentation), ADP-ribose (yellow sticks), and TSA (cyan sticks), His133 at the active site is represented in sticks. D) Interaction of TSA with Sirt6. Interacting residues are labeled, and polar interactions are indicated by dashed red lines. $2\text{Fo}-\text{Fc}$ electron density for the ligand is contoured at 1σ . E) LigPlot of Sirt6 and TSA interaction. F) Overlay of the Sirt6/TSA complex (gray cartoon, cyan ligand) with a Sirt3/Ac-ACS peptide/carba-NAD⁺ complex (PDB ID 4FVT, cartoon was hide, green carba-NAD⁺). G) Binding of TSA to apo-Sirt6 (\circ , K_d $227 \pm 35 \mu\text{M}$) and in the presence of 10 mM NAM (\blacktriangle , K_d $445 \pm 66 \mu\text{M}$). H) Structural overlay of the Sirt6/ADP-ribose/TSA complex (gray cartoon, cyan ligand) with a Sirt3/acetyl-ADP-ribose/Ex-527 complex (PDB ID 4BVH, yellow cartoon, magenta ligand). I)

Structures overlay of the Sirt6/ADP-ribose/TSA complex (gray color) with Sirt1 (yellow color; PDB ID 4IF6), Sirt2 (green color; PDB ID 3ZGV), Sirt3 (pink color; PDB ID 4FVT) and Sirt5 (red color; PDB ID 4G1C). Close view of the TSA (cyan ligand) binding site. Residues clashing with TSA are represented as sticks.

Binding studies revealed that TSA does not compete with either peptide substrate or ADP-ribose. However, decreased binding affinity of TSA for Sirt6 was observed in the presence of 10mM NAM (Fig. 18G), suggesting that TSA can act as a Sirt6 inhibitor like NAM and EX527, which occupy the C pocket after NAM release and stabilize the intermediate complex (Fig. 18H). Compared to other Sirtuin structures, the Sirt6/TSA complex structure presents an isoform-specific binding motif for inhibitor. The TSA binding site comprises the unique acyl binding channel of Sirt6, which is occupied by the cofactor binding loop and neighboring helix bundles in other Sirtuin isoforms contain Sirt1,2,3 and 5. The distal part of the aliphatic chain and the dimethylaminophenyl moiety of TSA are observed to form steric clashes with other Sirtuin isoforms in this region (Fig. 18I), and therefore display significant selectivity in inhibition of Sirt6. Our results demonstrate that TSA is able to interact more extensively with conserved residues from the C pocket compared to NAM and thus enhance the interaction with Sirt6, whereas the extended cap group of TSA helps to convey isoform selectivity.

3.3.2 Implication to develop class selective inhibitor based on TSA for HDACs

To investigate how to develop the selectivity of TSA analogues against Class I/II HDACs and Sirtuins respectively, we placed the human HDAC7/TSA complex on top of the Sirt6/TSA complex and aligned them at the TSA binding site. While the hydroxamate groups and the aliphatic chains can be well overlaid, the phenyl groups are found to display different binding orientations. The phenyl group of TSA forms a clash with Trp71 of Sirt6 with the indicated orientation in the HDAC7 binding mode (Fig. 18A). The other way round, the different orientation of the phenyl group in HDAC7 is needed to prevent a major clash between TSA and the $\alpha 1/\alpha 2$ loop as well as the $\alpha 14$ loop of HDAC7. SAHA has been identified as a specific inhibitor for Class I/II HDACs, and produces no effect on Sirtuins, in contrast to the inhibitory effect of its analogue TSA on Sirt6. To understand the mechanism underlying the specificity difference, we overlaid the complex structures of human HDAC2/SAHA and Sirt6/TSA. Notably, the aliphatic chain of SAHA serves to bind HDACs tightly like TSA, despite its high flexibility, likely due to energetically favourable binding conformation. However, the phenyl group of SAHA also forms a steric clash with Trp71 of Sirt6, according to the binding mode of SAHA with HDACs (Fig. 18B). Moreover, the long aliphatic chain of

SAHA is suggested to prevent the shift of the phenyl group like seen for TSA in its Sirt6 complex to avoid a steric clash with Trp71 of Sirt6, and lead to the improved selectivity for HDACs over Sirt6. Thus our results suggest that modification of the phenyl moiety by placing a larger group there or by extension of the aliphatic chain length can increase the clash more with Sirt6 Trp71, and decrease the effect against Sirt6. Conversely, rigidification of the aliphatic chain length and the conformation of the phenyl moiety might optimize the potency of compound for Sirt6 and abolish the effect for Class I/II HDACs.

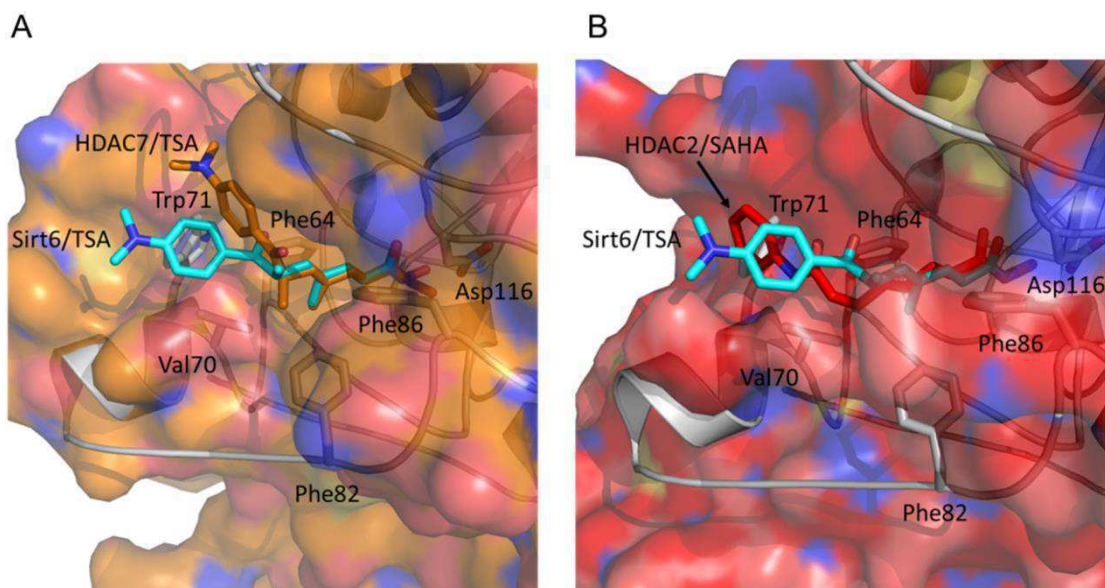


Figure 18: Structural comparisons among different class HDACs. A) Compare the binding mode of TSA by placing the human HDAC7/TSA complex (PDB ID 3C10; protein displayed as surface, gold ligand) on the top of the Sirt6/TSA complex (gray cartoon, cyan ligand, side chains involved in TSA interactions are displayed in gray sticks). B) Compare the binding mode of TSA and SAHA by placing the human HDAC2/SAHA complex (PDB ID 4LXZ; protein displayed as surface, red ligand) on the top of the Sirt6/TSA complex (gray cartoon, cyan ligand, side chains involved in TSA interactions are displayed in gray sticks).

3.4 Identification of a subdomain of Sirt7 for crystallization.

Sirt7 contains 400 amino acids and sequence alignments of Sirtuins reveal that its potential catalytic domain comprises residues 90-331. Both the N-terminal and C-terminal regions flanking the catalytic domain are identified to be low-complexity sequences. At the beginning, recombinant human Sirt7 constructs (residues 1-400, 59-356 and 81-356) were expressed using either the pOPIN-MBP vector system (encodes a cleavable N-terminal MBP tag) in E.coli BL21 (DE3) codon plus (residues 1-400) or using the pET-19b vector system (encodes an N-terminal his-tag) in E. coli C43 (DE3) Prep4 (residues 59-356 and 81-356). The recombinant proteins were expressed in an auto-induction system at 16°C for overnight. The purification was first performed by using Immobilized-metal affinity chromatography (IMAC), and the protein of interest was further purified by using cation exchange chromatography on a HiTrap SP-Sepharose Fast Flow column (GE Healthcare), followed by gel filtration using a Superdex 200 column (GE Healthcare). The N-terminal his tag attached to the residues 59-356 and 81-356 was cleaved by Tobacco Etch Virus (TEV) protease, and was purified by reverse affinity chromatography. In contrast, the MBP tag was kept for crystallization. However, when the oligomeric state of the recombinant proteins was evaluated in Blue Native Gel, they were found to form heavy aggregates and to remain in the sample well. In order to identify an improved protein subdomain for crystallization, the method of limited proteolysis was performed. Trypsin was selected for this experiment, various protease to protein ratios, reaction times and reaction temperatures were investigated. The digest was quenched by adding SDS PAGE loading buffer, and the result was displayed in SDS-PAGE. The N-terminal sequence of the subdomain was identified by protein sequencing and the C terminal sequence was determined by Mass spectrometry. Limited proteolysis of two Sirt7 subdomains including residues 59-356 and 81-356 yielded the same fragment 134-348 (Fig. 19A, B), but the treatment of Sirt7 full length generated two different fragments 134-388 and 134-372 (Fig. 19C). Thus, new protein constructs were designed by starting with residue 100, 121 or 134 and ending with various C terminuses, such as residue 356, 372 and 388. However, the expression of new constructs only yielded inclusion bodies and the secondary structure based sequence alignment of Sirtuins indicated that a conservative α -helix is located before residue 100, which is therefore thought to play an important role in stabilizing the overall structure. Next, we plan to extend N-terminus to include the potential helix and fusion protein to assist Sirt7 crystallization, and also consider expressing protein in different expression system like insect cell and mammalian cell.

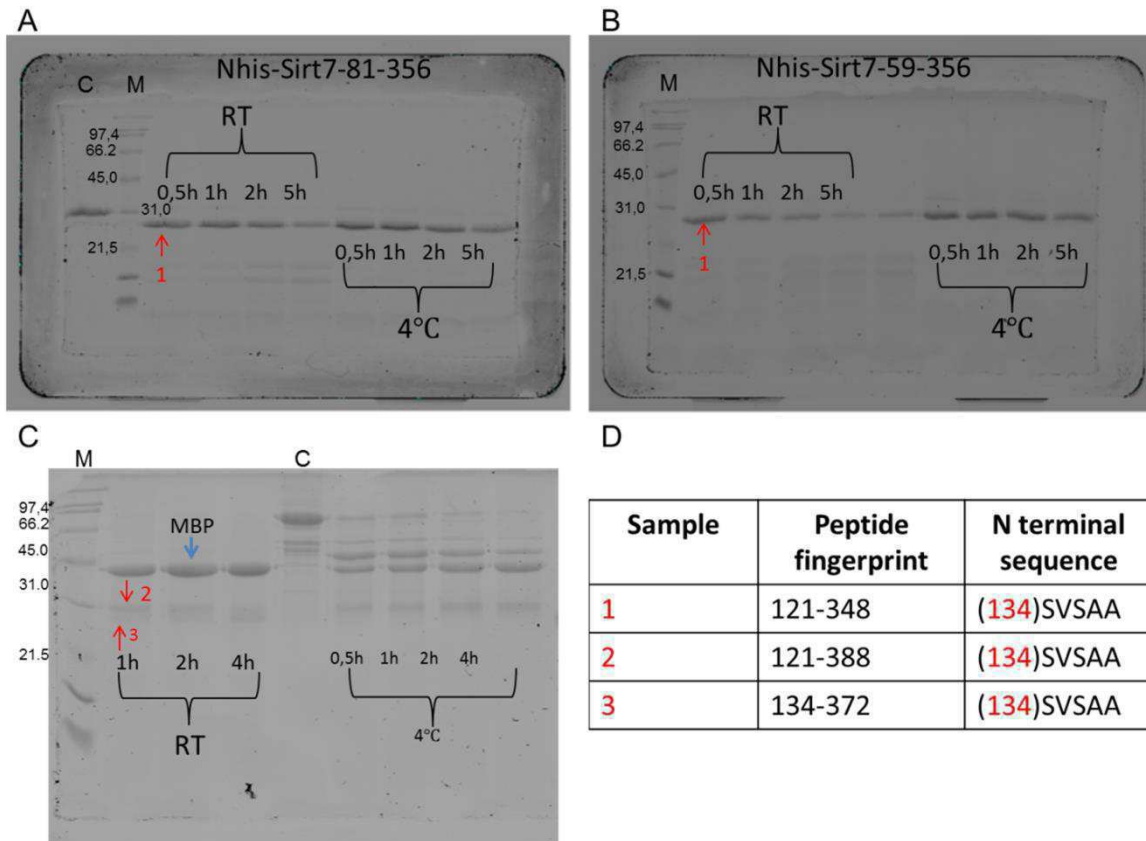


Figure 19: SDS-PAGE of limited proteolysis performed at a trypsin to Sirt7 ratio of 1:100.

A) Limited proteolysis of Sirt7 subdomain 81-356 at room temperature (RT) and 4°C with different incubation time. C indicates the sample of protein without proteolysis, and M refers to protein marker. B) Limited proteolysis of Sirt7 subdomain 59-356 at room temperature (RT) and 4°C with different incubation time. C) Limited proteolysis of full length Sirt7 at room temperature (RT) and 4°C with different incubation time. MBP refers to the Maltose-binding protein. D) Statistic of the fragment boundary analyzed by peptide mass fingerprint and protein sequencing.

4 References

1. Kirkwood, T. B. L. A systematic look at an old problem. *Nature* **451**, 644–647 (2008).
2. Blagosklonny, M. V. Aging: ROS or TOR. *Cell Cycle* **7**, 3344–3354 (2008).
3. Gems, D. & Partridge, L. Genetics of Longevity in Model Organisms: Debates and Paradigm Shifts. *Annu. Rev. Physiol.* **75**, 621–644 (2013).
4. Kenyon, C. J. The genetics of ageing. *Nature* **464**, 504–512 (2010).
5. Burtner, C. R. & Kennedy, B. K. Progeria syndromes and ageing: What is the connection? *Nat. Rev. Mol. Cell Biol.* **11**, 567–578 (2010).
6. Hoeijmakers, J. H. J. DNA Damage, Aging, and Cancer. *N. Engl. J. Med.* **361**, 1475–1485 (2009).
7. Moskalev, A. A. *et al.* The role of DNA damage and repair in aging through the prism of Koch-like criteria. *Ageing Res. Rev.* **12**, 661–684 (2013).
8. Lord, C. J. & Ashworth, A. The DNA damage response and cancer therapy. *Nature* **481**, 287–294 (2012).
9. Blackburn, E. H., Greider, C. W. & Szostak, J. W. Telomeres and telomerase: The path from maize, Tetrahymena and yeast to human cancer and aging. *Nat. Med.* **12**, 1133–1138 (2006).
10. Hayflick, L. & Moorhead, P. S. The serial cultivation of human diploid cell strains. *Exp. Cell Res.* **25**, 585–621 (1961).
11. Bodnar, A. G. *et al.* Extension of by Introduction of Telomerase Normal Human into Normal Human Cells. *Science (80-.).* **279**, 349–352 (1998).
12. Blasco, M. A. The epigenetic regulation of mammalian telomeres. *Nat. Rev. Genet.* **8**, 299–309 (2007).
13. Talens, R. P. *et al.* Epigenetic variation during the adult lifespan: Cross-sectional and longitudinal data on monozygotic twin pairs. *Ageing Cell* **11**, 694–703 (2012).
14. Powers, E. T., Morimoto, R. I., Dillin, A., Kelly, J. W. & Balch, W. E. Biological and Chemical Approaches to Diseases of Proteostasis Deficiency. *Annu. Rev. Biochem.* **78**, 959–991 (2009).
15. Colman, R. J. *et al.* Caloric restriction delays disease onset and mortality in rhesus monkeys. *Science (80-.).* **325**, 201–204 (2009).
16. Fontana, L., Partridge, L. & Longo, V. D. Extending healthy life span - From yeast to humans. *Science (80-.).* **328**, 321–326 (2010).
17. Barzilai, N., Huffman, D. M., Muzumdar, R. H. & Bartke, A. The critical role of metabolic pathways in aging. *Diabetes* **61**, 1315–1322 (2012).
18. Cornelius, C., Cuzzocrea, S., Iavicoli, I., Rizzarelli, E. & Calabrese, E. J. Hormesis, cellular stress response and vitagenes as critical determinants in aging and longevity. *Mol. Aspects Med.* **32**, 279–304 (2011).
19. Campisi, J. & D’Adda Di Fagagna, F. Cellular senescence: When bad things happen to good cells. *Nat. Rev. Mol. Cell Biol.* **8**, 729–740 (2007).
20. Collado, M., Blasco, M. A. & Serrano, M. Cellular Senescence in Cancer and Aging. *Cell* **130**, 223–233 (2007).
21. Thomas Kuilman, Chrysiis Michaloglou, Wolter J. Mooi & Daniel S. Peeper. The essence of senescence. *Genes Dev.* **24**, 2463–2479 (2010).
22. Shaw, A. C., Joshi, S., Greenwood, H., Panda, A. & Lord, J. M. Aging of the innate immune system. *Curr. Opin. Immunol.* **22**, 507–513 (2010).
23. Laplante, M. & Sabatini, D. M. mTOR Signaling in Growth Control and Disease. *Cell* **149**, 274–293 (2012).
24. Rando, T. A. & Chang, H. Y. Aging, rejuvenation, and epigenetic reprogramming: Resetting the aging clock. *Cell* **148**, 46–57 (2012).
25. López-Otín, C., Blasco, M. A., Partridge, L., Serrano, M. & Kroemer, G. The hallmarks of aging. *Cell* **153**, (2013).
26. McCay, C. M., Crowell, M. F. & Maynard, L. A. The Effect of Retarded Growth Upon the Length of Life Span and Upon the Ultimate Body SizeOne Figure. *J. Nutr.* **10**, 63–79 (1935).
27. Lin, S. J., Defossez, P. A. & Guarente, L. Requirement of NAD and *SIR2* for life-span extension by calorie restriction in *Saccharomyces cerevisiae*. *Science* **289**, 2126–2128 (2000).

28. Guarente, L. Calorie restriction and sirtuins revisited. *Genes Dev.* **27**, 2072–2085 (2013).
29. Houtkooper, R. H. & Auwerx, J. Exploring the therapeutic space around NAD⁺. *J. Cell Biol.* **199**, 205–209 (2012).
30. Chen, D., Steele, A. D., Lindquist, S. & Guarente, L. Medicine: Increase in activity during calorie restriction requires Sirt1. *Science (80-.)*. **310**, 1641 (2005).
31. Verdin, E., Hirschey, M. D., Finley, L. W. S. & Haigis, M. C. Sirtuin regulation of mitochondria: Energy production, apoptosis, and signaling. *Trends Biochem. Sci.* **35**, 669–675 (2010).
32. Konrad T. Howitz *et al.* Small molecule activators of sirtuins extend *Saccharomyces cerevisiae* lifespan. *Nature* **425**, 191–196 (2003).
33. Milne, J. C. *et al.* Small molecule activators of SIRT1 as therapeutics for the treatment of type 2 diabetes. *Nature* **450**, 712–716 (2007).
34. Dai, H. *et al.* SIRT1 activation by small molecules: Kinetic and biophysical evidence for direct interaction of enzyme and activator. *J. Biol. Chem.* **285**, 32695–32703 (2010).
35. Hubbard, B. P. & Sinclair, D. A. Small molecule SIRT1 activators for the treatment of aging and age-related diseases. *Trends Pharmacol. Sci.* **35**, 146–154 (2014).
36. Mercken, E. M. *et al.* SRT2104 extends survival of male mice on a standard diet and preserves bone and muscle mass. *Aging Cell* **13**, 787–796 (2014).
37. Bonkowski, M. S. & Sinclair, D. A. Slowing ageing by design: The rise of NAD⁺ and sirtuin-activating compounds. *Nat. Rev. Mol. Cell Biol.* **17**, 679–690 (2016).
38. Kennedy, B. K. *et al.* Redistribution of silencing proteins from telomeres to the nucleolus is associated with extension of life span in *S. cerevisiae*. *Cell* **89**, 381–391 (1997).
39. Braunstein, M., Sobel, R. E., Allis, C. D., Turner, B. M. & Broach, J. R. Efficient transcriptional silencing in *Saccharomyces cerevisiae* requires a heterochromatin histone acetylation pattern. *Mol. Cell. Biol.* **16**, 4349–56 (1996).
40. Rusche, L. N., Kirchmaier, A. L. & Rine, J. The Establishment, Inheritance, and Function of Silenced Chromatin in *Saccharomyces cerevisiae*. *Annu. Rev. Biochem.* **72**, 481–516 (2003).
41. Hecht, A. T., Laroche, T., Strahl-Bolsinger, S., Gasser, S. M. & Grunstein, M. Histone H3 and H4 N termini interact with SIR3 and SIR4 proteins: A molecular model for the formation of heterochromatin in yeast. **80**, 583–592 (1995).
42. Imai, S., Armstrong, C. M., Kaeberlein, M. & Guarente, L. Transcriptional silencing and longevity protein Sir2 is an NAD⁺-dependent histone deacetylase. *Nature* **403**, 795–800 (2000).
43. Sauve, A. A., Wolberger, C., Schramm, V. L. & Boeke, J. D. The Biochemistry of Sirtuins. *Annu. Rev. Biochem.* **75**, 435–465 (2006).
44. Frye, R. A. Phylogenetic classification of prokaryotic and eukaryotic Sir2-like proteins. *Biochem. Biophys. Res. Commun.* **273**, 793–798 (2000).
45. Nakagawa, T. & Guarente, L. SnapShot: Sirtuins, NAD, and aging. *Cell Metab.* **20**, 192–192.e1 (2014).
46. Haigis, M. C. & Sinclair, D. A. Mammalian Sirtuins: Biological Insights and Disease Relevance. *Annual review of pathology* **5**, 253–295 (2010).
47. Michishita, E., Park, J. Y., Burneskis, J. M., Barrett, J. C. & Horikawa, I. Evolutionarily Conserved and Nonconserved Cellular Localizations and Functions of Human SIRT Proteins. *Molecular Biology of the Cell* **16**, 4623–4635 (2005).
48. MICHAN, S. & SINCLAIR, D. Sirtuins in mammals: insights into their biological function. *The Biochemical journal* **404**, 1–13 (2007).
49. North, B. J., Marshall, B. L., Borra, M. T., Denu, J. M. & Verdin, E. The Human Sir2 Ortholog, SIRT2, Is an NAD⁺-Dependent Tubulin Deacetylase. *Mol. Cell* **11**, 437–444 (2003).
50. Black, J. C., Mosley, A., Kitada, T., Washburn, M. & Carey, M. The SIRT2 Deacetylase Regulates Autoacetylation of p300. *Molecular cell* **32**, 449–455 (2008).
51. Morris, B. J. Seven sirtuins for seven deadly diseases of aging. *Free Radic. Biol. Med.* **56**, 133–171 (2013).
52. Du, J. *et al.* Sirt5 is a NAD-dependent protein lysine demalonylase and desuccinylase. *Science (80-.)*. **334**, 806–809 (2011).
53. Roessler, C. *et al.* Chemical probing of the human sirtuin 5 active site reveals its substrate acyl

- specificity and peptide-based inhibitors. *Angew. Chemie - Int. Ed.* **53**, 10728–10732 (2014).
54. Hirschev, M. D. & Zhao, Y. Metabolic Regulation by Lysine Malonylation, Succinylation, and Glutarylation. *Molecular & Cellular Proteomics : MCP* **14**, 2308–2315 (2015).
 55. Jiang, H. *et al.* SIRT6 regulates TNF- α secretion through hydrolysis of long-chain fatty acyl lysine. *Nature* **496**, 110–3 (2013).
 56. Michishita, E. *et al.* SIRT6 is a histone H3 lysine 9 deacetylase that modulates telomeric chromatin. *Nature* **452**, 492–496 (2008).
 57. Michishita, E. *et al.* Cell cycle-dependent deacetylation of telomeric histone H3 lysine K56 by human SIRT6. *Cell cycle (Georgetown, Tex.)* **8**, 2664–2666 (2009).
 58. Liszt, G., Ford, E., Kurtev, M. & Guarente, L. Mouse Sir2 homolog SIRT6 is a nuclear ADP-ribosyltransferase. *J. Biol. Chem.* **280**, 21313–21320 (2005).
 59. Mostoslavsky, R. *et al.* Genomic instability and aging-like phenotype in the absence of mammalian SIRT6. *Cell* **124**, 315–329 (2006).
 60. Haigis, M. C. *et al.* SIRT4 Inhibits Glutamate Dehydrogenase and Opposes the Effects of Calorie Restriction in Pancreatic β Cells. *Cell* **126**, 941–954 (2006).
 61. Pannek, M. *et al.* Crystal structures of the mitochondrial deacylase Sirtuin 4 reveal isoform-specific acyl recognition and regulation features. *Nat. Commun.* **8**, (2017).
 62. Chalkiadaki, A. & Guarente, L. Sirtuins mediate mammalian metabolic responses to nutrient availability. *Nat. Rev. Endocrinol.* **8**, 287 (2012).
 63. Rodgers, J. T. *et al.* Nutrient control of glucose homeostasis through a complex of PGC-1 α and SIRT1. *Nature* **434**, 113 (2005).
 64. Eriko Michishita, Jean Y. Park, Jenna M. Burneskis, J. Carl Barrett & Horikawa, I. Evolutionarily Conserved and Nonconserved Cellular Localizations and Functions of Human SIRT Proteins. *Mol. Biol. Cell* **16**, 4623–4635 (2005).
 65. Lombard, D. B., Schwer, B., Alt, F. W. & Mostoslavsky, R. SIRT6 IN DNA REPAIR, METABOLISM, AND AGEING. *Journal of internal medicine* **263**, 128–141 (2008).
 66. Mostoslavsky, R. DNA repair, insulin signaling and sirtuins: at the crossroads between cancer and aging. *Front. Biosci.* **13**, 6966–6990 (2008).
 67. Zhong, L. *et al.* The Histone Deacetylase Sirt6 Regulates Glucose Homeostasis via Hif1 α . *Cell* **140**, 280–293 (2010).
 68. McCord, R. A. *et al.* SIRT6 stabilizes DNA-dependent Protein Kinase at chromatin for DNA double-strand break repair. *Aging (Albany NY)* **1**, 109–121 (2009).
 69. Kugel, S. & Mostoslavsky, R. Chromatin and beyond: The multitasking roles for SIRT6. *Trends Biochem. Sci.* **39**, 72–81 (2014).
 70. Li, Q., Withoff, S. & Verma, I. M. Inflammation-associated cancer: NF- κ B is the lynchpin. *Trends Immunol.* **26**, 318–325 (2005).
 71. Kawahara, T. L. A. *et al.* SIRT6 links histone H3 lysine 9 deacetylation to control of NF- κ B dependent gene expression and organismal lifespan. *Cell* **136**, 62–74 (2009).
 72. Denko, N. C. Hypoxia, HIF1 and glucose metabolism in the solid tumour. *Nat. Rev. Cancer* **8**, 705–713 (2008).
 73. Matt Kaerberlein & Kapahi, P. The Hypoxic Response and Aging. *Cell Cycle* **8**, 2324 (2009).
 74. Dominy, J. E. *et al.* The Deacetylase Sirt6 Activates the Acetyltransferase GCN5 and Suppresses Hepatic Gluconeogenesis. *Molecular cell* **48**, 900–913 (2012).
 75. Kanfi, Y. *et al.* The sirtuin SIRT6 regulates lifespan in male mice. *Nature* **483**, 218–221 (2012).
 76. Ford, E. *et al.* Mammalian Sir2 homolog SIRT7 is an activator of RNA polymerase I transcription. *Genes & Development* **20**, 1075–1080 (2006).
 77. Chen, S. *et al.* Repression of RNA Polymerase I upon Stress Is Caused by Inhibition of RNA-Dependent Deacetylation of PAF53 by SIRT7. *Mol. Cell* **52**, 303–313 (2013).
 78. Grob, A. *et al.* Involvement of SIRT7 in resumption of rDNA transcription at the exit from mitosis. *Journal of Cell Science* **122**, 489–498 (2009).
 79. Chen, S. *et al.* SIRT7-dependent deacetylation of the U3-55k protein controls pre-rRNA processing. *Nat. Commun.* **7**, 10734 (2016).
 80. Barber, M. F. *et al.* SIRT7 links H3K18 deacetylation to maintenance of oncogenic

- transformation. *Nature* **487**, 114–118 (2012).
81. Ryu, D. *et al.* A SIRT7-dependent acetylation switch of GABP β 1 controls mitochondrial function. *Cell Metab.* **20**, 856–869 (2014).
 82. Shin, J. *et al.* SIRT7 Represses Myc Activity to Suppress ER Stress and Prevent Fatty Liver Disease. *Cell reports* **5**, 654–665 (2013).
 83. Moniot, S., Weyand, M. & Steegborn, C. Structures, substrates, and regulators of mammalian sirtuins – opportunities and challenges for drug development. *Frontiers in Pharmacology* **3**, 16 (2012).
 84. Gertz, M. & Steegborn, C. Using mitochondrial sirtuins as drug targets: disease implications and available compounds. *Cell. Mol. Life Sci.* **73**, 2871–2896 (2016).
 85. Feldman, J. L., Dittenhafer-Reed, K. E. & Denu, J. M. Sirtuin catalysis and regulation. *J. Biol. Chem.* **287**, 42419–42427 (2012).
 86. Min, J., Landry, J., Sternglanz, R. & Xu, R. M. Crystal structure of a SIR2 homolog-NAD complex. *Cell* **105**, 269–279 (2001).
 87. Moniot, S., Schutkowski, M. & Steegborn, C. Crystal structure analysis of human Sirt2 and its ADP-ribose complex. *J. Struct. Biol.* **182**, 136–143 (2013).
 88. Feldman, J. L., Baeza, J. & Denu, J. M. Activation of the protein deacetylase SIRT6 by long-chain fatty acids and widespread deacetylation by mammalian sirtuins. *J. Biol. Chem.* **288**, 31350–31356 (2013).
 89. Feldman, J. L. *et al.* Kinetic and Structural Basis for Acyl-Group Selectivity and NAD⁺ Dependence in Sirtuin-Catalyzed Deacetylation. *Biochemistry* **54**, 3037–3050 (2015).
 90. Gai, W., Li, H., Jiang, H., Long, Y. & Liu, D. Crystal structures of SIRT3 reveal that the α 2- α 3 loop and α 3-helix affect the interaction with long-chain acyl lysine. *FEBS Lett.* **590**, 3019–3028 (2016).
 91. Schutkowski, M., Fischer, F., Roessler, C. & Steegborn, C. New assays and approaches for discovery and design of sirtuin modulators. *Expert Opin. Drug Discov.* **9**, 183–199 (2014).
 92. Yu, J., Haldar, M., Mallik, S. & Srivastava, D. K. Role of the substrate specificity-defining residues of human SIRT5 in modulating the structural stability and inhibitory features of the enzyme. *PLoS One* **11**, 1–26 (2016).
 93. Basil P. Hubbard *et al.* Evidence for a Common Mechanism of SIRT1 Regulation by Allosteric Activators. *Science (80-.)*. **339**, 1216–1219 (2013).
 94. Dai, H. *et al.* Crystallographic structure of a small molecule SIRT1 activator-enzyme complex. *Nat. Commun.* **6**, 7645 (2015).
 95. Pirola, L. & Fröjdö, S. Resveratrol: One molecule, many targets. *IUBMB Life* **60**, 323–332 (2008).
 96. Mai, A. *et al.* Study of 1,4-dihydropyridine structural scaffold: Discovery of novel sirtuin activators and inhibitors. *J. Med. Chem.* **52**, 5496–5504 (2009).
 97. Pillai, V. B. *et al.* Honokiol blocks and reverses cardiac hypertrophy in mice by activating mitochondrial Sirt3. *Nat. Commun.* **6**, 1–16 (2015).
 98. Cen, Y. Sirtuins inhibitors: The approach to affinity and selectivity. *Biochim. Biophys. Acta - Proteins Proteomics* **1804**, 1635–1644 (2010).
 99. Napper, A. D. *et al.* Discovery of indoles as potent and selective inhibitors of the deacetylase SIRT1. *J. Med. Chem.* **48**, 8045–8054 (2005).
 100. Gertz, M. *et al.* Ex-527 inhibits sirtuins by exploiting their unique NAD⁺-dependent deacetylation mechanism. *Proc. Natl. Acad. Sci.* **110**, E2772–E2781 (2013).
 101. Disch, J. S. *et al.* Discovery of thieno[3,2-d]pyrimidine-6-carboxamides as potent inhibitors of SIRT1, SIRT2, and SIRT3. *J. Med. Chem.* **56**, 3666–3679 (2013).
 102. Nguyen, G. T. T., Gertz, M. & Steegborn, C. Crystal structures of SIRT3 complexes with 4'-bromo-resveratrol reveal binding sites and inhibition mechanism. *Chem. Biol.* **20**, 1375–1385 (2013).
 103. Li, L. *et al.* SIRT7 is a histone desuccinylase that functionally links to chromatin compaction and genome stability. *Nat. Commun.* **7**, 1–17 (2016).
 104. Kiviranta, P. H. *et al.* N ϵ -Thioacetyl-Lysine-Containing Tri-, Tetra-, and Pentapeptides as SIRT1

- and SIRT2 Inhibitors. *J. Med. Chem.* **52**, 2153–2156 (2009).
105. He, B., Du, J. & Lin, H. Thiosuccinyl peptides as Sirt5-specific inhibitors. *J. Am. Chem. Soc.* **134**, 1922–1925 (2012).
106. Rajabi, N. *et al.* Mechanism-Based Inhibitors of the Human Sirtuin 5 Deacylase: Structure-Activity Relationship, Biostructural, and Kinetic Insight. *Angew. Chem. Int. Ed. Engl.* **56**, 14836–14841 (2017).
107. Parenti, M. D. *et al.* Discovery of novel and selective SIRT6 inhibitors. *J. Med. Chem.* **57**, 4796–4804 (2014).
108. Sociali, G. *et al.* Quinazolinedione SIRT6 inhibitors sensitize cancer cells to chemotherapeutics. *Eur. J. Med. Chem.* **102**, 530–539 (2015).
109. Y. Cen, D. Y. Youn & Sauve, A. A. Advances in characterization of human sirtuin isoforms: chemistries, targets and therapeutic applications. *Curr. Med. Chem.* **18**, 1919–1935 (2011).
110. Damonte, P. *et al.* SIRT6 inhibitors with salicylate-like structure show immunosuppressive and chemosensitizing effects. *Bioorg. Med. Chem.* **25**, 5849–5858 (2017).
111. Rahnasto-Rilla, M. *et al.* Natural polyphenols as sirtuin 6 modulators. *Sci. Rep.* **8**, 4163 (2018).
112. Shin, E. S. *et al.* Catechin gallates are NADP⁺-competitive inhibitors of glucose-6-phosphate dehydrogenase and other enzymes that employ NADP⁺ as a coenzyme. *Bioorganic Med. Chem.* **16**, 3580–3586 (2008).
113. Roche, J. & Bertrand, P. Inside HDACs with more selective HDAC inhibitors. *Eur. J. Med. Chem.* **121**, 451–483 (2016).
114. Vigushin, D. M. *et al.* Trichostatin A is a histone deacetylase inhibitor with potent antitumor activity against breast cancer in vivo. *Clin. Cancer Res.* **7**, 971–976 (2001).
115. Mann, B. S., Johnson, J. R., Cohen, M. H., Justice, R. & Pazdur, R. FDA Approval Summary: Vorinostat for Treatment of Advanced Primary Cutaneous T-Cell Lymphoma. *Oncologist* **12**, 1247–1252 (2007).
116. Wood, M., Rymarchyk, S., Zheng, S. & Cen, Y. Trichostatin A inhibits deacetylation of histone H3 and p53 by SIRT6. *Arch. Biochem. Biophys.* **638**, 8–17 (2018).
117. Schlicker, C., Boanca, G., Lakshminarasimhan, M. & Steegborn, C. Structure-based development of novel sirtuin inhibitors. *Aging (Albany NY)* **3**, 852–872 (2011).
118. Piia Kokkonen *et al.* Studying SIRT6 regulation using H3K56 based substrate and small molecules. *Eur J Pharm Sci* **63**, 71–76 (2014).
119. Smith, B. C., Hallows, W. C. & Denu, J. M. A continuous microplate assay for sirtuins and nicotinamide-producing enzymes. *Anal. Biochem.* **394**, 101–109 (2009).

5 List of publications

5.1 Publication 1

Structural basis of sirtuin 6 activation by synthetic small molecules

Weijie You, Dante Rotili, Tie-Mei Li, Christian Kambach, Marat Meleshin, Mike Schutkowski, Katrin F. Chua, Antonello Mai, and Clemens Steegborn. *Angew. Chemie - Int. Ed.* 2017, 56, 1007–1011.

Author Contributions

Dante Rotili and Antonello Mai synthesized the compounds; Clemens Steegborn and I solved the crystal structures; Christian Kambach, Tie-Mei Li and I performed binding and activity experiments, and we analyzed data supported by Katrin F. Chua, Antonello Mai, Dante Rotili, and Clemens Steegborn; Marat Meleshin and Mike Schutkowski synthesized peptides; all authors contributed to the manuscript, which was initially drafted by Clemens Steegborn.



Structural Basis of Sirtuin 6 Activation by Synthetic Small Molecules

Weijie You, Dante Rotili, Tie-Mei Li, Christian Kambach, Marat Meleshin, Mike Schutkowski, Katrin F. Chua, Antonello Mai,* and Clemens Steegborn*

Abstract: Sirtuins are protein deacylases regulating metabolism and stress responses, and are implicated in aging-related diseases. Small molecule activators for the human sirtuins Sirt1–7 are sought as chemical tools and potential therapeutics, such as for cancer. Activators are available for Sirt1 and exploit its unique N-terminus, whereas drug-like activators for Sirt2–7 are lacking. We synthesized and screened pyrrolo[1,2-*a*]quinoxaline derivatives, yielding the first synthetic Sirt6 activators. Biochemical assays show direct, substrate-independent compound binding to the Sirt6 catalytic core and potent activation of Sirt6-dependent deacetylation of peptide substrates and complete nucleosomes. Crystal structures of Sirt6/activator complexes reveal that the compounds bind to a Sirt6-specific acyl channel pocket and identify key interactions. Our results establish potent Sirt6 activation with small molecules and provide a structural basis for further development of Sirt6 activators as tools and therapeutics.

Sirtuins are NAD⁺-dependent protein lysine deacylases regulating processes such as energy metabolism and stress responses.^[1] They have been implicated in aging and life-span extending effects of caloric restriction (CR).^[1,2] Few potent sirtuin inhibitors are available, but it is the activation of sirtuins that can simulate CR effects and is considered attractive for the treatment of several aging-related diseases.^[2,3] Of the seven mammalian sirtuin isoforms (Sirt1–7),

Sirt1–3 feature strong deacetylase activities, while Sirt5 acts primarily as a desuccinylase.^[4] Sirt6 has much higher demyristoylation than deacetylation activity on peptide substrates,^[5] but catalyzes robust histone deacetylation on complete nucleosomes and chromatin.^[6] Sirtuins bind substrates between a Rossmann-fold and a Zn²⁺-binding subdomain of their conserved catalytic core, burying the substrate acyl group in a channel with isoform-specific features.^[3a,4,5] During catalysis, the acyl oxygen forms an alkylimidate with ADP-ribose produced from the co-substrate NAD⁺.^[3a] After rearrangement in a bicyclic intermediate, it is hydrolyzed to yield deacetylated polypeptide and 2'-*O*-acyl-ADP-ribose. The sirtuin catalytic core is flanked by isoform-specific extensions contributing to regulation and localization.^[3a] Sirtuins show protective effects against disorders such as cardiovascular diseases (Sirt1 and Sirt3) and neurodegeneration (Sirt1).^[1,3a] Sirt6 contributes to metabolic adaptations and DNA homeostasis, and it extends life-span in male mice and suppresses aging phenotypes and cancer growth, for example, in the pancreas.^[7] Pharmacological Sirt6 activation is thus considered a treatment for cancer and other aging-related conditions. Small molecule activation was first described for Sirt1.^[2] Although initially debated, it is now well documented and potent, drug-like Sirt1 activators are available.^[2,8] A large set of Sirt1 activators binds to a Sirt1-specific N-terminal domain, which is assumed to induce a closure of the substrate-containing active site and possibly a direct activator/substrate interaction.^[3a,8b,9] Few activating small molecule effects have been described for the other sirtuin isoforms, all of which lack the Sirt1 N-terminal domain. Sirt5 activation by resveratrol was observed with the artificial substrate “Fluor-de-Lys” (FdL), whose fluorophore mediates strong activator interactions and might mimic part of the Sirt1 mechanism, and with an acetylated protein, but not with its favored succinyl substrate.^[9] Weak and possibly non-specific activating effects were also reported for the plant metabolite honokiol (Sirt3) and fatty acids (Sirt6).^[3a,10] The fatty acid effect appeared to involve the acyl binding channel, but a structural characterization and the development of more potent and drug-like compounds had to be awaited. Herein, we report the discovery of pharmacological Sirt6 activators. The pyrrolo-[1,2-*a*]quinoxaline-based compounds increase Sirt6-dependent deacetylation of peptides and nucleosomes, and crystal structures of Sirt6/activator complexes reveal their binding site and provide a structural basis for drug development.

In an effort to identify scaffolds for isoform-specific sirtuin inhibition, we recognized a weak, apparently stimulatory effect of the 4-(pyridin-3-yl)-5-((3-(trifluoromethyl)phenyl)sulfonyl)-4,5-dihydropyrrolo[1,2-*a*]quinoxaline UBCS038/CSC38 (**1**; Figure 1a) on Sirt6 using FdL assays.^[11] To clarify whether the compound indeed activates Sirt6, we

[*] W. You, Dr. C. Kambach, Prof. Dr. C. Steegborn
Universität Bayreuth
Lehrstuhl Biochemie und Forschungszentrum für Biomakromoleküle
Universitätsstr. 30, 95447 Bayreuth (Germany)
E-mail: clemens.steegborn@uni-bayreuth.de

Dr. D. Rotili, Prof. Dr. A. Mai
Sapienza University Roma
Department of Drug Chemistry and Technologies and
Pasteur Institute of the Cenci–Bolognetti Foundation
P. le A. Moro 5, 00185 Rome (Italy)
E-mail: antonello.mai@uniroma1.it

Dr. T.-M. Li, Prof. Dr. K. F. Chua
Department of Medicine
Stanford University School of Medicine
300 Pasteur Drive Grant Bldg., Rm. S-025, Stanford, CA 94305 (USA)
and
Geriatric Research, Education, and Clinical Center
Department of Veterans Affairs Palo Alto Health Care System
Palo Alto, CA 94304 (USA)

Dr. M. Meleshin, Prof. Dr. M. Schutkowski
Abteilung Enzymologie
Institut für Biochemie und Biotechnologie
Martin-Luther-Universität
Kurt-Mothes-Str. 3, 06110 Halle (Saale) (Germany)

Supporting information for this article can be found under:
<http://dx.doi.org/10.1002/anie.201610082>.

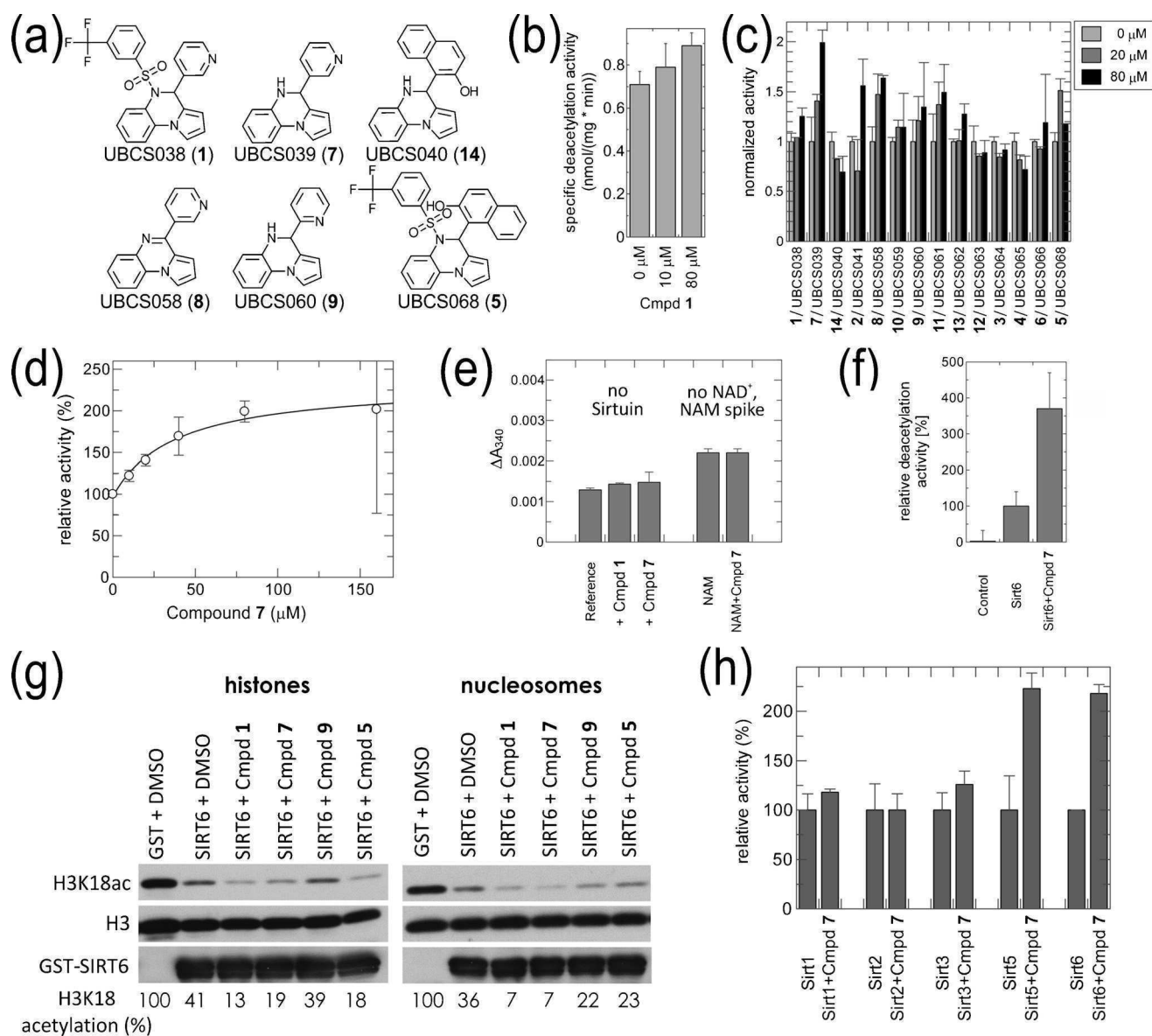


Figure 1. Pharmacological Sirt6 activation. a) Chemical structures of **1** and selected derivatives (complete set: Figure S1). b) Activation of Sirt6-dependent peptide deacetylation by **1**. c) A panel of **1** derivatives tested at 20 and 80 μM for effects on Sirt6 deacetylase activity. d) **7** titration showing concentration-dependent Sirt6 activation. e) Control reactions without sirtuin, in the absence and presence of 100 μM activator (**7**) and without co-substrate NAD⁺ but spiked with 100 μM NAM (substrate for downstream enzymes), in the absence and presence of 100 μM activator. f) Effect of **7** on Sirt6-dependent peptide deacetylation analyzed in a mass spectrometry-based assay. g) Western blot analysis of compound effects, at 100 μM, on the Sirt6-dependent deacetylation of H3K18 in a histone protein preparation (left) and HeLa nucleosomes (right). h) Selectivity of **7** (100 μM) among human sirtuin isoforms Sirt1, 2, 3, 5, and 6. Sirt5 was tested with succinylated substrate, all other isoforms with acetylated peptides.

first tested it in a coupled enzymatic assay (detecting the sirtuin product NAM^[12]) with an acetylated histone H3K9 peptide substrate. Adding 10 or 80 μM **1** caused weak activation at the higher concentration (Figure 1 b). To identify more potent compounds, we generated a panel of **1** derivatives **2–14** (Figure 1 a; Supporting Information, Figure S1 and Methods). Testing their effects on Sirt6-dependent H3K9 peptide deacetylation yielded activation for several compounds, with the highest activation for 4-(pyridin-3-yl)-4,5-dihydropyrrolo[1,2-*a*]quinoxaline (**7**; UBSC039; Figure 1 c). Titration with **7** yielded a dose-dependent increase in Sirt6

activity, with a maximum ≈ 2-fold stimulation and an EC₅₀ of 38 ± 13 μM (Figure 1 d). No effects were observed in control reactions without sirtuin, or without the sirtuin co-substrate NAD⁺ but spiked with NAM (Figure 1 e), showing that the activation effect is Sirt6-dependent. To further exclude assay artifacts, we also tested the compound in a mass spectrometry-based deacetylation assay. Sirt6 showed the expected weak deacetylation activity against the H3K9 peptide, and an ≈ 3.5-fold increase of this activity in the presence of 100 μM **7** (Figure 1 f). These results confirm that our pyrrolo[1,2-*a*]quinoxaline derivatives enable direct Sirt6 activation.

We next analyzed the effects of our compounds on the Sirt6-dependent deacetylation of physiological substrates, namely full-length histone proteins and complete HeLa nucleosomes. **1** and **7** showed robust activating effects on Sirt6-dependent H3K18ac deacetylation of both substrates (Figure 1g). No effect or weak stimulation was observed with **9**, while **5** also activated Sirt6 but had slightly weaker and more variable effects than **1** and **7** (Figure 1g), likely owing to its lower solubility in aqueous buffers. However, we can conclude that the pyrrolo[1,2-*a*]quinoxalines activate Sirt6-dependent deacetylation of peptides and physiological protein substrates. We then tested whether **7**-dependent activation is Sirt6-specific. The compound showed no statistically significant effects on basal Sirt1, 2, and 3 deacetylation activities (Figure 1h). For Sirt5, however, **7** caused a ≈ 2 -fold increase in its desuccinylation activity. Compound **7** thus shows specificity for Sirt6 among the deacetylase isoforms, but can also stimulate the physiologically dominant Sirt5 activity.

We next studied the Sirt6 activator-binding site and mechanism. Microscale thermophoresis binding experiments revealed an affinity of $44 \pm 12 \mu\text{M}$ for **7** to apo-Sirt6 (Figure 2a), comparable to its EC_{50} in activity assays. The Sirt6 affinity of **7** was not influenced substantially by the presence of either 2 mM acetyl substrate peptide ($K_{\text{d}}[\mathbf{7}] = 26 \pm 3 \mu\text{M}$) or 1 mM ADP-ribose ($K_{\text{d}}[\mathbf{7}] = 38 \pm 16 \mu\text{M}$), a moiety of the co-substrate NAD^+ (Figure 2a), indicating that activator binding is independent of these ligands. Consistent with their less potent activation, **8** and **5** bound with lower affinities to Sirt6/acetyl-H3K9 ($236 \pm 49 \mu\text{M}$ and $467 \pm 135 \mu\text{M}$, respectively), and the compound **9** that only weakly activates Sirt6 showed further decreased affinity ($K_{\text{d}} \approx 740 \pm 391 \mu\text{M}$; Figure 2b). Analyzing Sirt6 activity in substrate titrations in the absence and presence of the strongest binder, **7**, suggested an increase in turnover but allowed no definitive conclusions on K_{M} and v_{max} effects due to limited compound solubility and the low in vitro Sirt6 deacetylation activity (Figure S2a).

The substrates and activator appear to bind independently, and we therefore attempted to solve Sirt6/activator complex structures through co-crystallization and soaking experiments in different combinations with peptide and ADP-ribose. In this way, ternary Sirt6 complexes with ADP-ribose and **1**, **7**, **14**, or **8** could be solved at 1.87–2.10 Å resolution (Table S1). All of the compounds occupied the same Sirt6 catalytic core pocket, and the complex with **7** is described in detail as a representative example. Sirt6/ADP-ribose/**7** was solved at 1.87 Å resolution, featured well-defined electron density for the activator, and was refined to $R_{\text{cryst}}/R_{\text{free}}$ values of 19.0/22.0% (Figures 2c,d and S2b; Table S1). Compound **7** occupies a rather hydrophobic cone at an active site exit, exposing the bottom of the pyrrolo[1,2-*a*]quinoxaline to solvent (Figure 2c–e). The tricyclic system is located between Phe82/86, Ile185, Trp71, and Met136/157, possibly forming a methionine–aromatic ring interaction with Met136 (Figures 2e and S2c). Comparison with the additional modulator complexes (Figure 2f) shows that they share the hydrophobic pyrrolo[1,2-*a*]quinoxaline/cone interaction, albeit with variations in the compound plane orientation within this hydrophobic aperture owing to their differing

substitutions at the N5 (N-group) and C4 (C-group) positions. These variations indicate an only moderate interaction through the tricyclic system, consistent with the limited interaction surface complementarity and the fact that the quinoxaline ring can be either saturated (**1**, **7**) or unsaturated (**8**), and it suggests an important contribution from the substituents. Strikingly, the different binding orientations position the identical 3-pyridyl C-groups of **1**, **7**, and **8** almost identically in a binding pocket inside the catalytic core (Figure 2f). The hydrophobic “C-group pocket” is formed by Ile61, Pro62, Phe64/82/86, Val70, and Val115 (Figures 2d,e and S2c), and the pyridine nitrogen is in a position for a polar contact and potential H-bond (in the case of a protonated pyridine) to the backbone oxygen of Pro62. This similarity suggests that the pyridine C-group serves as a major anchoring point, and relevance for its interaction with Pro62 is indicated by the fact that **9**, in which the pyridine nitrogen is shifted from the *meta* to *ortho* position, shows much lower Sirt6 affinity and activation (Figures 1c, 2b). A dominant binding contribution from the C-group is also indicated by the Sirt6 complex with **1**, which features an N-group in addition. This 3-(trifluoromethyl)-phenylsulfonyl moiety is oriented toward the protein surface and packed on a patch comprising Trp71/188, Lys15, and Val70. This interaction, concomitant with the conserved C-group interaction, is enabled through a small shift and an $\approx 60^\circ$ rotation of the pyrrolo[1,2-*a*]quinoxaline of **1** within the hydrophobic binding cone, and an N-group-induced switch of the pyridine C-group into the axial position (Figure 2g). Even the hydroxynaphthyl C-group of the inactive compound **14** is placed with its distal ring superposing with the pyridine moiety of the activators (Figure 2g). This position of the larger C-group of **14** is enabled by a substantially rotated compound orientation that places its pyrrolo[1,2-*a*]quinoxaline on the Val70/Trp71 patch that interacts with the 3-(trifluoromethyl)-phenylsulfonyl N-group of **1**. Thus, the compounds appear to bind dominantly through the Sirt6 C-group pocket, and through weaker and less specific interactions of pyrrolo[1,2-*a*]quinoxaline and N-group to the Sirt6 exit surface. The latter compound moieties thus seem amenable to major modifications for improving solubility and potency, whereas our structures suggest only smaller pyridine modifications for optimization of C-group interactions.

Comparing Sirt6/**7** with a Sirt6/myristoyl-peptide complex^[5] revealed that the activators occupy the Sirt6 channel that accommodates distal parts of longer acyl substrates (Figure 2h). As expected for competitive binding of myristoyl group and activator, Sirt6 demyristoylation activity could not be stimulated with **7** (Figure S2d), in contrast to its deacetylation activity. The compound also caused no significant inhibition of demyristoylation, but with the **7** concentrations attainable this weak binder cannot compete with the well-binding myristoyl peptide. However, when added to **7** binding assays, 100 μM myristoyl peptide weakened compound binding by at least one order of magnitude ($K_{\text{d}} > 400 \mu\text{M}$) as compared to apo-Sirt6 and the acetyl peptide complex (Figure 2a). We thus conclude that our activators and their binding site enable differential modulation of Sirt6 deacetylation and demyristoylation activities.

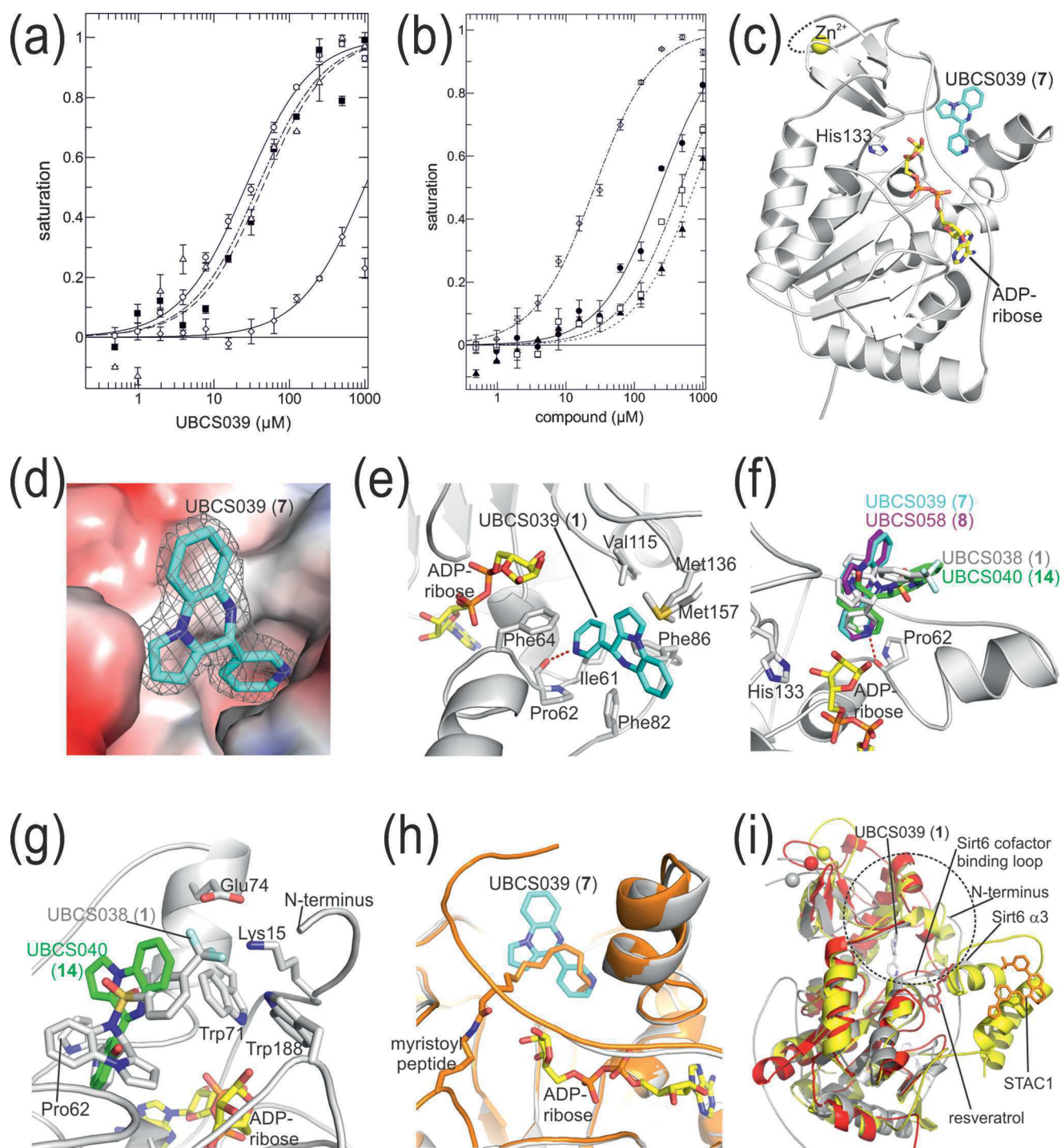


Figure 2. Structural and mechanistic characterization of Sirt6 activation. a) Binding of **7** to Sirt6 in the apo-state (■) and in the presence of acetylated H3K9 peptide (○), myristoylated TNFα peptide (◇), or ADP-ribose (△). b) Binding of Sirt6 activators in the presence of acetyl-H3K9 peptide: **7** (◇), **8** (●), **9** (▲), **5** (□). c) Overall structure of the complex between human Sirt6 (cartoon presentation), ADP-ribose (yellow sticks), and the activator **7** (cyan sticks). The conserved catalytic residue His133 indicates the active site. d) Closer view of the Sirt6 activator complex. The surface of Sirt6 is colored according to electrostatic potential, and **7** (cyan sticks) is overlaid with 2F_o-F_c density contoured at 1σ. e) Binding details for Sirt6 and **7**. Interacting residues are labeled. ADP-ribose is shown in yellow, **7** in cyan. The dashed line indicates a potential polar interaction. f) Overlay of Sirt6 complexes with **1** (gray), **7** (cyan), **14** (green), and **8** (magenta). g) Close-up of Sirt6 complexes with **1** (gray) and **14** (green), showing their interaction with the surface patch around Trp71/188. h) Overlay of the Sirt6/**7** complex (gray/cyan) with a Sirt6/myristoyl peptide complex (orange; PDB ID 3ZG6). i) Overlay of activator complexes of Sirt6 (gray; **7**), Sirt1 (yellow; STAC1; PDB ID 4ZZI), and Sirt5 (red; resveratrol; PDB ID 4HDA). Dotted circle: Cofactor-binding loop and neighboring helix bundle.

Small-molecule activation is established for Sirt1 but mechanistically only partially understood, and it is little studied for other isoforms.^[3a,8] Our results establish potent, pharmacological Sirt6 stimulation and reveal the activator-binding pocket at a Sirt6-specific acyl channel opening. It is covered by the cofactor-binding loop and neighboring helix bundle in Sirt1 and Sirt5, but accessible in Sirt6 due to their reduction to a short loop and single helix α 3 (Figure 2i). Conversely, the activator site in the Sirt5/resveratrol complex,^[9] which is speculated also to contribute to Sirt1 activation,^[3a,8b] is an active site opening that is covered in Sirt6 by its N-terminus (Figure 2i). Thus, two different active site openings are exploited in Sirt6 and Sirt1/5. Comparing Sirt6/7 with several Sirt6 states (apo, ADP-ribose complex, myristoyl peptide complex)^[5,13] reveals no significant conformational differences (Figure S2e). As for Sirt1/5, further mechanistic details of Sirt6 activation thus remain to be characterized. However, our identification of potent Sirt6 activators and of their Sirt6-specific binding sites provides an excellent basis for further development of Sirt6 activators as chemical tools and potential therapeutics.

Coordinates and structure factors for the Sirt6/compound complexes have been deposited with the Protein Data Bank (www.rcsb.org/pdb) under accession codes 5MGN (UBCS038), 5MF6 (UBCS039), 5MFZ (UBCS040), and 5MPF (UBCS058).

Acknowledgements

We thank Norbert Grillenbeck and Drs. Luisa Tasselli, Michael Weyand, Matt Fuszard and the beamline staff at BESSY II for experimental support. This work was supported by DFG (1701/15-1) and Oberfrankenstiftung (C.S.), PRIN 2012 (prot.2012CTAYSY to D.R.), AIRC-TRIDEO 2015 (Id.17515 to D.R.), and grants (to K.F.C.) from the NIH (R01AG050997) and U.S. Department of Veterans Affairs (Merit Review).

Conflict of interest

The authors declare no conflict of interest.

Keywords: deacetylases · drug discovery · enzymes · sirtuin activators · structural biology

How to cite: *Angew. Chem. Int. Ed.* **2017**, *56*, 1007–1011
Angew. Chem. **2017**, *129*, 1027–1031

- [1] B. J. Morris, *Free Radical Biol. Med.* **2013**, *56*, 133–171.
- [2] B. P. Hubbard, D. A. Sinclair, *Trends Pharmacol. Sci.* **2014**, *35*, 146–154.
- [3] a) M. Gertz, C. Steegborn, *Cell. Mol. Life Sci.* **2016**, *73*, 2871–2896; b) M. Schutkowski, F. Fischer, C. Roessler, C. Steegborn, *Expert Opin. Drug Discovery* **2014**, *9*, 183–199.
- [4] J. Du, Y. Zhou, X. Su, J. J. Yu, S. Khan, H. Jiang, J. Kim, J. Woo, J. H. Kim, B. H. Choi, B. He, W. Chen, S. Zhang, R. A. Cerione, J. Auwerx, Q. Hao, H. Lin, *Science* **2011**, *334*, 806–809.
- [5] H. Jiang, S. Khan, Y. Wang, G. Charron, B. He, C. Sebastian, J. Du, R. Kim, E. Ge, R. Mostoslavsky, H. C. Hang, Q. Hao, H. Lin, *Nature* **2013**, *496*, 110–113.
- [6] a) R. Gil, S. Barth, Y. Kanfi, H. Y. Cohen, *Nucleic Acids Res.* **2013**, *41*, 8537–8545; b) L. Tasselli, Y. Xi, W. Zheng, R. I. Tennen, Z. Odrowaz, F. Simeoni, W. Li, K. F. Chua, *Nat. Struct. Mol. Biol.* **2016**, *23*, 434–440.
- [7] a) Y. Kanfi, S. Naiman, G. Amir, V. Peshti, G. Zinman, L. Nahum, Z. Bar-Joseph, H. Y. Cohen, *Nature* **2012**, *483*, 218–221; b) S. Kugel, C. Sebastian, J. Fitamant, K. N. Ross, S. K. Saha, E. Jain, A. Gladden, K. S. Arora, Y. Kato, M. N. Rivera, S. Ramaswamy, R. I. Sadreyev, A. Goren, V. Deshpande, N. Bardeesy, R. Mostoslavsky, *Cell* **2016**, *165*, 1401–1415; c) B. Martinez-Pastor, R. Mostoslavsky, *Front. Pharmacol.* **2012**, *3*, 22.
- [8] a) M. Lakshminarasimhan, D. Rauh, M. Schutkowski, C. Steegborn, *Aging* **2013**, *5*, 151–154; b) H. Dai, A. W. Case, T. V. Riera, T. Considine, J. E. Lee, Y. Hamuro, H. Zhao, Y. Jiang, S. M. Sweitzer, B. Pietrak, B. Schwartz, C. A. Blum, J. S. Disch, R. Caldwell, B. Szczepankiewicz, C. Oalman, P. Yee Ng, B. H. White, R. Casaubon, R. Narayan, K. Koppetsch, F. Bourbonnais, B. Wu, J. Wang, D. Qian, F. Jiang, C. Mao, M. Wang, E. Hu, J. C. Wu, R. B. Perni, G. P. Vlasuk, J. L. Ellis, *Nat. Commun.* **2015**, *6*, 7645.
- [9] M. Gertz, G. T. Nguyen, F. Fischer, B. Suenkel, C. Schlicker, B. Franzel, J. Tomaschewski, F. Aladini, C. Becker, D. Wolters, C. Steegborn, *PLoS One* **2012**, *7*, e49761.
- [10] J. L. Feldman, J. Baeza, J. M. Denu, *J. Biol. Chem.* **2013**, *288*, 31350–31356.
- [11] C. Schlicker, G. Boanca, M. Lakshminarasimhan, C. Steegborn, *Aging* **2011**, *3*, 852–857.
- [12] B. C. Smith, W. C. Hallows, J. M. Denu, *Anal. Biochem.* **2009**, *394*, 101–109.
- [13] P. W. Pan, J. L. Feldman, M. K. Devries, A. Dong, A. M. Edwards, J. M. Denu, *J. Biol. Chem.* **2011**, *286*, 14575–14587.

Manuscript received: October 14, 2016

Revised: November 30, 2016

Final Article published: December 19, 2016

Supporting Information

Structural Basis of Sirtuin 6 Activation by Synthetic Small Molecules

Weijie You, Dante Rotili, Tie-Mei Li, Christian Kambach, Marat Meleshin, Mike Schutkowski, Katrin F. Chua, Antonello Mai, and Clemens Steegborn**

anie_201610082_sm_miscellaneous_information.pdf

Table of Contents

Materials and Methods	page 2
Supplementary Table 1: Diffraction data and refinement statistics for Sirt6/ADP-ribose/activator complexes.	page 14
Supplementary Table 2: Physical and Chemical Data for Compounds 1-14	page 15
Supplementary Figure 1	page 17
Supplementary Figure 2	page 18
References	page 19

Materials and Methods

Chemicals

All chemicals were obtained from Sigma if not stated otherwise. Myristoyl-TNF α peptide (Ac-EALPK-(myristoyl-K)-TGG-amide) was prepared using standard solid-phase-peptide synthesis using a nosyl protected Lys6 building block. Subsequent to selective removal of the nosyl protecting group Lys6 was myristoylated on resin as described before ^[1]. All other HPLC-purified synthetic peptides were from GL Biochem (acetyl-H3K9: TKQTAR-(acetyl-K)-STGGKA; acetyl- α -tubulin: MPSD-(acetyl-K)-TIG; acetyl-ACS2: TRSG-(acetyl-K)-VMR; succinyl-CPS1: RGVL-(succinyl-K)-EYGV). UBCS compounds were synthesized as described below and dissolved at 20 mM in DMSO to prepare stock solutions.

Protein production and purification

N-terminally his-tagged human Sirt6 constructs (residues 1-355, 1-318 and 13-308) were expressed using vector pQE80L.1 (internal pQE80 derivative with TEV cleavage site) in *E. coli* M15[pREP4] (construct 1-355) or vector pET151-D-TOPO in *E. coli* Rosetta2 (DE3) pLysS (shortened constructs). Proteins were expressed and purified essentially as described previously ^[2]. In brief, Sirt6 proteins were enriched through immobilized metal ion affinity chromatography (IMAC) on Talon resin (Clontech) or a HisTrap column (GE Healthcare), the tag removed using Tobacco Etch Virus (TEV) protease, and proteins subjected to reverse IMAC. The proteins were further purified through cation exchange chromatography on a HiTrap SP-Sepharose Fast Flow column (GE Healthcare), followed by gel filtration on a Superose 12 column (GE Healthcare) in 20 mM Na-HEPES pH 7.5, 100 mM NaCl, 2 mM DTT. Proteins were concentrated to ≥ 10 mg/ml, flash frozen in liquid nitrogen and stored at -80 °C.

Deacylation assays

For coupled enzymatic peptide deacylation assays, the setup of Smith *et al.* ^[3] was used. Assays were performed in 100 μ l 50 mM Na-phosphate buffer pH 7.5, 5 % DMSO, 0.6 mM DTT, and 0.05 % (v/v) Tween 20, 200 μ M acetylated histone H3K9 peptide, 500 μ M NAD⁺, and 2.5 – 5.0 μ M Sirt6 enzyme.

Reactions with the indicated compound concentrations were run at 25 °C for 120 min and the absorption at 340 nm monitored in an Epoch 2 plate reader (BioTek). Reference measurements were done by adding the solvent DMSO without compound. For demyristoylation assays, myristoylated TNF α peptide was used as the substrate. Control reactions were run with assay mixtures lacking either sirtuin enzyme, substrate peptide, or NAD⁺, and effects on downstream enzymes were tested by spiking control reactions with 5 – 40 μ M nicotinamide.

For mass spectrometry-based deacylation assays, reactions containing 50 mM Na-phosphate buffer pH 7.5, 5 % DMSO, 0.1 % (v/v) Tween 20, 200 μ M acetylated histone H3K9 peptide, 2 mM NAD⁺, and 5.0 μ M Sirt6 were incubated at 37 °C for up to 8 h and aliquots taken after several time-points. Reactions were stopped by adding an equal volume 0.1 % trifluoro acetic acid and peptide deacetylation was quantified as described ^[4].

In vitro deacetylation reactions on histone and nucleosome substrates were performed as previously described ^[5], with minor modifications. Briefly, 2 μ g of recombinant Sirt6 and 2 μ g of Calf thymus histones (CTH; Sigma), or 5 μ g mononucleosomes purified from HeLa cells were incubated in HDAC buffer (50 mM Tris-HCl pH 8.0, 2 mM NAD⁺, 150 mM NaCl) for 4 h (for CTH) or 80 min (for nucleosomes) at 30 °C. To test the effects of the compounds on Sirt6 activity, corresponding compound (100 μ M working concentration) or DMSO control was added before incubation. The reaction mixture was analyzed by western blotting and quantified using ImageJ.

Binding assays

Binding affinities were measured by using microscale thermophoresis (MST). Label-free measurements were done on a Monolith NT.label-free (NanoTemper Technologies) with 3 μ M Sirt6-1-355 protein in 50 mM Na-phosphate buffer pH 7.5, 0.6 mM DTT, and 0.05 % (v/v) Tween 20, and 10 % DMSO. After preincubation of protein and compound for 20min on ice, thermophoresis was analyzed at 25 °C with 20 % laser power and 15 % LED power. As some compounds induced a fluorescence quench in label-free MST, additional binding measurements were performed with labeled Sirt6 on a Monolith NT 115 (NanoTemper Technologies). Sirt6-1-355 was labeled by incubation with a 20 % molar fraction of FITC (Thermo Fischer) in 50 mM sodium borate, pH 8.5 at room temperature

for 30 min. Free dye was removed with a Nap5 column (GE Healthcare). 50 nM Sirt6 was preincubated with the compound for 20 min at room temperature in 50 mM phosphate pH 7.5, 0.05 % Tween-20 and 10 % DMSO, and thermophoresis was then measured at 25 °C at an excitation wavelength of 470 nm, emission wavelength of 520 nm, 10-20 % laser power and 15-20 % LED power. Binding curves were fitted with GraFit7 (Erithacus Software) with an equation for one binding site with background. All experiments were repeated at least twice.

Crystallization and Structure determination

Crystal structures of Sirt6 in complex with UBCS compounds were solved by crystallizing Sirt6-13-308/ADP-ribose complex (stock solution: 10 mg/ml Sirt6-13-308, 10 mM ADP-ribose) at 20 °C in hanging drops with 1.6 M (NH₄)₂SO₄, 10% PEG 400, and Bis-Tris buffer pH 5.7 as reservoir solution. Crystals appeared within 24 h and were subsequently soaked by adding 100 mM compound and incubation for one week. Crystals were transferred to cryoprotectant containing reservoir supplemented with 20% ethylene glycol, 2 mM compound, 10 % DMSO and 2 mM ADP-ribose, and then flash frozen in liquid nitrogen.

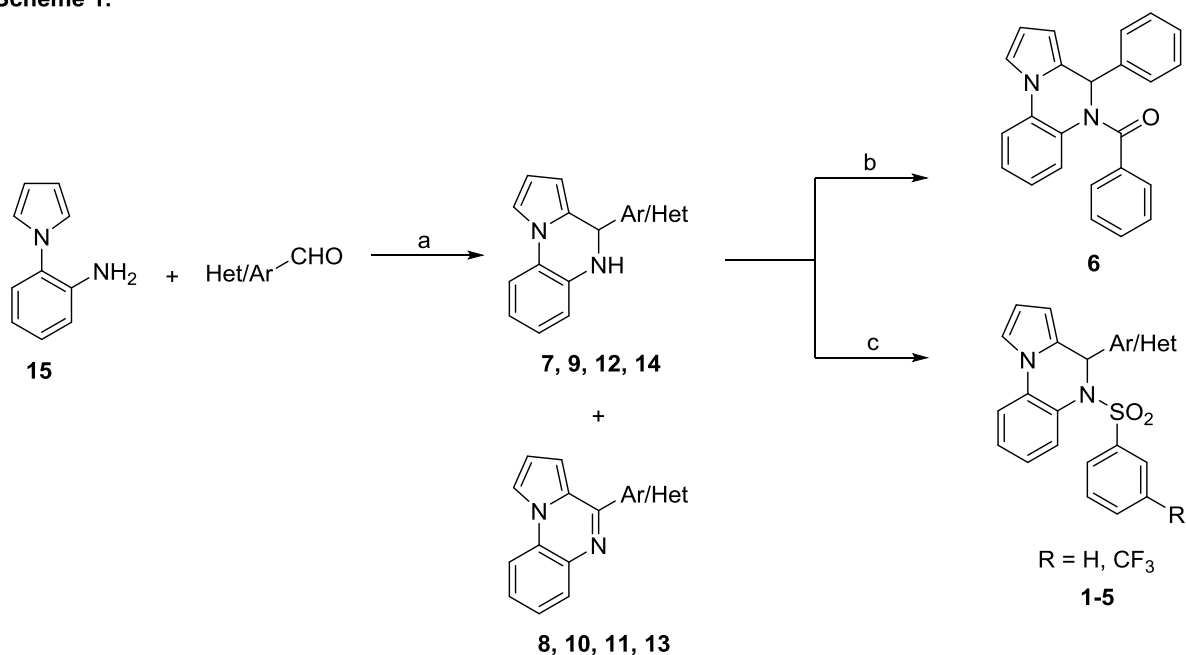
Diffraction data were collected at 100 K at BL14.1 operated by Helmholtz-Zentrum Berlin (HZB) at the BESSY II electron storage ring (Berlin-Adlershof, Germany) ^[6]. Data were processed with X-ray Detector Software (XDS) ^[7] and programs of the CCP4 software suite ^[8]. Crystals belonged to space group P6₃ and showed merohedral twinning with twin fractions of 20 - 46 % as determined by an L-test. Structures were solved by Patterson searches (“molecular replacement”) using Molrep and the protein part of a Sirt6/ADP-ribose structure (PDB code 3K35) ^[9] as a search model. Structures were rebuilt in COOT ^[10] and subjected to amplitude-based twin refinement in Refmac ^[11], with 5% of the reflections excluded from refinement for R_{free} calculation.

Synthesis and analysis of 1/UBCS038 derivatives

Melting points were determined on a Buchi 530 melting point apparatus and are uncorrected. ¹H-NMR and ¹³C-NMR spectra were recorded at 400 MHz on a Bruker AC 400 spectrometer; reporting chemical shifts in δ (ppm) units relative to the internal reference tetramethylsilane (Me₄Si). All compounds were routinely checked by TLC and ¹H-NMR. TLC was performed on aluminum-backed silica gel plates (Merck DC, Alufolien Kieselgel 60 F254) with spots visualized by UV light. Yields of all reactions refer to the purified products. All chemicals were purchased from Aldrich Chimica, Milan (Italy), and were of the highest purity. Mass spectra were recorded on an API-TOF Mariner by Perspective Biosystem (Stratford, TX, USA), and samples were injected with a Harvard pump using a flow rate of 5–10 μ L/min, infused in the Electrospray system. Elemental analyses were performed with a PE 2400 (Perkin-Elmer) analyzer and have been used to determine purity of the described compounds, which is > 95%. Analytical results are within \pm 0.40% of the theoretical values.

The synthetic pathway for the preparation of compounds **1-15** is depicted in Scheme 1. 4-(Hetero)aryl-4,5-dihydropyrrolo[1,2-*a*]quinoxalines **7**, **9**, **12**, **14** were obtained from the condensation between the 1-(2-aminophenyl)pyrrole **15**, prepared as reported,^[12] and the proper commercial (hetero)aromatic aldehyde in dry EtOH in the presence of a catalytic amount of glacial acetic acid while heating at 50 °C. This reaction usually gave the correspondent oxidized side compounds **8**, **10**, and **13** in low yield, with the only exception of compound **11** that was obtained in high yield as unique reaction product. Final compounds **1-5** resulted from reaction of the compounds **7**, **9**, **12**, and **14** with the proper commercially available benzenesulfonyl chloride in dry DCM in the presence of dry pyridine at room temperature, while compound **6** was obtained from the acylation reaction between the 4-phenyl-4,5-dihydropyrrolo[1,2-*a*]quinoxaline **12** and the benzoylchloride in dry DCM in the presence of TEA at room temperature.

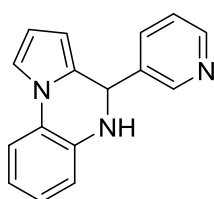
Scheme 1.



(a): Dry EtOH, cat. glacial AcOH, 50 °C; (b) PhCOCl, TEA, dry DCM, N₂, rt; (c) R-SO₂Cl, dry pyridine, dry DCM, N₂, rt.

General Procedure for the Preparation of the 4-Substituted-4,5-dihydropyrrolo[1,2-*a*]quinoxalines (7, 9, 12, 14) and 4-Substituted-pyrrolo[1,2-*a*]quinoxalines (8, 10, 11, 13).

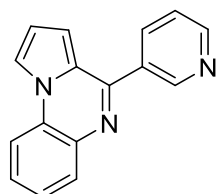
Example: 4-(Pyridin-3-yl)-4,5-dihydropyrrolo[1,2-*a*]quinoxaline (7, MC3154, UBCS039)^[13] and 4-(Pyridin-3-yl)pyrrolo[1,2-*a*]quinoxaline (8, MC3190, UBCS058).^[14]



A solution of 1-(2-aminophenyl)pyrrole **15** (2.53 mmol, 400 mg), prepared as reported in literature,^[12] and the commercial pyridine-3-carboxaldehyde (2.65 mmol, 284.4 mg) in dry ethanol (4 mL) was heated to 50 °C for 2h and 30 minutes in the presence of a catalytic amount of glacial acetic acid (15 drops). After cooling to room temperature, the reaction was quenched with water (25 mL) and stirred for 1h. The resulting solid in suspension was then filtered off, washed with water and purified by silica gel column chromatography eluting with a mixture ethyl acetate/chloroform/hexane 1/12/3 v/v/v to afford the pure compound **7** as a white solid. By continuing the elution with the same solvent mixture

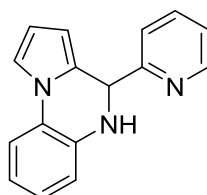
it was then collected the oxidized analogue 4-(pyridin-3-yl)pyrrolo[1,2-*a*]quinoxaline **8** as a white solid. mp 132-134 °C; yield 70%. ¹H-NMR (CDCl₃) δ 4.17 (s, broad, 1H, NH), 5.59 (m, 2H, C3-*H* and C4-*H*), 6.26 (t, 1H, C2-*H*), 6.77 (d, 1H, C6-*H*), 6.90 (m, 1H, C8-*H*), 6.99 (m, 1H, C7-*H*), 7.21 (s, 1H, C1-*H*), 7.22-7.37 (m, 2H, C9-*H* and pyridine-*H*), 7.82 (d, 1H, pyridine-*H*), 8.61 (d, 1H, pyridine-*H*), 8.69 (d, 1H, pyridine-*H*). ¹³C-NMR (CDCl₃) δ 53.9, 106.1, 110.3, 114.6, 114.8, 115.5, 119.8, 123.8, 124.8, 125.4, 128.9, 135.6, 135.7, 137.1, 149.3, 149.8 ppm. Anal. (C₁₆H₁₃N₃) Calcd. (%): C, 77.71; H, 5.30; N, 16.99. Found (%): C, 77.76; H, 5.31; N, 16.93. MS (ESI), m/z: 248 [M + H]⁺.

4-(Pyridin-3-yl)pyrrolo[1,2-*a*]quinoxaline (8, MC3190, UBCS058).^[14]



mp 152-155 °C; yield 22%. ¹H-NMR (CDCl₃) δ 6.97 (m, 1H, C3-*H*), 7.02 (m, 1H, C2-*H*), 7.46-7.54 (m, 2H, C6-*H* and C8-*H*), 7.56-7.61 (m, 1H, C7-*H*), 7.94 (m, 1H, C1-*H*), 8.07-8.08 (m, 2H, C9-*H* and pyridine-*H*), 8.35 (m, 1H, pyridine-*H*), 8.80 (d, 1H, pyridine-*H*), 9.29 (s, 1H, pyridine-*H*). ¹³C-NMR (CDCl₃) δ 107.9, 113.3, 113.9, 114.7, 123.2, 124.6, 125.1, 126.7, 127.6, 129.8, 133.8, 135.6, 135.8, 149.0, 150.1, 150.9 ppm. Anal. (C₁₆H₁₁N₃) Calcd. (%): C, 78.35; H, 4.52; N, 17.13. Found (%): C, 78.39; H, 4.53; N, 17.08. MS (ESI), m/z: 246 [M + H]⁺.

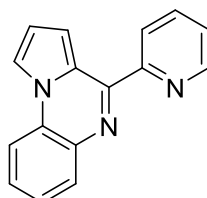
4-(Pyridin-2-yl)-4,5-dihydropyrrolo[1,2-*a*]quinoxaline (9, MC3148, UBCS060).



mp 128-129 °C. ¹H-NMR (CDCl₃) δ 4.73 (bs, 1H, NH), 5.64 (s, 1H, C4-*H*), 5.88 (d, 1H, C3-*H*), 6.26 (t, 1H, C2-*H*), 6.68 (dd, 1H, C6-*H*), 6.72-6.76 (m, 1H, C1-*H*), 6.84-6.88 (m, 1H, C8-*H*), 7.07-7.11 (m, 2H, C7-*H* and C9-*H*), 7.16-7.17 (m, 1H, pyridine-*H*), 7.23-7.26 (m, 1H, pyridine-*H*), 7.49-7.53 (m, 1H, pyridine-*H*), 8.50 (d, 1H, pyridine-*H*). ¹³C-NMR (CDCl₃) δ 56.3, 100.5, 111.0, 114.7, 115.8,

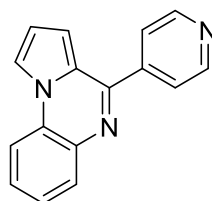
116.1, 119.4, 121.6, 122.4, 124.7, 126.5, 131.9, 136.8, 138.5, 148.6, 158.7 ppm. Anal. (C₁₆H₁₃N₃) Calcd. (%): C, 77.71; H, 5.30; N, 16.99. Found (%): C, 77.76; H, 5.31; N, 16.93. MS (ESI), m/z: 248 [M + H]⁺.

4-(Pyridin-2-yl)pyrrolo[1,2-*a*]quinoxaline (10, MC3155, UBCS059)^[15]



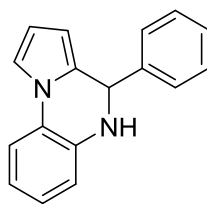
mp 104-105 °C. ¹H-NMR (CDCl₃) δ 6.90 (t, 1H, C3-*H*), 7.34-7.50 (m, 3H, C2-*H*, C7-*H* and C8-*H*), 7.68 (d, 1H, C9-*H*), 7.81-7.85 (m, 2H, C6-*H* and C1-*H*), 7.95-7.96 (m, 1H, pyridine-*H*), 7.99 (m, 1H, pyridine-*H*), 8.35 (d, 1H, pyridine-*H*), 8.75 (d, 1H, pyridine-*H*). ¹³C-NMR (CDCl₃) δ 110.5, 113.6, 114.3, 114.4, 123.3, 124.2, 124.5, 125.1, 127.5, 127.9, 130.3, 135.6, 136.6, 148.8, 151.2, 156.3 ppm. Anal. (C₁₆H₁₁N₃) Calcd. (%): C, 78.35; H, 4.52; N, 17.13. Found (%): C, 78.39; H, 4.53; N, 17.08. MS (ESI), m/z: 246 [M + H]⁺.

4-(Pyridin-4-yl)pyrrolo[1,2-*a*]quinoxaline (11, MC3226, UBCS061).^[14-15]



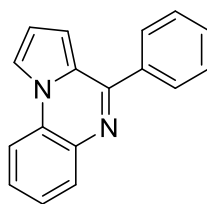
mp 196-199 °C. ¹H-NMR (CDCl₃) δ 6.97 (m, 1H, C3-*H*), 7.02 (m, 1H, C2-*H*), 7.53 (t, 1H, C6-*H*), 7.61 (t, 1H, C8-*H*), 7.92-7.95 (m, 3H, C1-*H*, C7-*H* and C9-*H*), 8.07 (m, 2H, pyridine-*H*), 8.85 (m, 2H, pyridine-*H*). ¹³C-NMR (CDCl₃) δ 108.1, 113.6, 114.3, 115.0, 123.0 (2C), 124.4, 125.9, 127.1, 128.3, 130.3, 135.7, 146.2, 149.7 (2C), 151.3 ppm. Anal. (C₁₆H₁₁N₃) Calcd. (%): C, 78.35; H, 4.52; N, 17.13. Found (%): C, 78.40; H, 4.53; N, 17.07. MS (ESI), m/z: 246 [M + H]⁺.

4-Phenyl-4,5-dihydropyrrolo[1,2-*a*]quinoxaline (12, MC3179, UBCS063).^[13, 16]



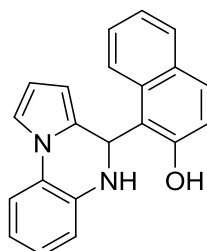
mp 92-94 °C. $^1\text{H-NMR}$ (CDCl_3) δ 4.20 (bs, 1H, NH), 5.57 (s, 1H, C4-H), 5.61 (m, 1H, C3-H), 6.27 (t, 1H, C2-H), 6.78 (dd, 1H, C6-H), 6.86 (m, 1H, C8-H), 7.00 (m, 1H, C7-H), 7.22 (m, 1H, C1-H), 7.36-7.42 (m, 4H, benzene-H), 7.49-7.51 (m, 2H, benzene-H and C9-H). $^{13}\text{C-NMR}$ (CDCl_3) δ 56.2, 106.0, 110.2, 114.5, 114.7, 115.5, 119.4, 124.9, 127.3 (2C), 128.4 (2C), 128.7, 128.9, 129.8, 135.9, 141.3 ppm. Anal. ($\text{C}_{17}\text{H}_{14}\text{N}_2$) Calcd. (%): C, 82.90; H, 5.73; N, 11.37. Found (%): C, 82.93; H, 5.74; N, 11.33. MS (ESI), m/z : 247 $[\text{M} + \text{H}]^+$.

4-Phenylpyrrolo[1,2-*a*]quinoxaline (13, MC3225, UBCS062).^[16]



mp 87-89 °C. $^1\text{H-NMR}$ (CDCl_3) δ 6.93 (m, 1H, C3-H), 7.03 (m, 1H, C2-H), 7.50 (m, 1H, benzene-H), 7.54-7.57 (m, 4H, C6-H, C7-H and benzene-H), 7.91-7.93 (d, 1H, C8-H), 8.02-8.08 (m, 4H, C1-H, C9-H and benzene-H). $^{13}\text{C-NMR}$ (CDCl_3) δ 108.6, 113.6, 114.0, 114.5, 125.2, 125.4, 127.1 (2C), 128.3, 128.5 (2C), 129.1, 129.7, 130.2, 136.2, 138.4, 154.4 ppm. Anal. ($\text{C}_{17}\text{H}_{12}\text{N}_2$) Calcd. (%): C, 83.58; H, 4.95; N, 11.47. Found (%): C, 83.61; H, 4.96; N, 11.43. MS (ESI), m/z : 245 $[\text{M} + \text{H}]^+$.

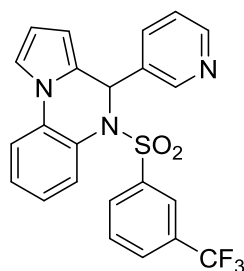
1-(4,5-Dihydropyrrolo[1,2-*a*]quinoxalin-4-yl)naphthalen-2-ol (14, MC3180, UBCS040).



mp 189-190 °C. $^1\text{H-NMR}$ (CDCl_3) δ 4.42 (bs, 1H, NH), 5.49 (m, 1H, C4-H), 6.22 (t, 1H, C3-H), 6.49 (s, 1H, C2-H), 6.94-6.97 (m, 1H, C6-H), 7.08-7.12 (m, 2H, C8-H and naphthalene-H), 7.20-7.22 (m,

1H, C7-*H*), 7.25 (m, 1H, C1-*H*), 7.35-7.39 (t, 1H, C9-*H*), 7.42-7.48 (m, 2H, naphthalene-*H*), 7.83-7.87 (m, 3H, naphthalene-*H*), 9.58 (bs, 1H, *OH*). ¹³C-NMR (CDCl₃) δ 48.0, 104.8, 110.1, 114.7, 115.1, 115.7, 116.7, 119.4, 123.1, 123.5, 124.2, 124.7, 126.4, 127.4, 129.2, 130.0, 130.1, 130.2, 134.4, 134.7, 155.1.ppm. Anal. (C₂₁H₁₆N₂O) Calcd. (%): C, 80.75; H, 5.16; N, 8.97. Found (%): C, 80.79; H, 5.17; N, 8.94 MS (ESI), m/z: 313 [M + H]⁺.

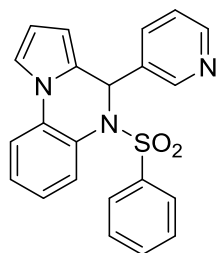
General Procedure for the Preparation of 4-[(Hetero)aryl]-5-((substituted)phenyl)sulfonyl 4,5-dihydropyrrolo[1,2-*a*]quinoxalines (1-5). Example: 4-(Pyridin-3-yl)-5-((3-(trifluoromethyl)phenyl)sulfonyl)-4,5-dihydropyrrolo[1,2-*a*]quinoxaline (1, MC3163, UBCS038).^[2]



To a solution of 4-(pyridin-3-yl)-4,5-dihydropyrrolo[1,2-*a*]quinoxaline **7** (0.505 mmol, 125 mg) in dry DCM (4 mL) in the presence of dry pyridine (2.02 mmol, 0.16 mL), was added dropwise at 0 °C, under nitrogen atmosphere the commercial 3-(trifluoromethyl)benzenesulfonyl chloride (1.01 mmol, 0.162 mL), and the resulting mixture was stirred at room temperature for 24h. After cooling to room temperature, the reaction mixture was diluted with DCM (25 mL) and washed with HCl 2N (2 x 5 mL) and brine (2 x 3 mL). The collected organic phases were dried and concentrated under vacuum to obtain a solid residue that was purified by silica gel column chromatography by eluting with a mixture ethyl acetate/petroleum ether 1/2.5 v/v to afford the pure compound **1** as a white solid; mp 169-170 °C; yield 72%. ¹H-NMR (CDCl₃) δ 6.14 (m, 2H, C3-*H* and C4-*H*), 6.64-6.66 (m, 2H, C2-*H* and C6-*H*), 7.14-7.20 (m, 3H, C1-*H*, C7-*H* and C8-*H*), 7.26-7.32 (m, 2H, C9-*H* and pyridine-*H*), 7.39 (m, 1H, benzene-*H*), 7.47 (s, 1H, benzene-*H*) 7.53 (d, 1H, pyridine-*H*), 7.59 (d, 1H, benzene-*H*), 7.75 (d, 1H, benzene-*H*), 8.37 (bs, 1H, pyridine-*H*), 8.43 (d, 1H, pyridine-*H*). ¹³C-NMR (CDCl₃) δ 66.8, 109.1, 113.7, 114.1, 118.5, 122.6, 122.8, 123.0, 124.3, 126.3, 128.3, 129.3, 129.5, 130.6, 131.1, 131.3, 131.5,

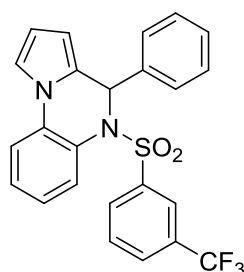
132.6, 134.9, 135.5, 140.1, 147.3, 150.3 ppm. Anal. (C₂₃H₁₆F₃N₃O₂S) Calcd. (%): C, 60.65; H, 3.54; F, 12.51; N, 9.23; S, 7.04. Found (%): C, 60.70; H, 3.55; F, 12.49; N, 9.22; S, 7.03. MS (ESI), m/z: 456 [M + H]⁺.

5-(Phenylsulfonyl)-4-(pyridin-3-yl)-4,5-dihydropyrrolo[1,2-*a*]quinoxaline (2, MC3178, UBCS041).



mp 183-185 °C. ¹H-NMR (CDCl₃) δ 6.13-6.16 (m, 2H, C4-*H* and C3-*H*), 6.68-6.70 (m, 2H, C2-*H* and C6-*H*), 7.13-7.16 (m, 5H, C1-*H*, C7-*H*, C8-*H*, C9-*H* and benzene-*H*), 7.23-7.28 (m, 3H, benzene-*H*), 7.32-7.36 (m, 1H, benzene-*H*) 7.56 (d, 1H, pyridine-*H*), 7.76 (d, 1H, pyridine-*H*), 8.37 (m, 1H, pyridine-*H*), 8.42 (d, 1H, pyridine-*H*). ¹³C-NMR (CDCl₃) δ 66.8, 103.6, 111.2, 115.7, 118.5, 120.6, 122.4, 123.7, 125.2, 127.6 (2C), 128.3, 128.5, 129.2 (2C), 131.5, 133.8, 134.9, 137.2, 138.2, 149.3, 150.7. ppm. Anal. (C₂₂H₁₇N₃O₂S) Calcd. (%): C, 68.20; H, 4.42; N, 10.85; S, 8.27. Found (%): C, 68.25; H, 4.43; N, 10.83; S, 8.26. MS (ESI), m/z: 388 [M + H]⁺.

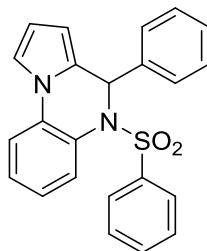
4-Phenyl-5-((3-(trifluoromethyl)phenyl)sulfonyl)-4,5-dihydropyrrolo[1,2-*a*]quinoxaline (3, MC3196, UBCS064).



mp 144-147 °C. ¹H-NMR (CDCl₃) δ 6.10 (m, 1H, C4-*H*), 6.12 (m, 1H, C3-*H*), 6.62 (m, 2H, C2-*H* and C6-*H*), 7.12-7.21 (m, 6H, C1-*H*, C7-*H*, C8-*H*, C9-*H* and benzene-*H*), 7.27-7.29 (m, 2H, benzene-*H*), 7.38-7.40 (m, 1H, benzene-*H*) 7.46 (m, 1H, benzene-*H*), 7.57-7.59 (m, 1H, benzene-*H*), 7.73 (d, 1H,

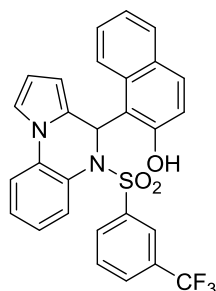
benzene-*H*). ^{13}C -NMR (CDCl_3) δ 69.5, 103.6, 111.0, 115.7, 118.2, 120.6, 122.4, 122.8, 125.2, 126.3, 126.7, 126.9 (2C), 128.2, 128.8 (2C), 129.2, 129.4, 130.4, 130.7, 131.5, 132.2, 138.8, 139.9 ppm. Anal. ($\text{C}_{24}\text{H}_{17}\text{F}_3\text{N}_2\text{O}_2\text{S}$) Calcd. (%): C, 63.43; H, 3.77; F, 12.54; N, 6.16; S, 7.05. Found (%): C, 63.49; H, 3.78; F, 12.52; N, 6.15; S, 7.04. MS (ESI), m/z : 455 $[\text{M} + \text{H}]^+$.

4-Phenyl-5-(phenylsulfonyl)-4,5-dihydropyrrolo[1,2-*a*]quinoxaline (4, MC3188, UBCS065).



mp 202-205 °C. ^1H -NMR (CDCl_3) δ 6.09 (m, 1H, C4-*H*), 6.14 (m, 1H, C3-*H*), 6.65 (s, 1H, C2-*H*), 6.68 (m, 1H, C6-*H*), 7.10-7.28 (m, 12H, C1-*H*, C7-*H*, C8-*H*, C9-*H* and benzene-*H*), 7.31-7.35 (m, 1H, benzene-*H*), 7.75 (d, 1H, benzene-*H*). ^{13}C -NMR (CDCl_3) δ 69.4, 103.7, 111.2, 115.9, 118.1, 120.3, 122.4, 125.2, 127.6, 127.8, 128.0 (2C), 128.5 (2C), 128.8 (2C), 128.9 (2C), 129.3, 131.7, 133.9, 138.3, 138.7 ppm. Anal. ($\text{C}_{23}\text{H}_{18}\text{N}_2\text{O}_2\text{S}$) Calcd. (%): C, 71.48; H, 4.69; N, 7.25; S, 8.30. Found (%): C, 71.52; H, 4.70; N, 7.24; S, 8.29. MS (ESI), m/z : 387 $[\text{M} + \text{H}]^+$.

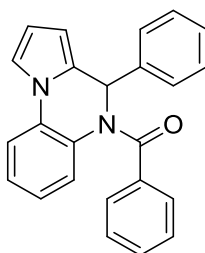
1-(5-((3-(Trifluoromethyl)phenyl)sulfonyl)-4,5-dihydropyrrolo[1,2-*a*]quinoxalin-4-yl)naphthalen-2-ol (5, MC3291, UBCS068).



mp 141-143 °C. ^1H -NMR (CDCl_3) δ 6.30 (m, 1H, C4-*H*), 6.71 (m, 1H, C3-*H*), 6.95 (t, 1H, C2-*H*), 7.24-7.35 (m, 3H, C6-*H*, C8-*H* and naphthalene-*H*), 7.39-7.55 (m, 6H, C1-*H*, C7-*H*, C9-*H* and naphthalene-*H*), 7.65 (d, 1H, benzene-*H*), 7.75-7.78 (m, 2H, naphthalene-*H* and benzene-*H*), 7.82 (m, 1H, benzene-*H*), 7.88 (d, 1H, benzene-*H*), 7.99-8.00 (d, 1H, naphthalene-*H*). ^{13}C -NMR (CDCl_3) δ

64.7, 107.8, 111.9, 114.2, 115.4, 117.7, 118.2, 122.4, 122.6, 123.1, 123.5, 125.1, 126.3, 126.5, 128.2 (2C), 128.5, 129.1, 129.3, 129.5, 130.0, 131.1, 131.5, 131.8, 134.3, 135.2, 139.8, 155.0 ppm. Anal. (C₂₈H₁₉F₃N₂O₃S) Calcd. (%): C, 64.61; H, 3.68; F, 10.95; N, 5.38; S, 6.16. Found (%): C, 64.63; H, 3.69; F, 10.92; N, 5.37; S, 6.18. MS (ESI), m/z: 521 [M + H]⁺.

Preparation of Phenyl(4-phenylpyrrolo[1,2-*a*]quinoxalin-5(4*H*)-yl)methanone (6, MC3217, UBCS066).



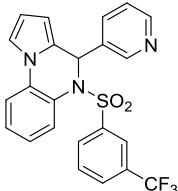
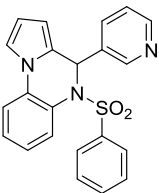
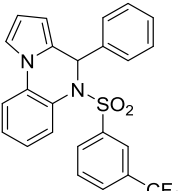
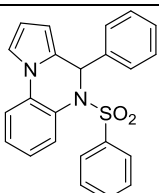
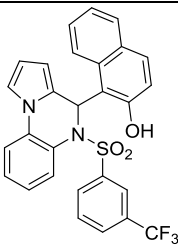
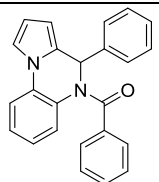
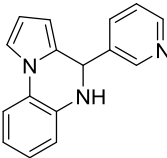
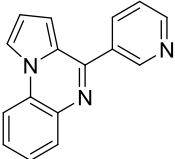
To a solution of 4-phenyl-4,5-dihydropyrrolo[1,2-*a*]quinoxaline **12** (0.333 mmol, 82 mg) in dry DCM (3 mL), in the presence of TEA (1.83 mmol, 0.25 mL), was added dropwise at 0 °C benzoylchloride (1.332 mmol, 0.15 mL), and the resulting mixture was stirred at room temperature for 3h and 30 minutes. At the end of the reaction, the solvent was removed under vacuum and the residue was suspended in water and then extracted with ethyl acetate (4 x 10 mL). The collected organic phases were washed with brine (2 mL), dried, and concentrated under reduced pressure to provide a crude residue that was purified by a silica gel flash chromatography (SNAP 25, Biotage Isolera One™) using a linear gradient of ethyl acetate (5% to 15%) in petroleum ether, giving the expected compound **6** as a white solid. mp 150-152 °C; yield 82%. ¹H-NMR (CDCl₃) δ 6.34 (m, 1H, C4-*H*), 6.48 (m, 1H, C3-*H*), 6.72 (m, 1H, C2-*H*), 7.10 (m, 1H, C1-*H*), 7.16-7.21 (m, 6H, aromatic-H), 7.27-7.33 (m, 4H, aromatic-H) 7.38-7.43 (m, 4H, aromatic-H). ¹³C-NMR (CDCl₃) δ 59.2, 111.0, 115.7, 117.3, 125.7, 126.9 (2C), 127.8 (2C), 128.5 (2C), 128.8 (2C), 128.9, 129.3, 129.9, 131.9, 132.1, 134.9, 138.2, 138.6, 139.2, 142.1, 168.1 ppm. Anal. (C₂₄H₁₈N₂O) Calcd. (%): C, 82.26; H, 5.18; N, 7.99. Found (%): C, 82.28; H, 5.19; N, 7.98. MS (ESI), m/z: 351 [M + H]⁺.

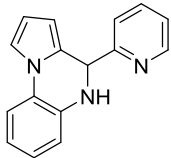
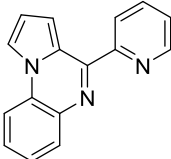
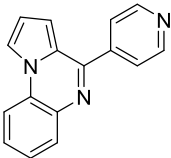
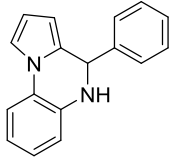
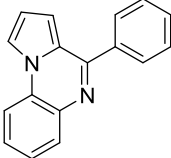
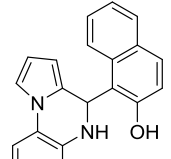
Supplementary Table 1: Diffraction data and refinement statistics for Sirt6/ADP-ribose/activator complexes.

	Sirt6/1	Sirt6/7	Sirt6/14	Sirt6/8
<i>Data collection</i>				
Space group	P 6 ₃	P 6 ₃	P 6 ₃	P 6 ₃
Cell dimensions				
<i>a, b, c</i> (Å)	91.9, 91.9, 145.4	91.3, 91.3, 144.3	91.4, 91.4, 144.2	91.4, 91.4, 144.2
Resolution (Å) ^[a]	48.45-2.07 (2.19-2.07)	45.65-1.87 (1.98-1.87)	48.07-2.10 (2.22-2.10)	48.05-1.97 (2.09-1.97)
<i>R</i> _{meas}	20.3 (110.3)	14.0 (132.0)	16.1 (109.5)	13.0 (96.0)
<i>I</i> / σ <i>I</i>	8.7 (2.3)	12.2 (1.9)	12.9 (2.3)	14.1 (2.3)
Completeness (%)	99.8 (99.0)	99.8 (99.1)	99.7 (98)	99.6 (97.3)
Redundancy	11.3 (11.5)	10.3 (10.2)	11.4 (11.6)	11.3 (10.7)
Twin fraction (%)	0.44	0.20	0.46	0.24
<i>Refinement</i>				
Resolution (Å)	45.93-2.07	45.65-1.87	45.68-2.10	45.69-1.98
No. reflections	40233	53308	37793	45143
<i>R</i> _{work} / <i>R</i> _{free}	14.4/19.2	19.0/22.0	16.7/20.8	15.7/18.5
No. atoms				
Protein	4309	4353	4353	4345
UBCS ligand	32	38	24	38
ADP-ribose	72	72	72	72
Solvent	143	238	97	264
<i>B</i> -factors				
Protein	32.1	32.8	39.3	33.4
UBCS ligand	70.0	45.9	54.7	42.9
ADP-ribose	21.8	22.6	28.0	23.5
Solvent	35.1	36.3	46.6	38.1
R.m.s. deviations				
Bond lengths (Å)	0.024	0.022	0.023	0.021
Bond angles (°)	2.41	2.32	2.45	2.24

^[a] Numbers in parentheses refer to highest-resolution shell.

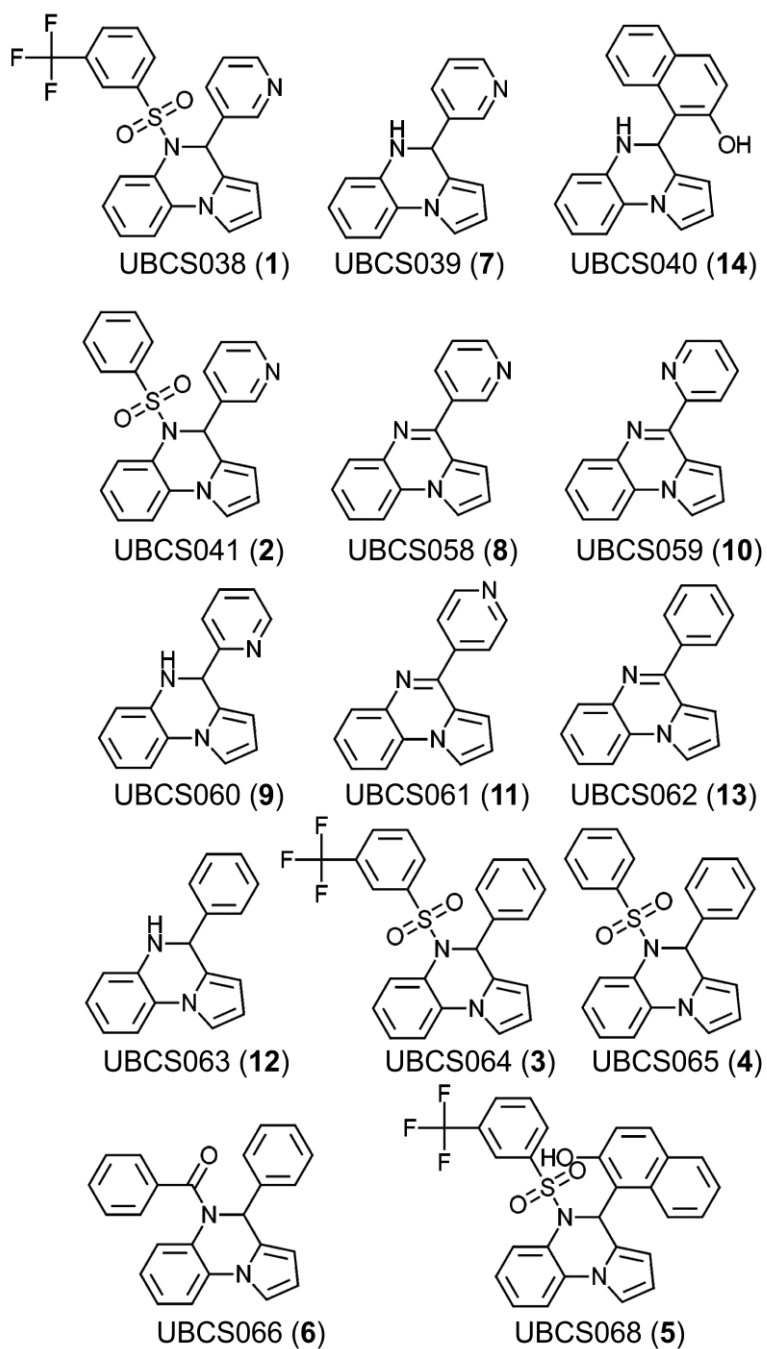
Supplementary Table 2: Physical and Chemical Data for Compounds **1-14**.

Compd	Synthesis Code	Assay Code	Structure	mp (°C)	recryst. System ^[a]	% yield
1	MC3163	UBCS038		165-168 °C	A	72
2	MC3178	UBCS041		183-185 °C	A	78
3	MC3196	UBCS064		144-147 °C	A	76
4	MC3188	UBCS065		202-205 °C	A	81
5	MC3291	UBCS068		141-143 °C	B	75
6	MC3217	UBCS066		165-168 °C	A	82
7	MC3154	UBCS039		132-134 °C	A	70
8	MC3190	UBCS058		152-155 °C	B	22

9	MC3148	UBCS060		128-129 °C	A	72
10	MC3155	UBCS059		104-105 °C	A	19
11	MC3226	UBCS061		196-199 °C	C	86
12	MC3179	UBCS063		92-94 °C	D	70
13	MC3225	UBCS062		87-89 °C	D	23
14	MC3180	UBCS040		182-183 °C	E	77

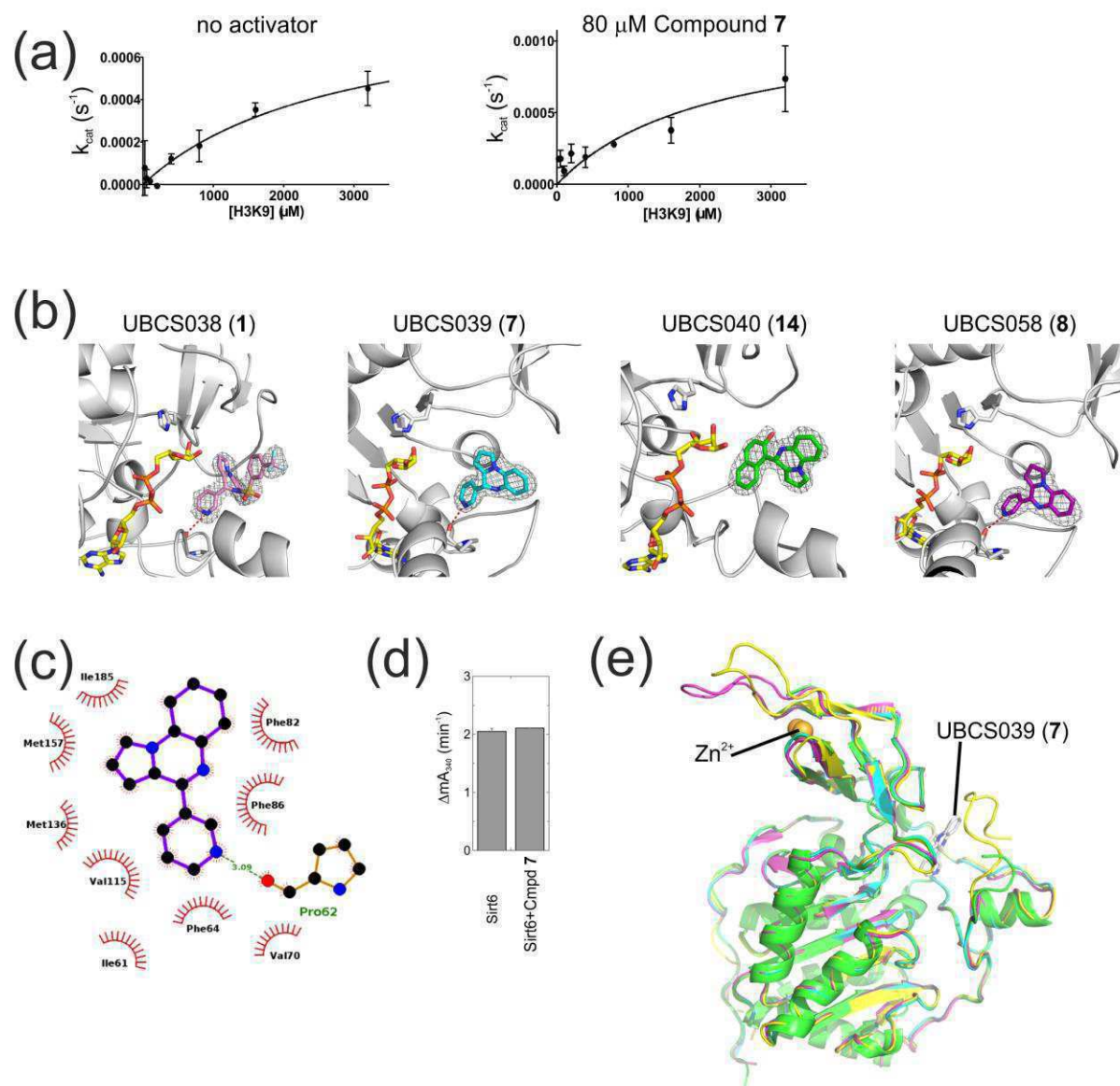
^[a] A: cyclohexane/benzene; B: benzene; C: ethanol; D: cyclohexane; E: acetonitrile.

Supplementary Figure 1



Supplementary Figure 1: Chemical structures of the compounds UBCS038 - UBCS068.

Supplementary Figure 2



Supplementary Figure 2: Interaction details and mechanism for Sirt6 activators. (a) Sirt6 deacetylation activity at increasing concentrations of substrate peptide, measured in absence (left) and presence of 80 μM **7**. (b) Close-up views of Sirt6 complexes with ADP-ribose and **1**, **7**, **14**, or **8**. The modulators are overlaid with their respective $2F_o - F_c$ electron density contoured at 1σ . (c) Schematic view of the Sirt6/7 interactions (prepared with LigPlot (Laskowski & Swindells (2011) *J. Chem. Info. Modeling* **51**, 2778–2786)). (d) Peptide demyristoylation activity of Sirt6 in absence and presence of 100 μM **7**. (e) Overlay of Sirt6/ADP-ribose/**7** (green) with Sirt6 apo (cyan; PDB ID 3K35), Sirt6/ADP-ribose (magenta; 3PKI) and Sirt6/myristoyl peptide (yellow; 3ZG6). The activator is shown as gray sticks, all other ligands are not shown.

References

- [1] S. Schuster, C. Roessler, M. Meleshin, P. Zimmermann, Z. Simic, C. Kambach, C. Schiene-Fischer, C. Steegborn, M. O. Hottiger, M. Schutkowski, *Sci Rep* **2016**, *6*, 22643.
- [2] C. Schlicker, G. Boanca, M. Lakshminarasimhan, C. Steegborn, *Aging (Albany NY)* **2011**, *3*, 852-857.
- [3] B. C. Smith, W. C. Hallows, J. M. Denu, *Anal Biochem* **2009**, *394*, 101-109.
- [4] F. Fischer, M. Gertz, B. Suenkel, M. Lakshminarasimhan, M. Schutkowski, C. Steegborn, *PLoS One* **2012**, *7*, e45098.
- [5] L. Tasselli, Y. Xi, W. Zheng, R. I. Tennen, Z. Odrowaz, F. Simeoni, W. Li, K. F. Chua, *Nat Struct Mol Biol* **2016**, *23*, 434-440.
- [6] U. Mueller, N. Darowski, M. R. Fuchs, R. Forster, M. Hellmig, K. S. Paithankar, S. Puhlinger, M. Steffien, G. Zocher, M. S. Weiss, *J Synchrotron Radiat* **2012**, *19*, 442-449.
- [7] W. Kabsch, *Acta Crystallogr D Biol Crystallogr* **2010**, *66*, 125-132.
- [8] M. D. Winn, C. C. Ballard, K. D. Cowtan, E. J. Dodson, P. Emsley, P. R. Evans, R. M. Keegan, E. B. Krissinel, A. G. Leslie, A. McCoy, S. J. McNicholas, G. N. Murshudov, N. S. Pannu, E. A. Potterton, H. R. Powell, R. J. Read, A. Vagin, K. S. Wilson, *Acta Crystallogr D Biol Crystallogr* **2011**, *67*, 235-242.
- [9] P. W. Pan, J. L. Feldman, M. K. Devries, A. Dong, A. M. Edwards, J. M. Denu, *J Biol Chem* **2011**, *286*, 14575-14587.
- [10] P. Emsley, K. Cowtan, *Acta Cryst Section D* **2004**, *60*, 2126-2132.
- [11] G. N. Murshudov, P. Skubak, A. A. Lebedev, N. S. Pannu, R. A. Steiner, R. A. Nicholls, M. D. Winn, F. Long, A. A. Vagin, *Acta Crystallogr D Biol Crystallogr* **2011**, *67*, 355-367.
- [12] Z. Zhang, C. Xie, X. Tan, G. Song, L. Wen, H. Gao, C. Ma, *Org. Chem. Frontiers* **2015**, *8*, 942-946.
- [13] R. Abonia, B. Insuasty, J. Quiroga, H. Kolshorn, H. Meier, *J. Heter. Chem.* **2001**, *38*, 671-674.
- [14] W. Lv, B. Budke, M. Pawlowski, P. P. Connell, A. P. Kozikowski, *J Med Chem* **2016**, *59*, 4511-4525.
- [15] A. Preetam, M. Nath, *RSC Advances* **2015**, *5*, 21843-21853.
- [16] A. K. Verma, R. R. Jha, V. K. Sankar, T. Aggarwal, R. P. Singh, R. Chandra, *Eur. J. Org. Chem.* **2011**, *34*, 6998-7010.

5.2 Publication 2

Structural Basis of Sirtuin 6 Inhibition by the Hydroxamate Trichostatin A: Implications for Protein Deacylase Drug Development

Weijie You and Clemens Steegborn. J. Med. Chem. 2018, acs.jmedchem.8b01455. [Epub ahead of print]

Author Contributions

Clemens Steegborn designed the study. I performed binding experiments and produced the complex crystal. Both authors contributed to the result analysis and the manuscript.

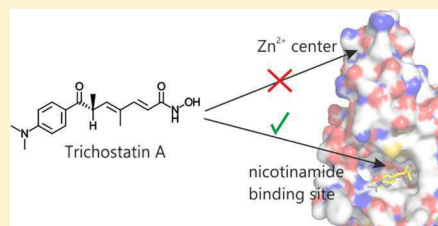
Structural Basis of Sirtuin 6 Inhibition by the Hydroxamate Trichostatin A: Implications for Protein Deacetylase Drug Development

Weijie You and Clemens Steegborn*[✉]

Department of Biochemistry, University of Bayreuth, Universitätsstraße 30, 95445 Bayreuth, Germany

Supporting Information

ABSTRACT: Protein lysine deacetylases comprise three zinc-dependent families and the NAD⁺-dependent sirtuins Sirt1–7, which contribute to aging-related diseases. Few Sirt6-specific inhibitors are available. Trichostatin A, which belongs to the potent, zinc-chelating hydroxamate inhibitors of zinc-dependent deacetylases, was recently found to potently and isoform-specifically inhibit Sirt6. We solved a crystal structure of a Sirt6/ADP-ribose/trichostatin A complex, which reveals nicotinamide pocket and acyl channel as binding site and provides interaction details supporting the development of improved deacetylase inhibitors.



INTRODUCTION

Sirtuins form class III of the protein lysine deacetylase family (also called histone deacetylases, HDACs) and regulate, for example, chromatin homeostasis and energy metabolism.¹ They require NAD⁺ as an essential cosubstrate, rendering them metabolic sensors, and they have been implicated in aging-related dysfunctions.¹ Mammals have seven sirtuin isoforms (Sirt1–7), with Sirt1, -6, and -7 being primarily localized in the nucleus. Sirt1 is the best characterized isoform, acts as deacetylase of histones and transcription factors, and is modulated by a variety of small molecules and used as therapeutic target for inflammatory diseases.^{1,2} Several biological Sirt6 functions are also established, but details of its activity and regulation and Sirt6-specific modulators are lacking.^{2,3} It associates with chromatin, modulates histones, transcription factors, and DNA repair proteins and thereby regulates gene expression and chromosome maintenance.³ Sirt6 supports longevity in male mice, suppresses aging phenotypes, and promotes proliferation of several cancer types,³ and small molecule Sirt6 modulators are thus sought for functional studies and therapy.

Sirt6 comprises the conserved sirtuin catalytic core of ~270 amino acids and small N- and C-terminal extensions that contribute to chromatin association.⁴ The sirtuin core consists of a Rossmann-fold subdomain and a small, more variable Zn²⁺-binding module, with the active site located between them.⁵ During catalysis, the cosubstrate's nicotinamide (NAM) moiety is placed in the so-called C-site for replacement of its glycosidic bond by a new bond to the substrate acyl oxygen, yielding an alkylimide intermediate.^{6,7} Rearrangement in a bicyclic intermediate and subsequent hydrolysis result in the products deacetylated peptide and 2'-O-acyl-ADP-ribose. Smaller variations in the substrate sites lead to isoform-specific substrate sequence and acyl preferences.^{8–10} Its particular small Zn²⁺-binding module and cofactor-binding loop render Sirt6's acyl pocket rather wide and extended, allowing it to

hydrolyze long chain acylations such as myristoylation more efficiently than acetylations *in vitro*.^{10,11} This Sirt6 activity regulates TNF- α secretion, but a broader relevance of this activity and of Sirt6's low mono-ADP-ribosylation activity remains to be confirmed.^{3,10} Sirt6 deacetylates histones and other target proteins efficiently *in vivo*, however, and the molecular reason for this discrepancy remains to be clarified.³

Few Sirt6 modulatory compounds are available. Fatty acids activate Sirt6-dependent deacetylations at high micromolar concentrations, and the flavonoid quercetin at millimolar levels.^{12,13} More potent activation was achieved with synthetic pyrrolo[1,2-*a*]quinoxalines, which bind to Sirt6's acyl channel exit, and with the quercetin derivative cyanidin.^{13,14} Sirt6 is inhibited by the pan-sirtuin inhibitor NAM (Figure 1A), which can rebound to the sirtuin/alkylimide complex to regenerate substrates (base-exchange reaction).⁷ The NAM related pyrazinamide appears to inhibit Sirt6 more specifically but with low (millimolar) potency.¹⁵ Salicylate derivatives and docking derived compounds show slightly improved Sirt6 potency (IC₅₀ \geq 89 μ M),^{16,17} and the quercetin derivatives catechin gallate and gallicocatechin gallate were reported as first potent small molecule Sirt6 inhibitors (IC₅₀ = 3–5 μ M) but affect various targets.^{13,18} Cyclic peptides can also potently inhibit Sirt6 but with limited selectivity.¹⁹ Recently, potent Sirt6 inhibition was further described for trichostatin A (TSA; Figure 1A).²⁰ TSA and related hydroxamates, such as suberoylanilide hydroxamic acid (SAHA, vorinostat; Figure 1A), inhibit class I and II HDACs by chelating their catalytic Zn²⁺ ion.²¹ TSA induces cell cycle arrest and potently inhibits proliferation of breast cancer cells, and the closely related SAHA has been FDA approved for the treatment of T-cell lymphoma.^{21–23} While sirtuins also feature a Zn²⁺ cofactor, it is remote from the active site, fully coordinated, and serves a

Received: September 19, 2018

Published: November 5, 2018

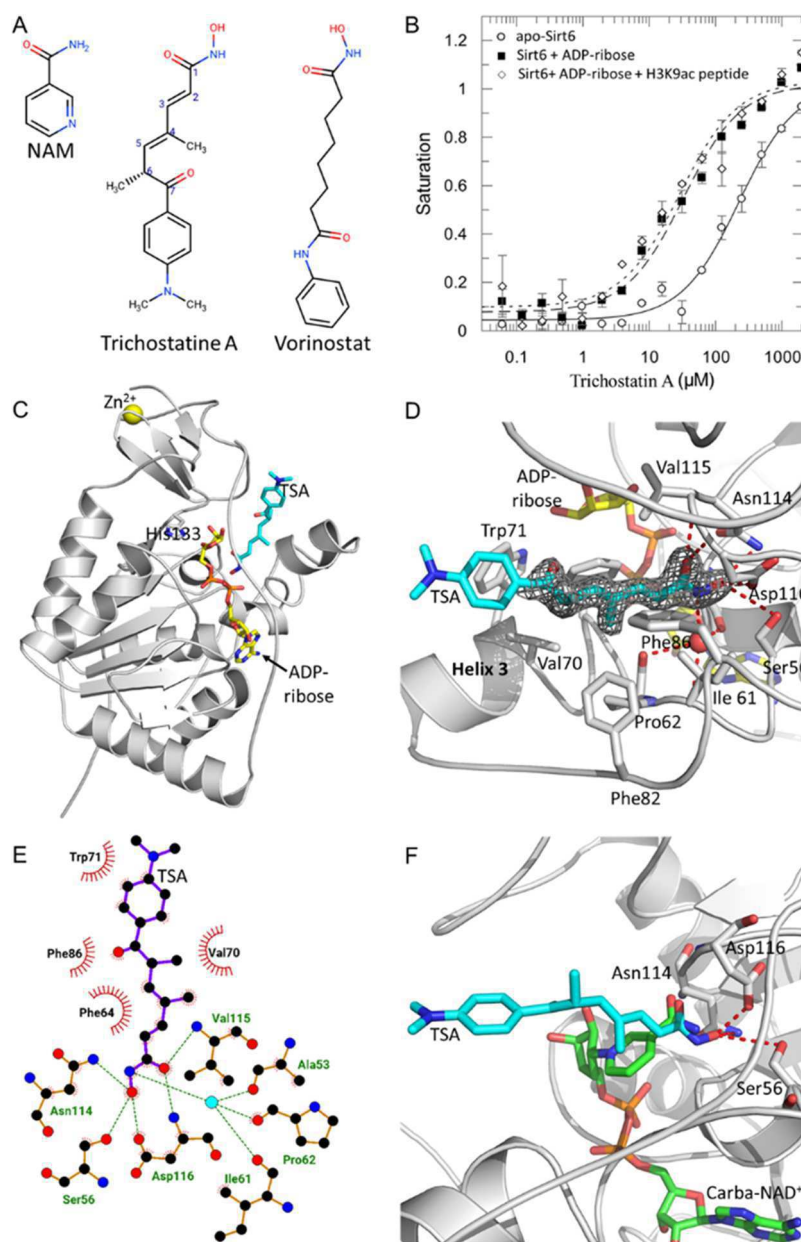


Figure 1. Crystal structure of a Sirt6/ADP-ribose/TSA complex. (A) Chemical structures of NAM, TSA, and SAHA (vorinostat). TSA carbons are numbered for referencing. (B) Binding of TSA to apo-Sirt6 ($K_d = 227 \pm 35 \mu\text{M}$) or in the presence of 1 mM ADP-ribose ($K_d = 33 \pm 6 \mu\text{M}$) or in the presence of 1 mM ADP-ribose and 1 mM acetylated H3K9 peptide ($K_d = 29 \pm 8 \mu\text{M}$). (C) Overall structure of Sirt6 in complex with ADP-ribose (yellow) and TSA (cyan). (D) TSA interactions with Sirt6. Ligand and interacting residues are shown as sticks, colored according to atom type. The ligand is overlaid with $2F_o - F_c$ electron density contoured at 1σ . (E) Scheme of the interactions between Sirt6 and TSA. (F) Overlay of the Sirt6/ADP-ribose/TSA complex (gray cartoon, cyan ligand) with a Sirt3/acetyl-peptide/carba-NAD⁺ complex (PDB code 4FVT; protein and peptide hidden, carba-NAD⁺ in green).

structural function, rendering the TSA effect on Sirt6 surprising.^{5,20} Activity assays indeed indicated that TSA appears to inhibit Sirt6 through competition with the acetyl substrate rather than by chelating its Zn²⁺ ion.²⁰ TSA potency against Sirt6 ($K_i = 2\text{--}5 \mu\text{M}$) is about 2–4 orders of magnitude lower than against class I/II HDACs, but it is still the most potent known Sirt6 inhibitor and shows no significant effects on Sirt1–3 and Sirt5.²⁰ Molecular details of Sirt6 inhibition by TSA thus would provide insights in a potent and isoform-selective Sirt6 inhibitor scaffold. Interestingly, the related SAHA had no effect on Sirt6,²⁰ indicating that small scaffold variations enable selectivity for class I/II HDACs. Other

modifications of this scaffold will likely also enable to specifically target sirtuins.

To exploit TSA scaffold and binding site for Sirt6 inhibitor development, we characterized the Sirt6 inhibition by TSA through binding assays and crystal structure analysis of a Sirt6/ADP-ribose/TSA complex. We find that TSA binds to Sirt6's acyl channel extension, which explains its isoform specificity. Binding is supported by ADP-ribose and noncompetitive with acetyl substrate, indicating that active site closure supports TSA binding. The inhibitor's hydroxamate group occupies the C-site and mimics NAM interactions, revealing a novel moiety for exploiting this site and a scaffold for concomitantly occupying NAM site and acyl channel extension. These results

provide molecular insights in potent and isoform-selective Sirt6 inhibition and will support further development of inhibitors for Sirt6, other sirtuins, and other HDAC families.

RESULTS

Crystal Structure of a Sirt6/TSA Complex. To identify TSA's Sirt6 binding site and inhibition mechanism, we aimed for solving a crystal structure of a Sirt6/TSA complex. For this purpose, we first analyzed whether the two Sirt6 substrates, acetyl peptide and NAD⁺, influence the TSA interaction. Binding measurements using microscale thermophoresis revealed that the ADP-ribose fragment of NAD⁺, which suffices for inducing nucleotide binding site closure, supports TSA binding and that adding substrate peptide has no significant effect on inhibitor affinity (Figure 1B). We thus soaked crystals of a Sirt6/ADP-ribose complex with TSA and solved the structure of the trimeric complex by molecular replacement phasing (Table 1). The Sirt6/ADP-ribose/TSA

site. Nitrogen and carbonyl oxygen of the hydroxamate overlay perfectly with the NAM carbamide and thus show the same interactions (Figure 1F). The carbonyl oxygen interacts with the backbone nitrogens of Val115 and Asp116, and the nitrogen forms a hydrogen bond to Asp116, a possible polar contact to Asn114, and water-mediated hydrogen bonds to the backbone oxygens of Ala53, Ile61, and Pro62. The hydroxamate's additional hydroxyl group is oriented deeper into the carbamide recognition pocket and forms additional hydrogen bonds to Asp116, Asn114, and Ser56 (Figure 1E,F), which are likely to contribute significantly to the higher affinity of TSA ($K_i(\text{NAM})$ against Sirt6, 0.45 mM; IC_{50} for other sirtuins, 0.02 to several mM).^{24,25}

The aliphatic linker of TSA is bound in a hydrophobic region that also accommodates the NAM pyridine moiety and interacts with Phe64/82/86, Ile61, and Val70/115 (Figure 1D,E). The TSA phenyl ring is oriented toward the acyl exit and positioned between Val70, Trp71, Met157, with one face of the aromatic ring and the complete dimethylamino group exposed to solvent (Figure 1D,E). In addition to this incomplete shielding of hydrophobic compound surfaces from solvent, the plane of the keto group is significantly distorted and the oxygen rotated out of the phenyl plane. These distortions are necessary to avoid a clash with Trp71, and compound modifications relieving this strain should improve Sirt6 affinity further (see discussion). However, the larger interaction interface through TSA's extended linker and additional diaminomethylphenyl moiety as compared to NAM likely also contribute to its already higher affinity. In particular the linker seems relevant, since it is well-defined by electron density, while the diaminomethylphenyl moiety is hardly defined and likely flexible (Figure 1D).

Inhibition Mechanism and Implications for Sirtuin Inhibitor Development. Our structure shows that TSA occupies the C-site, which might suggest that it competes with NAD⁺ (Figure 1F). No TSA/NAD⁺ competition was observed in activity assays,²⁰ however, similar to the behavior of the pan-sirtuin inhibitor NAM and the Sirt1 inhibitor Ex527. NAM inhibits via rebinding to the C-site of the long-lived alkyl imidate intermediate complex and re-formation of substrates, and Ex527 binds to the C-site after NAM dissociation to block product release.^{7,26} A TSA binding titration to Sirt6 in the presence of 10 mM of the low-affinity ligand NAM indeed revealed weak but statistically significant competition with isolated NAM (Figure 2A). Our structure further shows that TSA interacts extensively with Sirt6's short cofactor binding loop (around Pro62) and $\alpha 3$ (Figure 1D), which undergo rearrangements upon nucleotide binding.²⁷ We thus propose that TSA acts similar to NAM and Ex527 (Figure 2B) by occupying the C-site after NAM release, consistent with the requirement of the NAD⁺ fragment ADP-ribose for tight TSA binding, the competition with NAM and lack of competition with NAD⁺, and the binding mode in the structure. It causes the reported peptide competition²⁰ indirectly, by inducing a conformation of cofactor-binding loop and nucleotide that would create clashes with the substrate acyl.

TSA inhibits HDACs orders of magnitude stronger than Sirt6, but as the most potent and specific Sirt6 inhibitor known, it can nevertheless provide important information for Sirt6 inhibitor development. Compared to NAM, TSA shows increased affinity due to more extensive interactions with the C-site's carbamide pocket and its larger interaction interface. Interactions in the highly conserved C-site are useful for

Table 1. Data Collection and Refinement Statistics

Sirt6/ADP-ribose/TSA complex	
Data Collection	
space group	$P6_3$
cell dimensions	
<i>a</i> , <i>b</i> , <i>c</i> (Å)	91.29, 91.29, 143.68
α , β , γ (deg)	90.00, 90.00, 120.00
resolution (Å) ^a	47.89–1.70 (1.80–1.70)
R_{meas} ^a	0.15 (2.47)
$I/\sigma(I)$ ^a	10.56 (0.87)
completeness (%) ^a	99.9 (99.6)
redundancy ^a	11.4 (11.6)
Refinement	
resolution (Å) ^a	45.65–1.70 (1.74–1.70)
no. reflections	72292
twin fractions ^b	0.684/0.316
$R_{\text{work}}/R_{\text{free}}$ (%)	15.4/18.5
no. atoms	
protein	4378
TSA ligand	44
ADP ribose	72
solvent	333
<i>B</i> -factors	
protein	36.2
TSA ligands	53.5
ADP ribose	27.3
solvent	39.7
rms deviation	
bond length (Å)	0.015
bond angle (deg)	2.2

^aHighest-resolution shell is shown in parentheses. ^bTwo twin domains were found; twin fractions were estimated using the L-test in CCP4 aimless.

complex was refined at 1.7 Å resolution to $R_{\text{cryst}}/R_{\text{free}}$ values of 15.5%/18.4% and revealed one TSA molecule bound per protein monomer (Figure 1C). The inhibitor is positioned in the Sirt6 substrate acyl binding channel, with its phenyl group oriented toward the acyl channel exit and exposed to solvent (Figure 1D,E). The hydroxamate group occupies the C-site, which normally accommodates the NAM moiety of NAD⁺ (Figure 1D–F). It mimics and possibly even improves the interactions with the carbamide-binding motif of the sirtuin C-

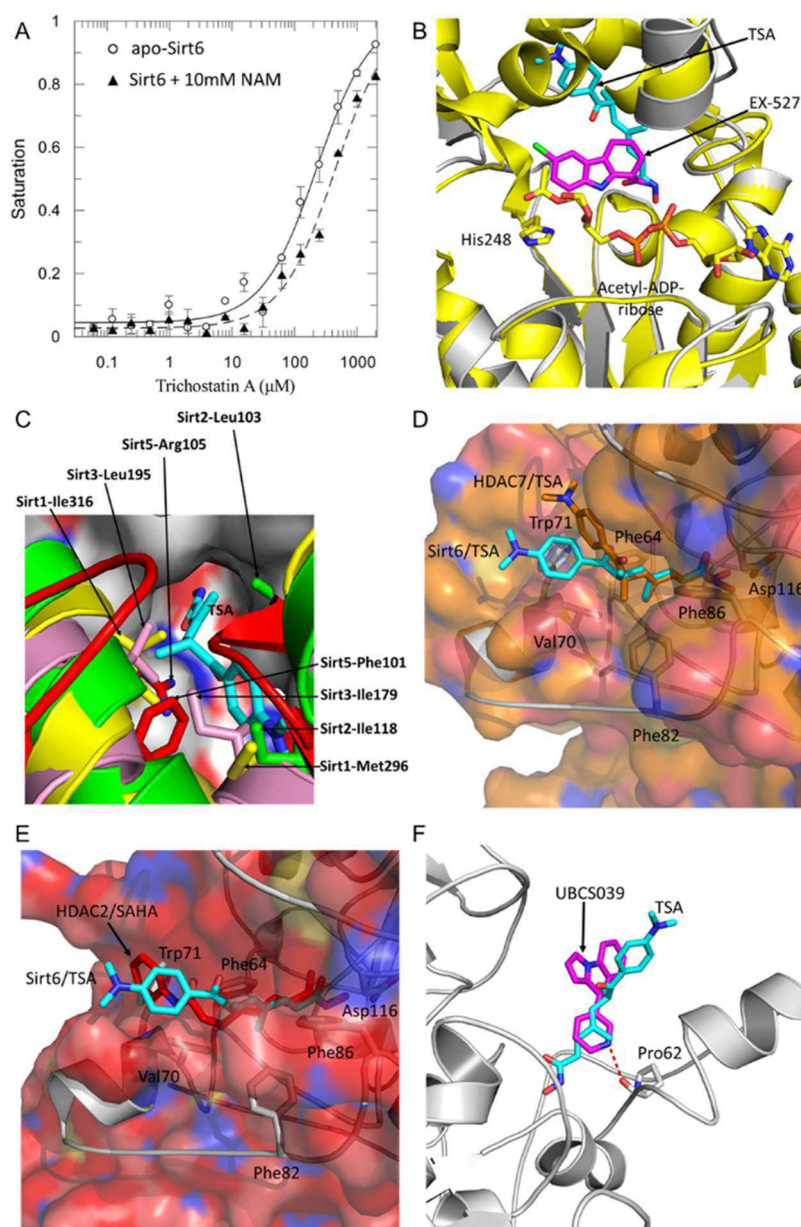


Figure 2. TSA inhibition mechanism and specificity. (A) Binding of TSA to apo Sirt6 ($K_d = 227 \pm 35 \mu\text{M}$) or in the presence of 10 mM NAM ($K_d = 445 \pm 66 \mu\text{M}$). (B) Overlay of the Sirt6/ADP-ribose/TSA complex (gray cartoon, cyan ligand) with a Sirt3/acetyl-ADP-ribose/Ex-527 complex (PDB code 4BVH, yellow cartoon, magenta ligand). (C) Overlay of the Sirt6/ADP-ribose/TSA complex (protein as surface, TSA in cyan) with Sirt1 (yellow; PDB code 4IF6), Sirt2 (green; 3ZGV), Sirt3 (pink; 4FVT), and Sirt5 (red; 4G1C). Examples for residues clashing with TSA are shown as sticks. (D) Overlay of TSA complexes of Sirt6 (gray cartoon, cyan ligand) and HDAC7 (PDB code 3C10; protein displayed as surface, gold ligand). (E) Overlay of Sirt6/TSA (gray cartoon, cyan ligand) and HDAC2/SAHA complexes (PDB code 4LXZ; protein displayed as surface, red ligand). (F) Overlay of Sirt6/TSA (gray cartoon, cyan ligand) with Sirt6/UBCS039 (PDB code 5MF6; protein hidden, magenta ligand).

affinity but less suitable for isoform specificity. The TSA extensions thus should provide the information of how to achieve selectivity for Sirt6 or also other sirtuin isoforms. Analyzing an overlay of the Sirt6/ADP-ribose/TSA complex with structures of Sirt1, -2, -3, and -5 indicates that the TSA phenyl group and its position are keys to its specificity (Figure 2C). The moiety is oriented into the acyl channel exit and packed on its hydrophobic rim (Figure 1D,E). This region is a unique Sirt6 feature and covered by more extended cofactor binding loops and neighboring helix bundles in other sirtuin isoforms, leading to clashes, e.g., with Sirt1-Met296, Sirt2-Ile118, Sirt3-Ile179, or Sirt5-Phe101 (Figure 2C).

The directly phenyl-connected part of the TSA linker (C5–7; Figure 1A) contributes to these selectivity-mediating interactions directly (e.g., clashes with Sirt1-Ile316, Sirt2-Leu103, Sirt3-Leu195, Sirt5-Arg105) and through positioning of the dimethylaminophenyl moiety (Figure 2C). The proximal linker part (C2–4), in contrast, occupies the binding region for the NAM pyridine group, which is conserved among sirtuins and can mainly be exploited for affinity but not selectivity (Figures 1F and 2C).

Our isoform comparison thus indicates that TSA modifications in the proximal linker region can further improve general sirtuin affinity and that modifications in the distal linker and terminal dimethylaminophenyl moiety can improve

sirtuin isoform selectivity (see also discussion); they can further abrogate activity against class I/II HDACs (see below).

Implications for Development of Specific HDAC Inhibitors. Hydroxamate-based HDAC inhibitors were assumed to be specific for class I/II HDACs, and several family members are in clinical trials or have entered the clinic, in particular also SAHA.^{21,23} Indeed, SAHA is specific for HDACs, in contrast to the closely related TSA with its Sirt6 inhibitory effect.²⁰ To analyze the molecular basis of these specificities and differences, we compared our Sirt6/ADP-ribose/TSA complex with a human HDAC2/SAHA and a human HDAC7/TSA complex, respectively, by overlaying them based on an optimized superposition of their ligands (Figure 2D,E). TSA hydroxamate and linker of the HDAC7 complex overlay well with the Sirt6/TSA ligand, but a different orientation of the TSA dimethylaminophenyl group is caused mostly by different torsions along the C5–6 bond. The different orientation in HDAC7 is necessary to avoid clashes with its $\alpha 1/\alpha 2$ loop and $\alpha 14$, which embrace the distal compound group like forceps. Rigidifying this compound section in its Sirt6-bound, HDAC7-incompatible conformation thus would be an approach to abrogate HDAC7 activity and to achieve Sirt6 specificity. In fact, overall structure and this HDAC7 binding site feature are similar in other HDAC isoforms,²¹ and stabilizing the Sirt6-bound conformation thus will generally prevent HDAC effects. Reinforcing this notion, the HDAC2/SAHA ligand can also be overlaid with Sirt6/TSA for hydroxamate and proximal linker and deviates for the distal part in the same way as the TSA in HDAC7, reflecting that the HDAC binding groove for the distal compound part is generally narrower than in Sirt6 and kinked. Notably, the SAHA ligand overlays well with the HDAC7-bound TSA despite its higher degree of rotational freedom, illustrating that this conformation is required for HDAC binding. We assume that the HDAC ligand conformation is also energetically favorable, with the TSA carbonyl oxygen in plane with the phenyl group and the TSA/SAHA carbonyl/carbamide mostly in planar conformation, which should contribute to the higher potency against HDACs. However, in contrast to the tight packing of the ligands' phenyl ends in the HDAC complexes, Sirt6 provides a wide funnel for the distal compound part (Figure 1D, Figure 2D,E). It would in principle allow for a variation of orientations, but it also limits the binding interactions that can be formed simultaneously. Also, the HDAC2/7 binding mode is prevented in Sirt6 due to a clash between the SAHA/TSA phenyl group and Sirt6-Trp71. Adding groups to the distal inhibitor end thus appears attractive to prevent activity against Sirt6, and shortening or modifying this part might improve Sirt6 inhibition (see discussion). In fact, the additional amino bridge between inhibitor chain and phenyl group in SAHA might contribute to its higher selectivity for HDACs over Sirt6 via this mechanism: It prevents a TSA-like orientation of the phenyl group that avoids clashes with Sirt6-Trp71. Another factor that might contribute to TSA's higher Sirt6 affinity compared to SAHA is its two methyl groups branching off from the carbon chain and interacting with hydrophobic Sirt6 patches.

DISCUSSION AND CONCLUSIONS

Despite Sirt6's physiological relevance and huge interest in small molecule modulators, few compounds have been described, all of which lack the combination of potency, specificity, and bioavailability required for pharmacological

applications.^{1,2,28} The most potent inhibition was so far described for quercetin derivatives, which show pleiotropic effects.¹⁸ For isoform-specific Sirt6 inhibition, NAM derivatives were proposed.¹⁵ NAM can inhibit with medium potency ($IC_{50} = 20\text{--}200\ \mu\text{M}$) through a base-exchange reaction or with low potency (IC_{50} millimolar) through NAD^+ competition, depending on isoform and substrate acyl.^{7,25} The NAM derivatives pyrazinamide and pyrazinoic acid showed only low potency effects, rendering them unsuitable for pharmacological applications despite a certain Sirt6 specificity.¹⁵ The C-site inhibitor Ex527 shows higher potency (IC_{50} against Sirt1, $\sim 1\ \mu\text{M}$) but only weak selectivity caused by different kinetics of acetyl-ADP-ribose formation, which is required as coligand.²⁶ However, our complex structure reinforces the idea to exploit the conserved sirtuin C site for specific Sirt6 inhibition based on a new compound class and binding mode. The TSA hydroxamate mimics and improves the carbamide interaction of NAM and constitutes a new and improved moiety for exploiting the C-site. Replacing the NAM carbamide with a hydroxamate moiety thus should improve the affinity of this scaffold, but specificity should remain low due to the conservation of the C-site. However, the Sirt6/TSA complex shows that the distal compound part occupies a binding region specific to Sirt6, explaining its isoform selectivity.²⁰ This region belongs to the Sirt6 acyl channel exit, which is also exploited by pyrrolo[1,2-*a*]quinoxalines but with different orientations and interacting patches (Figure 2F).¹⁴ We speculate that adding a related extension to the existing TSA carbon branch at C6 would combine these interactions in one molecule and could lead to superior affinity. Another modification that might potentially increase potency would be to change the methyl group at C4 to an amino group to simulate the Pro62 interaction of the ring nitrogens of NAM and UBCS activators (Figure 2F). The comparison with the Sirt3/Ex527 complex (Figure 2B) also suggests that larger moieties added to C3, such as a methylindole, might improve sirtuin affinity, and they would also abrogate HDAC affinity due to steric hindrance. This moiety would occupy the so-called "extended C-site" (ECS) II, which is conserved among sirtuins and thus will improve general sirtuin affinity as discussed for the C-site.^{26,29} Linker and distal moiety, in contrast, occupy the ECS III region, which differs between isoforms and thus can contribute to isoform specificity.^{29,30}

Generally, rigidifying the TSA linker and proximal group conformation of the Sirt6 complex should allow abolishing of effects on HDACs (see above). A possible strategy could be to insert a double bond between C6 and C7, since the carbonyl oxygen appears not to contribute significantly to Sirt6 binding. Alternatively, several modifications to the TSA dimethylaminophenyl group can be envisioned for improving sirtuin binding and specificity. The TSA phenyl plane is distorted against the carbonyl oxygen and the carbonyl plane is bent, likely causing an energetically less favorable conformation, to avoid clashes with Trp71. Making the terminal group smaller could thus lead to tighter binding. Also, making it less hydrophobic might lessen its unfavorable solvent interactions through the unbound surface and ridge, and it would weaken interactions with the hydrophobic pocket it occupies in HDACs. Also, shortening this group and adding an interaction partner for other, isoform-specific residues, such as Sirt3-Arg158, could allow exploiting of the TSA scaffold for the development of compounds specific for sirtuin isoforms other than Sirt6.

The strong HDAC inhibition by hydroxamates is mostly based on their Zn chelate interaction, and methylation of the hydroxamate hydroxyl group might retain the activity against Sirt6 but prevent HDAC binding. The other way round, improving HDAC inhibitors can be achieved by rigidifying the ligand conformation observed in HDACs, for example, through ring formation between the carbonyl and phenyl moieties in SAHA. Also, extending the distal moiety with hydrophobic groups might also increase HDAC over sirtuin specificity, since it would further fill the corresponding HDAC binding site and increase the steric hindrance in Sirt6.

In summary, we provide molecular insights in Sirt6 binding mode and interaction details for TSA, the most potent small molecule Sirt6 inhibitor reported so far. These insights provide a rational basis for developing compounds that inhibit Sirt6, other sirtuins, and HDACs with improved potency and/or selectivity. Such compounds, in particular those targeting sirtuins, are rare and urgently needed for functional studies and as lead compounds for the development of therapeutic drugs. Our data reveal the role of the hydroxamate as interactor for the sirtuin C-site, identifying this moiety, or a modified version abolishing binding to the HDAC active site Zn²⁺, as an attractive group for sirtuin inhibitor development. They further identify the relevance of chain modifications and conformation for discrimination of Sirt6 versus other sirtuin isoforms and Zn²⁺-dependent HDACs. These insights now allow for the design of improved inhibitors.

EXPERIMENTAL SECTION

Chemicals. TSA was purchased from Invivogen. All other chemicals were purchased from Sigma if not stated differently.

Protein Production and Purification. Human Sirt6 protein was recombinantly produced and purified as described previously.^{14,31} Briefly, full-length Sirt6 (residues 1–355) in pQE80L.1 was expressed in *E. coli* M15[pREP4] and Sirt6(13–308) in pET151-D-TOPO in *E. coli* Rosetta2 (DE3) pLysS. Sirt6 protein was affinity purified using Talon resin (Clontech) and the his-tag removed through tobacco etch virus (TEV) protease cleavage and reverse affinity chromatography. Sirt6 protein was then further purified through cation exchange chromatography on SP Sepharose (GE Healthcare) and gel filtration on a Superdex 200 column (GE Healthcare). The purified protein was concentrated to 10 mg/mL, flash frozen in liquid nitrogen, and stored at –80 °C.

Binding Assays. Binding of TSA to Sirt6 was analyzed through label-free microscale thermophoresis measurements on a Monolith NT.label-free (NanoTemper Technologies). Full-length Sirt6 at a final concentration of 2 μM in 50 mM Na-phosphate buffer, pH 7.5, 0.6 mM DTT, and 5% DMSO was titrated with TSA stock solution (12.1 mg/mL in DMSO). Prior to measurements, mixtures were incubated for 20 min at room temperature. Thermophoresis was analyzed at 25 °C with 20% laser power and 15% LED power. A concentration-dependent fluorescence quenching was observed upon binding, and the SDS-denaturation test indicated that the change of the fluorescence signal was caused by the Sirt6/TSA interaction. Data were fitted in GraFit7 with an equation for one binding site with background. All experiments were repeated at least twice.

Crystallization and Structure Determination. Protein solution containing 10 mg/mL Sirt6 (13–308) and 10 mM ADP-ribose was mixed with an equal volume of reservoir solution (1.6 M (NH₄)₂SO₄, 10% PEG 400, and Bis-Tris buffer, pH 5.7) and crystallized by the hanging-drop vapor diffusion method at 20 °C. The Sirt6/ADP-ribose/TSA was generated by soaking 10 mM TSA into Sirt6/ADP-ribose crystals overnight. Crystals were transferred to a cryoprotectant solution of reservoir supplemented with 20% ethylene glycol, 10 mM compound, and 2 mM ADP-ribose before being frozen in liquid nitrogen.

Diffraction data for the Sirt6/ADP-ribose/TSA complex were collected at 100 K at BL14.1 at the BESSY II electron storage ring operated by the Helmholtz-Zentrum Berlin (HZB), Germany.³² Data were processed with “X-ray detector software” (XDS)³³ and initial phases determined by molecular replacement with Phaser³⁴ from the CCP4 software suite³⁵ and a Sirt6/ADP-ribose structure (PDB code 3K35) as search model. The structure was rebuilt in COOT³⁶ and refined with Refmac.³⁷ Since the crystal showed significant twinning (twin fraction 34%), the amplitude-based twin refinement mode of Refmac was employed.

ASSOCIATED CONTENT

Supporting Information

The Supporting Information is available free of charge on the ACS Publications website at DOI: 10.1021/acs.jmedchem.8b01455.

SMILES strings for the small molecules of Figure 1A (CSV)

Accession Codes

Coordinates and structure factors of the Sirt6/ADP-ribose/TSA complex have been deposited with the PDB (www.PDB.org) under accession code 6HOY. Authors will release the atomic coordinates and experimental data upon article publication.

AUTHOR INFORMATION

Corresponding Author

*Phone: (49)(921)557831. Fax: (49)(921)557832. E-mail: clemens.steegborn@uni-bayreuth.de.

ORCID

Clemens Steegborn: 0000-0002-0913-1467

Notes

The authors declare no competing financial interest.

ACKNOWLEDGMENTS

We thank the beamline staff at BESSY for excellent technical support.

ABBREVIATIONS USED

HDAC, histone deacetylase; NAM, nicotinamide; SAHA, suberoylanilide hydroxamic acid; TSA, trichostatin A

REFERENCES

- (1) Morris, B. J. Seven sirtuins for seven deadly diseases of aging. *Free Radical Biol. Med.* **2013**, *56*, 133–171.
- (2) Dai, H.; Sinclair, D. A.; Ellis, J. L.; Steegborn, C. Sirtuin activators and inhibitors: promises, achievements, and challenges. *Pharmacol. Ther.* **2018**, *188*, 140–154.
- (3) Tasselli, L.; Zheng, W.; Chua, K. F. SIRT6: novel mechanisms and links to aging and disease. *Trends Endocrinol. Metab.* **2017**, *28*, 168–185.
- (4) Tennen, R. I.; Berber, E.; Chua, K. F. Functional dissection of SIRT6: identification of domains that regulate histone deacetylase activity and chromatin localization. *Mech. Ageing Dev.* **2010**, *131*, 185–192.
- (5) Moniot, S.; Weyand, M.; Steegborn, C. Structures, substrates, and regulators of mammalian sirtuins—opportunities and challenges for drug development. *Front. Pharmacol.* **2012**, *3*, 16.
- (6) Schutkowski, M.; Fischer, F.; Roessler, C.; Steegborn, C. New assays and approaches for discovery and design of sirtuin modulators. *Expert Opin. Drug Discovery* **2014**, *9*, 183–199.
- (7) Cen, Y.; Youn, D. Y.; Sauve, A. A. Advances in characterization of human sirtuin isoforms: chemistries, targets and therapeutic applications. *Curr. Med. Chem.* **2011**, *18*, 1919–1935.

- (8) Rauh, D.; Fischer, F.; Gertz, M.; Lakshminarasimhan, M.; Bergbrede, T.; Aladini, F.; Kambach, C.; Becker, C. F. W.; Zerweck, J.; Schutkowski, M.; Steegborn, C. An acetylole peptide microarray reveals specificities and deacetylation substrates for all human sirtuin isoforms. *Nat. Commun.* **2013**, *4*, 2327.
- (9) Roessler, C.; Nowak, T.; Pannek, M.; Gertz, M.; Nguyen, G. T. T.; Scharfe, M.; Born, I.; Sippl, W.; Steegborn, C.; Schutkowski, M. Chemical probing of the human sirtuin 5 active site reveals its substrate acyl specificity and peptide-based inhibitors. *Angew. Chem., Int. Ed.* **2014**, *53*, 10728–10732.
- (10) Jiang, H.; Khan, S.; Wang, Y.; Charron, G.; He, B.; Sebastian, C.; Du, J.; Kim, R.; Ge, E.; Mostoslavsky, R.; Hang, H. C.; Hao, Q.; Lin, H. SIRT6 regulates TNF- α secretion through hydrolysis of long-chain fatty acyl lysine. *Nature* **2013**, *496*, 110–113.
- (11) Pan, P. W.; Feldman, J. L.; Devries, M. K.; Dong, A.; Edwards, A. M.; Denu, J. M. Structure and biochemical functions of SIRT6. *J. Biol. Chem.* **2011**, *286*, 14575–14587.
- (12) Feldman, J. L.; Baeza, J.; Denu, J. M. Activation of the protein deacetylase SIRT6 by long-chain fatty acids and widespread deacetylation by mammalian sirtuins. *J. Biol. Chem.* **2013**, *288*, 31350–31356.
- (13) Rahnasto-Rilla, M.; Tyni, J.; Huovinen, M.; Jarho, E.; Kulikowicz, T.; Ravichandran, S.; Bohr, V. A.; Ferrucci, L.; Lahtela-Kakkonen, M.; Moaddel, R. Natural polyphenols as sirtuin 6 modulators. *Sci. Rep.* **2018**, *8*, 4163.
- (14) You, W.; Rotili, D.; Li, T.-M.; Kambach, C.; Meleshin, M.; Schutkowski, M.; Chua, K. F.; Mai, A.; Steegborn, C. Structural basis of sirtuin 6 activation by synthetic small molecules. *Angew. Chem., Int. Ed.* **2017**, *56*, 1007–1011.
- (15) Bolívar, B. E.; Welch, J. T. Studies of the binding of modest modulators of the human enzyme, sirtuin 6, by STD NMR. *ChemBioChem* **2017**, *18*, 931–940.
- (16) Damonte, P.; Sociali, G.; Parenti, M. D.; Soncini, D.; Bauer, I.; Boero, S.; Grozio, A.; von Holtey, M.; Piacente, F.; Becherini, P.; Sanguineti, R.; Salis, A.; Damonte, G.; Cea, M.; Murone, M.; Poggi, A.; Nencioni, A.; Del Rio, A.; Bruzzone, S. SIRT6 inhibitors with salicylate-like structure show immunosuppressive and chemosensitizing effects. *Bioorg. Med. Chem.* **2017**, *25*, 5849–5858.
- (17) Parenti, M. D.; Grozio, A.; Bauer, I.; Galeno, L.; Damonte, P.; Millo, E.; Sociali, G.; Franceschi, C.; Ballestrero, A.; Bruzzone, S.; Del Rio, A.; Nencioni, A. Discovery of novel and selective SIRT6 inhibitors. *J. Med. Chem.* **2014**, *57*, 4796–4804.
- (18) Shin, E. S.; Park, J.; Shin, J. M.; Cho, D.; Cho, S. Y.; Shin, D. W.; Ham, M.; Kim, J. B.; Lee, T. R. Catechin gallates are NADP⁺-competitive inhibitors of glucose-6-phosphate dehydrogenase and other enzymes that employ NADP⁺ as a coenzyme. *Bioorg. Med. Chem.* **2008**, *16*, 3580–3586.
- (19) Liu, J.; Zheng, W. Cyclic peptide-based potent human SIRT6 inhibitors. *Org. Biomol. Chem.* **2016**, *14*, 5928–5935.
- (20) Wood, M.; Rymarchyk, S.; Zheng, S.; Cen, Y. Trichostatin A inhibits deacetylation of histone H3 and p53 by SIRT6. *Arch. Biochem. Biophys.* **2018**, *638*, 8–17.
- (21) Roche, J.; Bertrand, P. Inside HDACs with more selective HDAC inhibitors. *Eur. J. Med. Chem.* **2016**, *121*, 451–483.
- (22) Vigushin, D. M.; Ali, S.; Pace, P. E.; Mirsaidi, N.; Ito, K.; Adcock, I.; Coombes, R. C. Trichostatin A is a histone deacetylase inhibitor with potent antitumor activity against breast cancer in vivo. *Clin. Cancer Res.* **2001**, *7*, 971–976.
- (23) Damaskos, C.; Valsami, S.; Kontos, M.; Spartalis, E.; Kalampokas, T.; Kalampokas, E.; Athanasiou, A.; Moris, D.; Daskalopoulou, A.; Davakis, S.; Tsourouflis, G.; Kontzoglou, K.; Perrea, D.; Nikiteas, N.; Dimitroulis, D. Histone deacetylase inhibitors: an attractive therapeutic strategy against breast cancer. *Anticancer Res.* **2017**, *37*, 35–46.
- (24) Schuster, S.; Roessler, C.; Meleshin, M.; Zimmermann, P.; Simic, Z.; Kambach, C.; Schiene-Fischer, C.; Steegborn, C.; Hottiger, M. O.; Schutkowski, M. A continuous sirtuin activity assay without any coupling to enzymatic or chemical reactions. *Sci. Rep.* **2016**, *6*, 22643.
- (25) Fischer, F.; Gertz, M.; Suenkel, B.; Lakshminarasimhan, M.; Schutkowski, M.; Steegborn, C. SIRT5 deacetylation activities show differential sensitivities to nicotinamide inhibition. *PLoS One* **2012**, *7*, No. e45098.
- (26) Gertz, M.; Fischer, F.; Nguyen, G. T. T.; Lakshminarasimhan, M.; Schutkowski, M.; Weyand, M.; Steegborn, C. Ex-527 inhibits sirtuins by exploiting their unique NAD⁺-dependent deacetylation mechanism. *Proc. Natl. Acad. Sci. U. S. A.* **2013**, *110*, E2772–E2781.
- (27) Sanders, B. D.; Jackson, B.; Marmorstein, R. Structural basis for sirtuin function: what we know and what we don't. *Biochim. Biophys. Acta, Proteins Proteomics* **2010**, *1804*, 1604–1616.
- (28) Yoon, Y. K.; Oon, C. E. Sirtuin inhibitors: an overview from medicinal chemistry perspective. *Anti-Cancer Agents Med. Chem.* **2016**, *16*, 1003–1016.
- (29) Gertz, M.; Steegborn, C. Using mitochondrial sirtuins as drug targets: disease implications and available compounds. *Cell. Mol. Life Sci.* **2016**, *73*, 2871–2896.
- (30) Nguyen, G. T. T.; Gertz, M.; Steegborn, C. Crystal structures of SIRT3 complexes with 4'-bromo-resveratrol reveal binding sites and inhibition mechanism. *Chem. Biol.* **2013**, *20*, 1375–1385.
- (31) Schlicker, C.; Boanca, G.; Lakshminarasimhan, M.; Steegborn, C. Structure-based development of novel sirtuin inhibitors. *Aging* **2011**, *3*, 852–872.
- (32) Mueller, U.; Darowski, N.; Fuchs, M. R.; Förster, R.; Hellmig, M.; Paithankar, K. S.; Pühringer, S.; Steffien, M.; Zocher, G.; Weiss, M. S. Facilities for macromolecular crystallography at the Helmholtz-Zentrum Berlin. *J. Synchrotron Radiat.* **2012**, *19*, 442–449.
- (33) Kabsch, W. Integration, scaling, space-group assignment and post-refinement. *Acta Crystallogr., Sect. D: Biol. Crystallogr.* **2010**, *66*, 133–144.
- (34) McCoy, A. J.; Grosse-Kunstleve, R. W.; Adams, P. D.; Winn, M. D.; Storoni, L. C.; Read, R. J. Phaser crystallographic software. *J. Appl. Crystallogr.* **2007**, *40*, 658–674.
- (35) Winn, M. D.; Ballard, C. C.; Cowtan, K. D.; Dodson, E. J.; Emsley, P.; Evans, P. R.; Keegan, R. M.; Krissinel, E. B.; Leslie, A. G. W.; McCoy, A.; McNicholas, S. J.; Murshudov, G. N.; Pannu, N. S.; Potterton, E. A.; Powell, H. R.; Read, R. J.; Vagin, A.; Wilson, K. S. Overview of the CCP4 suite and current developments. *Acta Crystallogr., Sect. D: Biol. Crystallogr.* **2011**, *67*, 235–242.
- (36) Emsley, P.; Cowtan, K. Coot: model-building tools for molecular graphics. *Acta Crystallogr., Sect. D: Biol. Crystallogr.* **2004**, *60*, 2126–2132.
- (37) Murshudov, G. N.; Vagin, A. A.; Dodson, E. J. Refinement of macromolecular structures by the maximum-likelihood method. *Acta Crystallogr., Sect. D: Biol. Crystallogr.* **1997**, *53*, 240–255.

5.3 Publication 3

Structural basis for the activation and inhibition of Sirtuin 6 by quercetin and its derivatives

Weijie You, Sandra Riemer, Wei Zheng, Katrin F. Chua, and Clemens Steegborn. Manuscript in preparation

Author Contributions

Wei Zheng and I performed the activity experiments, and we analyzed data supported by Katrin F. Chua and Clemens Steegborn; Sandra Riemer and I produced complex crystals; Sandra Riemer, I and Clemens Steegborn solved the crystal structures; all authors contributed to the manuscript, which was initially drafted by me and Clemens Steegborn.

**Structural basis for the activation and inhibition of Sirtuin 6
by quercetin and its derivatives**

Weijie You¹, Sandra Riemer¹, Wei Zheng^{2,3}, Katrin F. Chua^{2,3}, Clemens Steegborn^{2*}

¹Department of Biochemistry, University of Bayreuth, 95445 Bayreuth, Germany

²Department of Medicine, Stanford University School of Medicine, Stanford, CA 94305,
USA

³Geriatric Research, Education, and Clinical Center, Veterans Affairs Palo Alto Health Care
System, Palo Alto, CA 94304, USA

* **Corresponding author.** email: Clemens.Steegborn@uni-bayreuth.de

Summary

Mammalian Sirtuin 6 (Sirt6) is an NAD⁺-dependent protein deacylase regulating metabolism and DNA homeostasis. Sirt6 activation protects against metabolic and aging-related diseases, and Sirt6 inhibition is considered for cancer therapy. Available Sirt6 modulators show insufficient potency and specificity, and partially contradictory effects were reported for the plant flavone quercetin and its derivatives. To understand Sirt6 modulation by this compound family and to support drug development, we analysed binding and activity effects of quercetin-based compounds on Sirt6 and other Sirtuin isoforms and solved crystal structures of compound complexes with Sirt6 and Sirt2. We find that quercetin activates Sirt6 via the isoform-specific binding site for pyrrolo[1,2-a]quinoxalines. Inhibition of other isoforms is based on an alternative binding site at the active site entrance. Based on these insights, we identified isoquercetin as a Sirt6 activator with increased specificity. Our results provide a structural basis for Sirtuin effects of quercetin-based compounds and Sirt6-targeted drug development.

Key Words

Sirtuins, deacylase, activator, inhibitor, complex structure, isoquercetin, cyanidin, catechin gallate

Introduction

Sirtuins are NAD⁺-dependent protein lysine deacylases that sense the cellular nutrient status, regulate energy metabolism and stress responses, and have been implicated in aging processes and aging-related diseases (Morris, 2013). Of the seven mammalian Sirtuin isoforms, Sirt1-7, three are localized in the nucleus (Sirt1,6,7). Sirt1 is the most studied isoform, functions as deacetylase of histones and transcription factors, and it is modulated by a variety of small molecule inhibitors and activators and used as a therapeutic target (Dai et al., 2018). Sirt6 associates with chromatin and modulates the functions of histones, transcription factors, and stress response proteins to regulate gene expression, telomere maintenance, and DNA repair (Kugel and Mostoslavsky, 2014). Sirt6 promotes longevity in male mice, and it suppresses aging phenotypes and induces apoptosis in cancer cells (Kugel et al., 2016). Thus, small molecule Sirt6 modulators are sought for functional studies and therapy of aging-related diseases, such as cancer and type 2 diabetes (Tasselli et al., 2017).

Sirtuins feature differing substrate acyl selectivities (Roessler et al., 2014, Gertz et al., 2016, Pannek et al., 2017). Sirt6 hydrolyses lysine acylations by long chain fatty acids, such as myristoylations, more efficiently than acetylations *in vitro*, and TNF- α demyristoylation regulates its secretion, but a broader relevance of this activity remains to be confirmed (Jiang et al., 2013). The same applies to Sirt6's low mon-ADP-ribosylation activity, which can activate PARP1 to stimulate DNA repair (Mao et al., 2011). Despite its low *in vitro* deacetylase activity, Sirt6 efficiently deacetylates histones and proteins involved in glucose metabolism and DNA repair *in vivo* (Gil et al., 2013, Tasselli et al., 2017). It features the conserved Sirtuin catalytic core of ~275 amino acids, with a large Rossmann-fold domain and a smaller Zn²⁺-binding domain, which shows larger variations among isoforms. The active site cleft between these domains comprises a substrate acyl-binding channel, and Sirt6's particular small Zn²⁺-binding domain and cofactor-binding loop render it larger and more hydrophobic than in most other Sirtuins, enabling efficient accommodation of long-chain acyls. The Sirtuin

catalytic core is flanked by isoform-specific N- and C- terminal extensions, which in Sirt6 contribute to chromatin localization (Tennen et al., 2010).

Only few Sirt6 modulators are available. Sirtuin-activating compounds (STACs) were initially described for Sirt1 (Dai et al., 2018). They bind to a Sirt1-specific STAC binding domain (SBD) (Dai et al., 2018), which might suggest that other Sirtuin isoforms are not amenable to activation. However, free fatty acids and fatty acid ethanolamides at high micromolar concentrations were found to stimulate Sirt6 deacetylation activity (Feldman et al., 2013, Rahnasto-Rilla et al., 2016). They inhibit Sirt6-dependent hydrolysis of long chain acylations, implicating the acyl binding channel in this effect. Recently, we identified synthetic pyrrolo[1,2-a]quinoxaline derivatives as more potent Sirt6 deacetylase activators (Schlicker et al., 2011, You et al., 2017). Crystal structures of Sirt6/activator complexes identified a Sirt6-specific modulator binding site in the acyl binding channel and provided a rational basis for further development (You et al., 2017), which will be necessary for *in vivo* applications due to their limited efficacy and solubility. Another low potency Sirt6 activator appears to be the flavonoid quercetin (**Fig. 1A**), which is present in fruits and vegetables and has anti-inflammatory and anti-diabetic effects (Williams RJ et al., 2004, Russo GL et al., 2014). Quercetin was among the Sirt1 activating polyphenols identified with the fluorogenic “Fluor-de-Lys” (FdL) substrate (Howitz et al., 2003) and was reported to inhibit Sirt6 in the same assay (Kokkonen et al., 2014). Later, quercetin was reported to act as a Sirt6 inhibitor at low and a Sirt6 activator at high concentrations based on mass spectrometry (MS) assays (Rahnasto-Rilla et al., 2016), but a recent MS study by the same group yielded only Sirt6 activating effects for quercetin and an improved derivative (Rahnasto-Rilla et al., 2018). It further indicated the quercetin derivatives catechin gallate and gallocatechin gallate as first potent Sirt6 inhibitors (IC₅₀ 2.5 and 5.4 μM, respectively; **Fig. 1A**). Although quercetin and its derivatives affect several cellular targets (Russo GL et al., 2014), their Sirtuin binding site and modulation mechanism would be highly helpful for the development of potent and soluble

Sirt6 modulators. A pharmacophore model (Ravichandran et al., 2014) and docking calculations (Rahnasto-Rilla et al., 2018) failed to rationalize the limited and partially contradictory experimental data on Sirt6 modulation, hindering their use for drug development.

Here, we analyse modulation of Sirt6 and other isoforms by quercetin and its derivatives in activity and binding assays and through crystal structure analysis of modulator complexes of Sirt6 and Sirt2. We find that quercetin-based compounds can activate or inhibit Sirt6-dependent deacetylation through binding to the Sirt6-specific acyl binding channel. Quercetin inhibits other Sirtuin isoforms through binding at the active site entrance, and isoquercetin can distinguish the binding sites and thus activates Sirt6 selectively. Our results hence provide structural insights in Sirtuin modulation by quercetin-based compounds and a rational basis for further Sirt6 modulator development.

Results

Quercetin and its derivative luteolin activate Sirt6-dependent deacetylation

To clarify the effects of quercetin and its derivatives on Sirt6 deacetylation activity, we tested them in several assays. In the FdL assay, quercetin appeared to inhibit Sirt6 but control reactions showed that it quenches FdL fluorescence, preventing reliable measurements (**Supplementary Fig. 1A**). In a coupled enzymatic assay with acetylated H3K9 peptide (H3K9Ac), which represents a physiological Sirt6 deacetylation site, quercetin also appeared to inhibit Sirt6 but control reactions revealed suppressive effects on the assay's downstream enzymes (**Supplementary Fig. 1B**). To overcome the artifacts in these widely used assays, we tested the compounds by using a robust MS-based assay (Fischer et al., 2012) and the H3K9Ac substrate. Quercetin and luteolin tested from 9.8 μ M to 10 mM revealed a dose-

dependent increase in Sirt6 activity, with a maximum stimulation of more than 2-fold and EC₅₀ values of ~1.2 mM (**Fig. 1B**). We did not observe any evidence for Sirt6 inhibition by these compounds.

Acetyl-peptides are poor substrates for Sirt6 and may not fully mimic physiologic conditions of histone deacetylation in cells (Michishita et al., 2008, Gil et al., 2013). We therefore examined the effects of quercetin on the deacetylation activity of Sirt6 on purified nucleosomes and free full-length histones (**Fig. 1C**). We observed substantial activation of Sirt6 by quercetin in deacetylating nucleosomal H3K18ac (H3K9ac levels were below the detection limit on these nucleosomes). Moreover, quercetin also augmented the H3K18ac and H3K9ac deacetylase activities of Sirt6 on free full-length histones (**Fig. 1C**), which are otherwise poor substrates for Sirt6. These findings demonstrate that quercetin has activating effects on Sirt6-dependent deacetylation of its physiological histone substrates.

A Sirt6/quercetin crystal structure reveals binding site and interaction details

To identify Sirt6's quercetin binding site and interaction details, we determined a crystal structure of a Sirt6/ADP-ribose/quercetin complex. The structure was solved at 1.84 Å resolution (**Table 1**) and contained well-defined electron density for one quercetin ligand per Sirt6 monomer (**Fig. 1D,E**). The binding site is located in the hydrophobic funnel that comprises the distal end of Sirt6's extended acyl binding channel (**Fig 1D,E**). Quercetin's catechol moiety (ring B) is buried in a protein pocket and its 4'-hydroxyl group forms a hydrogen bond to the Pro62 backbone oxygen, and the 4'- and 3'-hydroxyls form water-mediated interactions with the backbone of Ala53 and Ile61 and the side chain of Asp116 (**Fig. 1E,F**). Asp116 also forms a hydrogen bond to the NAM moiety of the cosubstrate NAD⁺ in its binding site known as "C-site", illustrating that catechol pocket and C-site are partly overlapping (see also below). The quercetin chromen-4-one system forms no polar interactions but contributes to complex formation through hydrophobic contacts with funnel

surface patches formed by Phe64/82/86 and Val70/115, and Met136/157 (**Fig. 1F**). Comparison of the Sirt6/querletin complex with a Sirt6 complex with the pyrrolo[1,2-a]quinoxaline-based activator UBCS039 shows that they share most of their binding sites (**Fig. 1F**). Querletin's catechol group overlays well with the UBCS039 pyridine moiety and reproduces its key interaction to Pro62 (You et al., 2017). The chromen-4-one substitutes for the hydrophobic pyrrolo[1,2-a]quinoxaline of UBCS039-related compounds, which varies between UBCS039 derivatives due to the non-directed nature of its interactions and the wide and hydrophobic architecture of the Sirt6 funnel (You et al., 2017). It thus appears that the buried catechol group of querletin functions as an anchor in Sirt6 binding, while the chromen-4-one provides smaller and non-specific binding contributions. The chromen-4-one thus appears particularly attractive for modifications to improve compound binding and potency.

Since querletin occupies the distal end of the extended Sirt6 acyl channel it is compatible with binding of acetylated substrates but would overlap with longer substrate acylations such as myristoylations (**Supplementary Fig. 1C**). Consistently, testing querletin on Sirt6-dependent demyristoylation revealed a concentration-dependent inhibition (**Fig. 1G**). Thus, querletin activates Sirt6's deacetylation activity and inhibits Sirt6-dependent demyristoylations, as observed for UBCS039 and consistent with their binding to the remote end of the Sirt6 acyl channel.

Sirt6 complex structures with inhibitory and activating querletin derivatives reveal interaction differences and suggest modulation mechanisms

Catechin gallate (CG) was reported to be the most potent compound among querletin derivatives that inhibit Sirt6-dependent deacetylation (Rahnasto-Rilla et al., 2018). Testing CG in our MS assay confirmed the inhibition, albeit with lower potency ($IC_{50} 80 \pm 15 \mu M$; **Fig 2A**) than reported ($IC_{50} 2.5 \pm 0.1 \mu M$). To rationalize the inhibitory effect, we determined a crystal structure of a Sirt6/CG complex. The structure was solved at 2.0 Å resolution and

comprised well-defined electron density for one CG ligand per Sirt6 monomer (**Table 1; Fig. 2B**). CG occupied the same binding region as quercetin (**Fig. 2C,D**), with identical positions for their catechol moieties but with a rotated chromen-4-one orientation in GC to accommodate its additional, bulky trihydroxy benzoyl group (**Fig. 2E**). The chromen-4-one now interacts with Trp71 of the acyl channel exit, and the trihydroxy benzoyl group forms hydrophobic interactions with the other side of the exit funnel and a polar contact to the backbone nitrogen of Gly155. The inhibitor does not overlap with the binding pocket for acetyl substrate but catechol group assumes a position perpendicular to, and partly overlapping with the NAM moiety of the NAD⁺ cosubstrate (**Supplementary Fig. 2A**). The inhibition could thus be based on NAD⁺ competition, but the fact that closely related compounds with identical catechol binding mode act as activators suggests that binding occurs only after NAM release from NAD⁺ during catalysis (see discussion).

Cyanidin is an quercetin derivative that was reported to activate Sirt6 with increased potency and efficacy (EC₅₀ 460 ± 20 μM; 55-fold stimulation) (Rahnasto-Rilla et al., 2018). In our activity assays, cyanidin showed some Sirt6 activation at lower concentrations (20-80 μM) but caused heavy precipitation at higher concentrations, preventing reliable measurements (**Fig. 2F**). Our data indicate indeed a higher potency than for quercetin, albeit lower than reported, and they do not allow conclusions on the efficacy. To obtain insights in activation mechanism and compound optimization options, we solved a crystal structure of a Sirt6/ADP-ribose/cyanidin complex (**Table 1; Fig. 2G**). The activator is well-defined by electron density for its B-ring catechol, but features weaker density for the A and C ring system, which could have functional relevance but might also be caused by the lower solubility (and resulting occupancy) of cyanidin. The A/C rings nevertheless can be positioned unequivocally in the same acyl exit funnel region as for quercetin (**Fig 2H**), and the compounds thus show the same binding mode.

The keto group at C-ring position 4 of quercetin that is missing in cyanidin and also in the potent inhibitor CG removes an unfavourable interaction with Met157 and might be a key difference causing their increased potency. Comparing the activating and inhibiting compounds and their Sirt6 complexes further suggests modulation mechanisms and relevant differences causing their differing effects. An overlay of the complex structures shows that the inhibitor CG differs from activators in a slight rotation of the catechol moiety and a bulky substituent extended toward the N-terminus, but the observed differences in protein conformation are subtle. Both compound types, however, overlap with the C-site that accommodates the NAM moiety of the substrate NAD^+ until NAM is released in the first catalytic step. Such a binding mode for activators implies that they bind during or after NAM release. Such a scheme was thoroughly characterized for the Sirtuin inhibitor Ex-527 (Gertz et al., 2013), and we speculate that the quercetin-based activators and inhibitors, which are very similar to each other, share this mechanistic feature. Different effects on the stabilization of the acyl channel conformation of Sirt6/product complexes, possibly due to the chromene group pointing toward the N-terminus, might cause their differing effects on Sirt6 deacetylase activity, but details remain to be established.

Quercetin inhibits other Sirtuin isoforms by exploiting an alternative binding site

Due to the isoform-specific features of the Sirt6 acyl channel, in particular its wide and hydrophobic architecture (**Supplementary Fig. 2B**), its ligands should be Sirt6 specific. However, effects of quercetin and related polyphenols were also reported for Sirt1 (Howitz et al., 2003)– Format not correct, no initials are given for other references!. We thus tested the quercetin isoform specificity in activity assays with human Sirt1, Sirt2, Sirt3, Sirt6 (all with acetylated substrate), and Sirt5 (with succinylated substrate). Quercetin caused a concentration-dependent inhibition of all Sirtuin isoforms except for Sirt6, with more than 80% activity reduction at 1250 μM (**Fig. 3A**). Due to the lack of a Sirt6-like binding site, quercetin

has to exploit an alternative binding site of the other isoforms to cause this opposite, inhibitory effect.

To identify the alternative quercetin binding site and modulation mechanism, we determined a crystal structure of a Sirt2/quercetin complex. The structure was solved at 2.2 Å resolution and revealed well-defined electron density for one quercetin molecule per Sirt2 monomer (**Table 1; Fig. 3B,C**). Quercetin binds on the protein surface at the active site entrance, through π - π stacking with Tyr-114 and Phe-235 and anion- π interaction with Glu-116 and Glu-120 (**Fig. 3C,D**). Interestingly, the bound quercetin locates between two symmetry-related Sirt2 monomers and interacts with the same surface region of the second monomer, albeit through fewer contacts and with rotated orientation (**Supplementary Fig. 2C**). An overlay with a Sirt2/substrate peptide complex reveals that quercetin partly occupies the pocket accommodating substrate residues C-terminal from the acetyl-Lys (respective the C-terminal fluorophore in FdL substrate) and thus sterically prevents substrate binding (**Fig. 3E**). Such a peptide competitive mechanism is supported by Sirt2 inhibition tests at different substrate concentrations, which showed that increasing substrate concentrations lead to weaker inhibitory effects of a fixed inhibitor concentration (**Fig. 3F**).

Comparing the Sirt2/quercetin complex to other Sirtuin isoforms reveals that its binding site is also accessible in Sirt1, 3, and 5, whereas it is occupied in Sirt6 by the protein's N-terminus (**Fig. 3G**). Since Sirt6's quercetin binding site is blocked in these other isoforms by cofactor loop and a helix bundle (**Supplementary Fig. 2D**), our structures define two mutually exclusive modulator binding sites for Sirt6 and for Sirt1,2,3,5, respectively.

Isoquercetin is an activating ligand for the quercetin site with improved specificity

Since the quercetin sites of Sirt6 and Sirt1,2,3,5 are mutually exclusive, suitable derivatives should exploit specific features of either side and thus show improved selectivity. We thus tested the isoform selectivity of the quercetin derivative isoquercetin, which features a bulky

sugar moiety that might be accommodated in one binding site but not the other. Indeed, isoquercetin retained the Sirt6 stimulating activity, albeit with even lower potency, but it showed no significant effects on Sirt1-3-dependent deacetylation and Sirt5-dependent desuccinylation (**Fig. 3G**). To clarify the molecular basis of isoquercetin's improved Sirt6 selectivity, we tried to determine a crystal structure of a Sirt6/ADP-ribose/isoquercetin complex. Initial soaking experiments failed, however, and we speculated that a PEG molecule bound to the acyl site and potentially overlapping with the isoquercetin sugar prevents binding. Substituting PEG with ethylene glycol indeed enabled us to solve the Sirt6/isoquercetin complex structure at 1.8 Å resolution (**Table 1; Fig. 3H**). The quercetin moiety of isoquercetin occupies the activator site identical to the parent compound (**Fig. 3H,I**). The additional sugar moiety of isoquercetin is thereby placed in the acyl channel and would indeed overlap with the PEG molecule of the quercetin complex. The density for the isoquercetin sugar is weaker than for its quercetin moiety, likely due to flexibility, and it indeed forms no significant positive interactions (**Fig. 3H,I**). Placing isoquercetin instead on top of the ligand of our Sirt2/quercetin structure reveals that the sugar moiety would clash with Tyr-114, rationalizing the improved selectivity for Sirt6 (**Fig. 3J**). The sugar thus acts as a negative selector, i.e. does not disturb Sirt6 binding significantly but hinders accommodation in the alternative binding site of the other isoforms, indicating this position as an attractive site for improvement of the compounds selectivity and – with more appropriate moieties for beneficial interactions – of its potency.

Discussion

Sirt6 supports longevity and suppresses aging phenotypes, and it is considered an attractive drug target for aging-related diseases (Morris, 2013, Howitz et al., 2003, Kugel et al., 2016). For pharmacological applications, the few available Sirt6 modulators require improvements concerning potency, selectivity, and bioavailability (You et al., 2018, Dai et al., 2018). They

comprise quercetin and some of its derivatives, a family of plant flavones with beneficial health impact, for example through anti-inflammatory and anti-diabetic effects (Williams et al., 2004, Russo et al., 2014). Partly contradictory effects were reported for quercetin effects on Sirt6 activity (Kokkonen et al., 2014, Rahnasto-Rilla et al., 2016, Ravichandran et al., 2014), and we find that the compound interferes with two popular Sirtuin activity assays, which is a common problem for optical assays (Fischer et al., 2012). Our tests in a robust MS assay confirm, however, that quercetin and luteolin act as low potency activators for Sirt6-dependent deacetylation. Previously reported inhibitory quercetin effects at lower concentrations could not be observed and likely are assay artifacts, possibly due to the compounds' optical effects or the use of Sirt6 tagged with GST, which is known to bind quercetin tightly (Ahmad et al., 2017). Excitingly, more potent quercetin-based Sirt6 activators such as cyanidin were reported recently (Rahnasto-Rilla et al., 2018), indicating that potency and specificity of this scaffold can be improved for pharmacological applications and that Sirt6 modulation might contribute to physiological effects of compound family members. Despite some discrepancies in EC₅₀ and efficacy values (**Supplementary Table 1**), which might be due to competition with NAD⁺ or NAM or an influence of the previously used GST-tag, our MS data confirm the activating effect and improved potency compared to quercetin. Quercetin itself affects a variety of other cellular targets, such as kinases, with much higher potency than Sirt6 (IC₅₀ values in the 0.1-15 μM range (Kokkonen et al., 2014)), which thus appears not to be a direct target mediating the compound's beneficial health effects. It might contribute indirectly, though, for example through its activation by increased NAD⁺ levels from quercetin inhibition of CD38 (Kellenberger et al., 2011). However, Sirt6 might be a relevant direct target for physiological effects of the identified, more potent quercetin-based compounds and/or for yet to be identified, even more potent derivatives or metabolites. Due to the wide Sirt6 binding site and the few specific interactions, it can even be envisioned that other natural compound families with a catechol group or a related moiety

for binding in this pocket can exploit this binding mode, possibly with even higher affinity and physiological relevance. They could be the explanation why the deacetylase activity of Sirt6 is weak in vitro yet robust and significant in vivo (Tasselli et al., 2017), and it would thus be exciting if such compounds could be identified. Interestingly, some quercetin derivatives show an inhibitory rather than activating effect on Sirt6. We could confirm this finding and the increased potency, albeit of differences in IC₅₀ values (**Supplementary Table 1**) possibly caused by the previously used GST-tag (Rahnasto-Rilla et al., 2018). Our assays further establish that quercetin inhibits other human Sirtuin isoforms with low potency, but more potent quercetin derivatives might also exist for these isoforms. Inhibition of Sirt6 and possibly also of other Sirtuin isoforms thus might also contribute to physiological effects of flavones or flavone-containing food or extracts.

For understanding the effects of quercetin-based compounds on Sirtuins and for exploiting them for drug development, details of the Sirtuin/compound interactions are required. A pharmacophore model for Sirt6-binding of quercetin derivatives was based on binding competition among these ligands and suggested four relevant hydrogen bonds (Ravichandran et al., 2014). Docking models for Sirt6-modulating quercetin derivatives suggested binding in the active site and acyl channel region, with partly peptide-competitive interactions for inhibitors and more external binding for activators (Rahnasto-Rilla et al., 2018). Both models were based on experimental data that were limited – binding of few compounds, without information on effects on activity respective activity effects of few derivatives – and partially incorrect (see discussion of dual effects on Sirt6 activity above). Our complex crystal structures in fact identify a deviating Sirt6 binding mode and provide detailed insights in interactions and modulation mechanisms. The complexes identify quercetin's catechol moiety as a key interaction moiety, which binds to the bottom of the Sirt6-specific acyl channel similar to the pyridine ring of activating pyrrolo[1,2-a]quinoxalines (You et al., 2017), leading to an overlap with the C-site that accommodates the

NAM moiety of NAD⁺. The larger chromene moiety, in contrast, contributes mostly non-directional hydrophobic contacts and thus can assume different orientations within the Sirt6 acyl exit funnel, depending on its substituents. This compound part thus appears most attractive for modifications to improve the interaction by introducing groups for polar interactions. Chromene substituents also seem dominant in determining whether a ligand activates or inhibits, but the details of this mechanistic difference remain to be clarified. However, the comparison with the pyrrolo[1,2-a]quinoxalines show that the more soluble quercetin moieties can substitute for rather hydrophobic moieties without significant loss of potency, which can be exploited in chimeric compounds or stimulate the development of other polar ligand moieties. Importantly, the general binding mode is identical for activators and inhibitors, and they would thus both overlap with the NAM moiety of NAD⁺. Rather than proposing competitive inhibition, which would leave the activating effects unexplained and require a different interaction scheme among ligands, we assume that the compounds bind only after NAM release from NAD⁺ within the first catalytic step (Fischer et al., 2012). Such a binding mode has already been established for the Sirtuin inhibitor Ex-527 (Gertz et al., 2013) and was also indicated for the inhibition of Sirt6 by trichostatin A (You et al., 2018). The distinct presence and orientation of chromene substituents of quercetin derivatives seem to contribute to the different potencies and effects (inhibition versus activation), and likely also interaction details yet to be identified from larger SAR studies and their analysis based on our complex structures. There might also be quercetin derivatives that occupy this site without a significant effect on Sirt6 deacetylase activity, as observed for the pyrrolo[1,2-a]quinoxaline UBCS059 (You et al., 2017). Due to the competition of these compounds with myristoylated substrate, but not with acetylated polypeptides, they constitute another interesting family of modulators specifically inhibiting the demyristoylation activity of Sirt6 without effects on its deacetylation activity.

Our structures readily explain the Sirt6-specific activation effects, the weak inhibition against other isoforms, and how derivatives can have isoform specific effects. Quercetin can occupy two largely different binding sites in Sirt6 versus all other isoforms. Our assay and structural data on isoquercetin show that this derivative extends with its additional sugar moiety into the acyl channel, whereas it would lead to a clash in the binding sites of Sirt1,2,3,5. This finding suggests modifications on the quercetin C ring as possibility to increase Sirt6 affinity as well as selectivity. In principle, our structures also provide information for improving the inhibitory binding to other Sirtuin isoforms, but strong and isoform-specific binding might be difficult to achieve due to their related and rather flat and exposed sites. Thus, our complex structures primarily provide vast information for further development of Sirt6 activators and inhibitors, based on the quercetin scaffold but also for development based on chimeras with other known ligands or novel, to be identified scaffolds that can occupy this binding region.

Significance

Quercetin is a plant flavone with beneficial health effects. It affects many targets and shows weak effects on Sirt6, an NAD⁺-dependent deacetylase that supports longevity and suppresses aging phenotypes. Sirt6-targeting drugs, in particular activators, are considered attractive for therapy of aging-related diseases. Contradictory quercetin effects on Sirt6 deacetylase activity have been reported, and we could clarify that inhibitory effects are assay artifacts and that the compound acts as Sirt6 activator. Importantly, more potent Sirt6-activating quercetin derivatives were recently identified and confirmed in our study, and also potentially Sirt6-inhibiting derivatives. Sirt6 modulation thus might contribute to physiological effects of such flavones, and the quercetin scaffold and insights in its Sirt6 binding mode can provide a basis for the development of pharmacological modulators. We therefore solved and analysed crystal structures of Sirt6 complexes with quercetin and activating as well as inhibiting derivatives to

identify their binding site and interaction details. Quercetin binds to with its chromene group to the Sirt6 acyl channel exit and with its catechol group in a deep target pocket. All quercetin derivatives bind with identical catechol group positions, while the chromene orientation can slightly vary depending on substituents. The compounds further bind similar to previously described pyrrolo[1,2-a]quinoxaline-based activators that suffer from low solubility and efficacy. Our data suggest a mechanism for Sirt6 modulation and factors that render a compound activating or inhibitory, and they provide a scaffold with improved solubility and details for derivative design for further development of Sirt6 deacetylase activators and inhibitors. They also support development of compounds that solely inhibit Sirt6's alternative demyristoylation activity. Quercetin-based compounds further showed weak inhibition of other Sirtuin isoforms, and solving a Sirt2/quercetin complex structure revealed an alternative binding site in Sirt1,2,3,5 but covered in Sirt6 by its N-terminus. This site is rather exposed and less promising for drug development, but rationalized the improved Sirt6 specificity of isoquercetin, illustrating that it can support Sirt6 drug development. Our findings further indicate how additional natural compounds might exploit this Sirt6 binding site, suggesting that a cytosolic ligand for this site might be responsible for the discrepancy between Sirt6's low in vitro and robust in vitro deacetylase activity.

Acknowledgements

We thank Dr. Di Fonzo for help with mass spectrometry assays and the staff at BESSY (operated by Helmholtz-Zentrum Berlin) for excellent beamline support. This work was supported by Deutsche Forschungsgemeinschaft (grant STE1701/15-1 to CS), and grants to K.F.C from the NIH/NIA (R01AG050997) and the Department of Veterans Affairs (Merit Award).

Author Contributions

Conceptualization, methodology, peptide experiments and data analysis and visualization, Sirt6 structures, manuscript drafting, WY and CS; Sirt2 structure, SR, WY, CS; histone and nucleosome experiments, WZ and KFC; supervision, funding Acquisition, CS and KFC; all authors contributed to writing of the manuscript.

Declaration of Interests

The authors declare no competing interests.

Materials and Methods

Chemicals

All chemicals were purchased from Sigma (Saint Louis, USA) if not stated differently. All other synthetic peptides were from GL Biochem (Shanghai, China; myristoyl-TNF: EALPK-(myristoyl-K)-TGG); acetyl-H3K9: MARTKQTAR-(acetyl-K)-STGGKAPRKQL; acetyl-p53: RHK-(acetyl-K)-LMFK; acetyl- α -tubulin: MPSD-(acetyl-K)-TIG; acetyl-ACS2: TRSG-(acetyl-K)-VMR; succinyl-CPS1: RGVL-(succinyl-K)-EYGV).

Protein production and purification

The recombinant N-terminal his-tagged human Sirt6 proteins were produced as previously described (Schlicker et al., 2011). Briefly, Sirt6(1-355) in pQE80L.1 was fermented in *E. coli* M15[pREP4]; Sirt6(13-308) in pET151-D-TOPO was expressed in *E. coli* Rosetta2 (DE3) pLysS. Human Sirt2(55-356) was expressed from a pET-SUMO vector in *E. coli* BL21 (DE3) codon+. The proteins were purified by affinity chromatography with Talon resin (Clontech), followed by tag cleavage with Tobacco Etch Virus (TEV) protease. Tag and protease were removed through a second Talon affinity chromatography, and the proteins were further

purified using cation exchange and gel filtration chromatography. Purified protein was concentrated to 10 mg/ml for Sirt6 and 36.5 mg/ml for Sirt2, flash frozen in liquid nitrogen, and stored at -80 °C.

Peptide deacylation assays

For coupled enzymatic peptide deacylation assays, reactions were run in a total volume of 100 μ l containing 50 mM Na-phosphate pH 7.50, 5% DMSO, 0.6 mM DTT, 0.1% (v/v) Tween 20, 200 μ M acetylated histone H3K9 peptide, 500 μ M NAD⁺ and 10 μ M Sirt6. The reactions were monitored in an Epoch 2 plate reader (BioTek) at 340 nm wavelengths. Control reactions to check for compound effects on downstream enzymes contained no Sirt6 and were spiked with 40 μ M nicotinamide.

For FdL assays, reactions were run in a total volume of 50 μ l containing 50 mM Tris-HCl pH 7.50, 100 mM NaCl, 5% DMSO, 100 μ M acetylated FdL1-peptide, 500 μ M NAD⁺ and 10 μ M Sirt6. After incubation at 37 °C for 1h, reactions were stopped by adding 2 mM NAM and 10 mg/ml trypsin, incubated 20 min, and measured in a FluoDia T70 (Photon Technology) at wavelengths 460 nm. Control reactions for fluorescence quenching effects of the compounds were run by adding compound at different concentrations after the deacetylation and development steps.

For MS deacetylation assays, reactions contained 50 mM Na-phosphate pH 7.5, 200 μ M H3K9ac peptide, 2.5 mM NAD⁺, 5% DMSO, the indicated amount of compound and 20 μ M Sirt6(1-355). Demyristoylation assays were done with 50 μ M myristoyl-TNF α peptide. Reference reactions contained 5% DMSO and no compound, and control reactions were run without Sirt6. After incubation for 2 h at 37 °C, reactions were stopped by adding equal volumes of 0.5% (v/v) trifluoroacetic acid and diluted 10-fold with 0.1% formic acid. Samples were filtered in 10 kDa MWCO concentrators and analyzed on an LTQ-XL mass spectrometer (Thermo Scientific) coupled to an HPLC-system with a self-packed ReproSil-

Pur C18-AQ column. Demyristoylation samples were analyzed on a TripleTOF 5600+ System (SCIEX) coupled to an HPLC-system with a Jupiter 5u C4 300A column (Phenomenex) without prior filtration. Peptide quantification was done with Skyline (Maclean et al., 2010). For the Sirt1, 2, 3, and 5 deacylation assays, the reaction mixtures contained 100 μ M acetyl-p53 (Sirt1), 100 μ M acetyl- α -tubulin (Sirt2), 100 μ M acetyl-ACS2 (Sirt3), or 100 μ M succinyl-CPS1 (Sirt5), respectively. Sirt3 samples contained in addition 0.05 mg/ml nicotinamidase. All reactions further contained 500 μ M NAD⁺ and indicated amounts of compounds in 50 mM Na-phosphate buffer with 5% DMSO and were incubated for 5 min at 37 °C. MS analyses of the peptides were done as described for Sirt6

In vitro histone and nucleosome deacetylation assays

2 μ g GST or GST-Sirt6 protein was pre-incubated with 5 mM quercetin or DMSO vehicle at room temperature for 10 minutes. *In vitro* deacetylation reactions were then performed by adding 5 μ g calf thymus histones or 2 μ g HeLa mononucleosomes (Epiccypher) in NAD⁺ deacetylation buffer (20 mM Tris pH 8, 150 mM NaCl, 1 mM NAD⁺, 1.5 mM DTT), incubated at 30 °C for 3 hours in a total volume of 20 μ l. Histone deacetylation was assessed by western blot with H3K9ac (ab4441) or H3K18ac (ab1191) specific antibodies. Signals were quantified with Image Studio™ Lite software (LI-COR Biosciences), and relative acetylation determined by normalization to total H3 and control samples.

Crystallization and Structure determination

Sirt6/ADP-ribose crystals were grown from 1.6 M (NH₄)₂SO₄, 10% PEG 400, and Bis-Tris buffer pH 5.7 with 10 mg/ml Sirt6(13-308) and 10 mM ADP-ribose by the hanging drop vapor diffusion method at 20 °C (You et al., 2017). The Sirt6/ADPr/quercetin and Sirt6/ADP-ribose/cyanidin complexes were obtained by soaking Sirt6/ADP-ribose crystals with 40 mM compound for one week, and the Sirt6/ADP-ribose/CG complex by soaking with 1 mM CG

overnight. The structure in complex with isoquercetin was produced by transferring crystals in a new drop containing 1.6 M $(\text{NH}_4)_2\text{SO}_4$, 10% ethylene glycol, and Bis-Tris buffer pH 5.7 with 40 mM isoquercetin and incubation for one week. A solution of reservoir supplemented with 20% ethylene glycol, 10 mM compound and 2 mM ADP-ribose was used as cryoprotectant.

Sirt2/ADP-ribose crystals were grown in hanging drops at 20 °C with 14 % PEG 10.000 and 0.1 M ammonium acetate pH 5.8 as reservoir solution (Rumpf et al., 2015). The protein solution contained 13 mg/ml Sirt2 (55-356) and 20 mM ADP-ribose. The Sirt2/ADP-ribose crystals were soaked with 40 mM quercetin for 3 days. Crystals were then transferred to a drop of reservoir supplemented with 20% glycol, 10 mM quercetin and 2 mM ADP-ribose before flash freezing in liquid nitrogen.

Diffraction data were collected at 100 K at BL14.1 operated by Helmholtz-Zentrum Berlin (HZB) at the BESSY II electron storage ring (Berlin-Adlershof, Germany) {Mueller, 2012}. Diffraction data were processed with the X-ray Detector Software (XDS) using XDSapp (Kabsch, 2010a, Kabsch, 2010b). Structure were solved by “molecular replacement” phasing with Phaser (McCoy et al., 2007) from the CCP4 software suite (Winn et al., 2011), using the Sirt6/ADP-ribose structure (PDB code 3K35) as a search model for the Sirt6 complexes and Sirt2/1,2,4-Oxadiazole/ADP-ribose structure (PDB code 5MAR) for the Sirt2 complex. The structures were manually rebuilt in COOT (Emsley and Cowtan, 2004) and refined with Refmac (Murshudov GN et al., 1997). The Sirt6 crystals were detected to be twinned (twin fractions 28 % for Sirt6/isoquercetin/ADP-ribose, 44 % for Sirt6/CG/ADP-ribose, 26 % for Sirt6/cyanidin/ADP-ribose, and 22 % for Sirt2/quercetin/ADP-ribose) and refinements were performed with amplitude-based twin refinement.

References

Ahmad, L., Rylott, E.L., Bruce, N.C., Edwards, R., and Grogan, G. (2017). Structural

evidence for Arabidopsis glutathione transferase At GSTF2 functioning as a transporter of small organic ligands. *7*, 122–132.

Dai, H., Sinclair, D.A., Ellis, J.L., and Steegborn, C. (2018). Sirtuin activators and inhibitors: promises, achievements, and challenges. *Pharmacol. Ther.* *188*, 140–154.

Emsley, P., and Cowtan, K. (2004). Coot: model-building tools for molecular graphics. *Acta Crystallogr. Sect. D* *60*, 2126–2132.

Feldman, J.L., Baeza, J., and Denu, J.M. (2013). Activation of the protein deacetylase SIRT6 by long-chain fatty acids and widespread deacylation by mammalian sirtuins. *J. Biol. Chem.* *288*, 31350–31356.

Fischer, F., Gertz, M., Suenkel, B., Lakshminarasimhan, M., Schutkowski, M., and Steegborn, C. (2012). SIRT5 deacylation activities show differential sensitivities to nicotinamide inhibition. *PLoS One* *7*, e45098.

Gertz, M., and Steegborn, C. (2016). Using mitochondrial sirtuins as drug targets: disease implications and available compounds. *Cell. Mol. Life Sci.* *73*, 2871–2896.

Gertz, M., Fischer, F., Nguyen, G.T.T., Lakshminarasimhan, M., Schutkowski, M., Weyand, M., and Steegborn, C. (2013). Ex-527 inhibits sirtuins by exploiting their unique NAD⁺-dependent deacetylation mechanism. *Proc. Natl. Acad. Sci.* *110*, E2772–E2781.

Gil, R., Barth, S., Kanfi, Y., and Cohen, H.Y. (2013). SIRT6 exhibits nucleosome-dependent deacetylase activity. *Nucleic Acids Res.* *41*, 8537–8545.

Howitz, K.T., Bitterman, K.J., Cohen, H.Y., Lamming, D.W., Lavu, S., Wood, J.G., Zipkin, R.E., Chung, P., Kisielewski, A., Zhang, L.-L., et al. (2003). Small molecule activators of sirtuins extend *Saccharomyces cerevisiae* lifespan. *Nature* *425*, 191–196.

Jiang, H., Khan, S., Wang, Y., Charron, G., He, B., Sebastian, C., Du, J., Kim, R., Ge, E., Mostoslavsky, R., et al. (2013). SIRT6 regulates TNF- α secretion through hydrolysis of long-chain fatty acyl lysine. *Nature* *496*, 110–113.

Kabsch, W. (2010a). XDS. *Acta Crystallogr. D. Biol. Crystallogr.* *66*, 125–132.

Kabsch, W. (2010b). Integration, scaling, space-group assignment and post-refinement. *Acta Crystallogr. Sect. D Biol. Crystallogr.* *66*, 133–144.

Kellenberger, E., Kuhn, I., Schuber, F., and Muller-Steffner, H. (2011). Flavonoids as inhibitors of human CD38. *Bioorganic Med. Chem. Lett.* *21*, 3939–3942.

Kugel, S., and Mostoslavsky, R. (2014). Chromatin and beyond: The multitasking roles for SIRT6. *Trends Biochem. Sci.* *39*, 72–81.

Kugel, S., Sebastián, C., Fitamant, J., Ross, K.N., Saha, S.K., Jain, E., Gladden, A., Arora, K.S., Kato, Y., Rivera, M.N., et al. (2016). SIRT6 suppresses pancreatic cancer through control of Lin28b. *Cell* *165*, 1401–1415.

Maclean, B., Tomazela, D.M., Shulman, N., Chambers, M., Finney, G.L., Frewen, B., Kern, R., Tabb, D.L., Liebler, D.C., and Maccoss, M.J. (2010). Skyline : an open source document editor for creating and analyzing targeted proteomics experiments. *26*, 966–968.

Mao, Z., Hine, C., Tian, X., Van Meter, M., Au, M., Vaidya, A., Seluanov, A., and Gorbunova, V. (2011). SIRT6 promotes DNA repair under stress by activating PARP1. *Science* *332*, 1443–1446.

McCoy, A.J., Grosse-Kunstleve, R.W., Adams, P.D., Winn, M.D., Storoni, L.C., and Read, R.J. (2007). Phaser crystallographic software. *J. Appl. Crystallogr.* *40*, 658–674.

Michishita, E., McCord, R.A., Berber, E., Kioi, M., Padilla-Nash, H., Damian, M., Cheung, P., Kusumoto, R., Kawahara, T.L.A., Barrett, J.C., et al. (2008). SIRT6 is a histone H3 lysine 9 deacetylase that modulates telomeric chromatin. *Nature* *452*, 492–496.

Morris, B.J. (2013). Seven sirtuins for seven deadly diseases of aging. *Free Radic. Biol. Med.* *56*, 133–171.

Murshudov GN, Vagin AA, and Dodson EJ (1997). Refinement of macromolecular structures by the maximum-likelihood method. *Acta Crystallogr. D Biol. Crystallogr.* *53*, 240–255.

Pannek, M., Simic, Z., Fuszard, M., Meleshin, M., Rotili, D., Mai, A., Schutkowski, M., and Steegborn, C. (2017). Crystal structures of the mitochondrial deacylase Sirtuin 4 reveal

isoform-specific acyl recognition and regulation features. *Nat. Commun.* 8.

Piia Kokkonen, Minna Rahnasto-Rilla, Paolo Mellini, Elina Jarho, Maija Lahtela-Kakkonen, and Tarja Kokkola (2014). Studying SIRT6 regulation using H3K56 based substrate and small molecules. *Eur J Pharm Sci* 63, 71–76.

Rahnasto-Rilla, M., Kokkola, T., Jarho, E., Lahtela-Kakkonen, M., and Moaddel, R. (2016). N-Acylethanolamines Bind to SIRT6. *ChemBioChem* 17, 77–81.

Rahnasto-Rilla, M., Tyni, J., Huovinen, M., Jarho, E., Kulikowicz, T., Ravichandran, S., A. Bohr, V., Ferrucci, L., Lahtela-Kakkonen, M., and Moaddel, R. (2018). Natural polyphenols as sirtuin 6 modulators. *Sci. Rep.* 8, 4163.

Ravichandran, S., Singh, N., Donnelly, D., Migliore, M., Johnson, P., Fishwick, C., Luke, B.T., Martin, B., Maudsley, S., Fugmann, S.D., et al. (2014). Pharmacophore model of the quercetin binding site of the SIRT6 protein. *J. Mol. Graph. Model.* 49, 38–46.

Roessler, C., Nowak, T., Pannek, M., Gertz, M., Nguyen, G.T.T., Scharfe, M., Born, I., Sippl, W., Steegborn, C., and Schutkowski, M. (2014). Chemical probing of the human sirtuin 5 active site reveals its substrate acyl specificity and peptide-based inhibitors. *Angew. Chemie - Int. Ed.* 53, 10728–10732.

Rumpf, T., Gerhardt, S., Einsle, O., and Jung, M. (2015). Seeding for sirtuins: microseed matrix seeding to obtain crystals of human Sirt3 and Sirt2 suitable for soaking. *Acta Crystallogr. Sect. F, Struct. Biol. Commun.* 71, 1498–1510.

Russo GL, Russo M, Spagnuolo C, Tedesco I, Bilotto S, Iannitti R, and Palumbo R (2014). Quercetin: a pleiotropic kinase inhibitor against cancer. *Cancer Treat. Res.* 159, 185–205.

Schlicker, C., Boanca, G., Lakshminarasimhan, M., and Steegborn, C. (2011). Structure-based development of novel sirtuin inhibitors. *Aging (Albany NY)* 3, 852–872.

Tasselli, L., Zheng, W., and Chua, K.F. (2017). SIRT6: novel mechanisms and links to aging and disease. *Trends Endocrinol. Metab.* 28, 168–185.

Tennen, R.I., Berber, E., and Chua, K.F. (2010). Functional dissection of SIRT6:

identification of domains that regulate histone deacetylase activity and chromatin localization. *Mech. Ageing Dev.* *131*, 185–192.

Williams RJ, Spencer JP, and Rice-Evans C. (2004). Flavonoids: antioxidants or signalling molecules? *Free Radic Biol Med.* *36*, 838–849.

Winn, M.D., Ballard, C.C., Cowtan, K.D., Dodson, E.J., Emsley, P., Evans, P.R., Keegan, R.M., Krissinel, E.B., Leslie, A.G.W., McCoy, A., et al. (2011). Overview of the CCP4 suite and current developments. *Acta Crystallogr. Sect. D Biol. Crystallogr.* *67*, 235–242.

You, W., and Steegborn, C. (2018). Structural basis of Sirtuin 6 inhibition by the hydroxamate trichostatin A – implications for protein deacetylase drug development. *J. Med. Chem.* [acs.jmedchem.8b01455](https://doi.org/10.1021/acs.jmedchem.8b01455).

You, W., Dante, R., Li, T.-M., Kambach, C., Meleshin, M., Schutkowski, M., Chua, K.F., Mai, A., and Steegborn, C. (2017). Structural basis of sirtuin 6 activation by synthetic small molecules. *Angew. Chemie - Int. Ed.* *56*, 1007–1011.

Tables

Table 1 Diffraction data and refinement statistics

	Sirt6 and quercetin	Sirt6 and isoquercetin	Sirt6 and CG	Sirt6 and cyanidin	Sirt2 and quercetin
Data collection					
Space group	P6 ₃	P6 ₃	P6 ₃	P6 ₃	P2 ₁ 2 ₁ 2 ₁
Cell dimensions					
<i>a</i> = <i>b</i> , <i>c</i> (Å)	91.4, 143.9	91.4, 144.2	91.8, 144.2	91.4, 143.8	78.2, 114.5
Resolution (Å) ^a	47.98-1.84 (1.95-1.84)	45.71-1.90 (2.01-1.90)	48.12-2.01 (2.14-2.01)	47.94-2.10 (2.22-2.10)	46.22-2.23 (2.37-2.23)
<i>R</i> _{merge} ^a	0.12 (1.76)	0.10 (1.63)	0.16 (1.90)	0.16 (1.84)	0.28 (1.90)
CC _{1/2} ^a	0.999 (0.479)	0.999 (0.378)	0.996 (0.710)	0.998 (0.634)	0.976 (0.282)
<i>I</i> / σ ^a	11.6 (1.1)	13.2 (1.2)	9.7 (1.3)	11.0 (1.3)	4.4 (0.7)
Completeness (%) ^a	99.7 (98.5)	99.9 (99.3)	98.9 (96.2)	99.9 (99.5)	99.5 (97.1)
Redundancy ^a	6.9 (6.9)	6.9 (6.6)	10.1 (8.5)	11.3 (11.3)	7.4 (7.4)
Refinement					
Resolution (Å) ^a	45.68-1.84 (1.89-1.84)	43.57-1.90 (1.95-1.90)	45.96-2.01 (2.07-2.01)	45.69-2.10 (2.15-2.10)	46.22-2.23 (2.29-2.23)
No. reflections	56832	51587	42989	37769	32823
Twin fractions ^b	none	0.72/0.28	0.56/0.44	0.74/0.26	0.78/0.22
<i>R</i> _{work} / <i>R</i> _{free} (%)	16.8/20.3	15.3/18.7	16.3/19.3	16.3/20.0	21.1/23.0
No. atoms					
Protein	4382	4381	4350	4341	4735
Compound	44	66	64	42	22
ADP ribose	72	72	72	72	72
Water	346	224	166	117	28
<i>B</i> -factors					
Protein	38.9	46.7	41.9	54.0	53.9
Compound	59.3	77.9	51.2	80.1	67.3
ADP ribose	28.7	36.1	30.2	41.8	34.8
Water	43.9	46.2	38.0	48.5	46.4
R.m.s. deviations					
Bond lengths (Å)	0.013	0.014	0.015	0.012	0.014
Bond angles (°)	1.84	2.11	2.26	1.95	2.2

^aHighest-resolution shell is shown in parentheses.

^bTwo twin domains were found in structure determination; twin fractions were estimated by L-test from CCP4 aimless.

Figure Legends

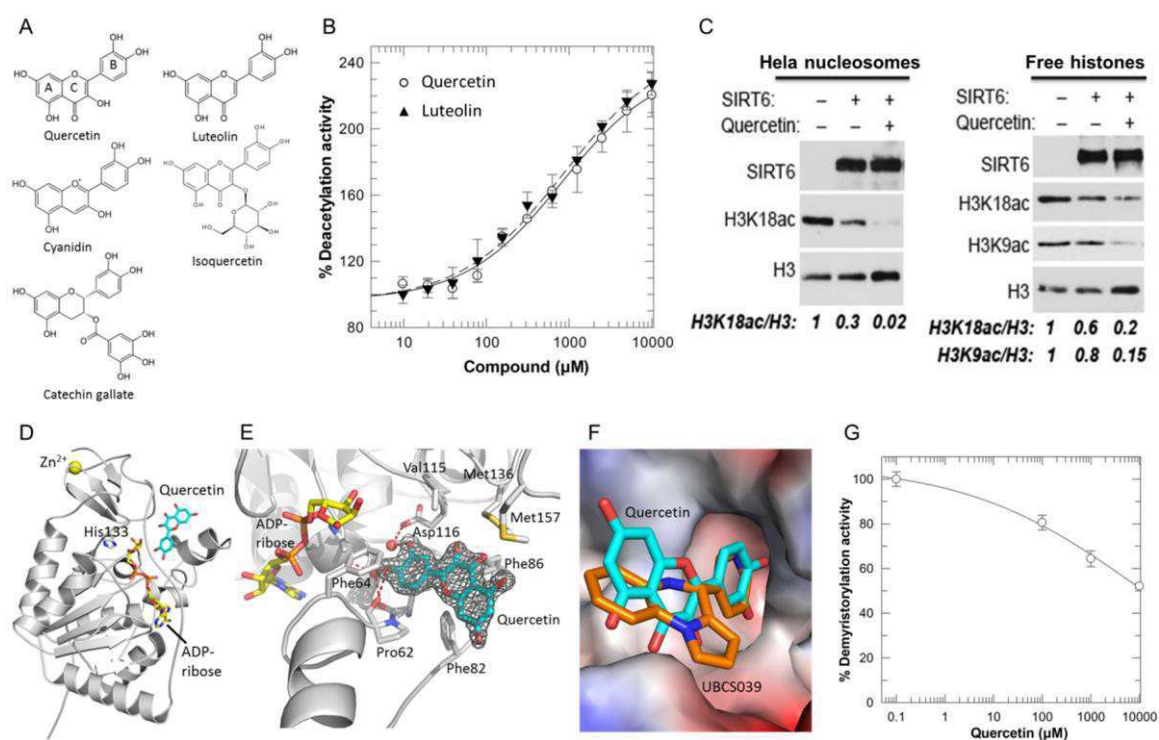


Figure 1: Activation of Sirt6-dependent deacetylation and crystal structure of a Sirt6/quercetin complex. (A) Chemical structures of quercetin and its derivatives. (B) Dose-dependent effects of quercetin and luteolin on Sirt6 deacetylation activity. (C) Western blots showing deacetylation activity of SIRT6 on purified HeLa cell nucleosomes (left) or free histones (right), and activation by quercetin (5mM) compared to DMSO vehicle control. Data are representative of 3 independent experiments. Relative acetylation on the indicated sites was determined by normalization to total H3 and control samples. (D) Overall structure of the complex between human Sirt6 (cartoon), ADP-ribose (yellow sticks), and quercetin (cyan sticks); His133 is shown as sticks to indicate the active site. (E) Interaction of quercetin with Sirt6. Interacting residues are labeled, and polar interactions are indicated by dashed red lines. $2F_o - F_c$ electron density for the ligand is contoured at 1σ . (F) Protein surface of the Sirt6/quercetin complex colored according to the electrostatic potential. The ligand is shown as cyan sticks and overlaid with UBCS039 (orange sticks). (G) Titration with quercetin inhibits Sirt6-dependent demyristoylation. Data are shown as means \pm SD ($n = 3$).

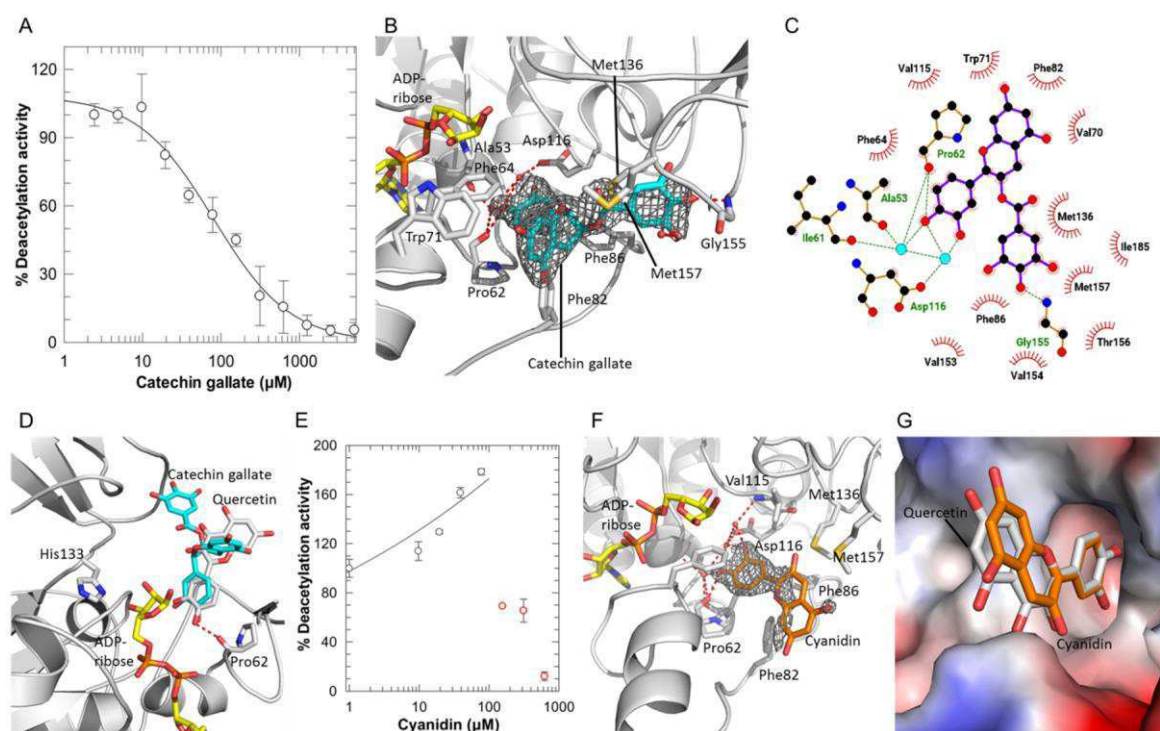


Figure 2: Effects of quercetin derivatives on Sirt6 and crystal structures of Sirt6/quercetin derivative complexes. (A) Dose-dependent effects of CG on Sirt6 deacetylation activity. (B) Interaction of CG with Sirt6. Interacting residues are labeled, and polar interactions are indicated by dashed lines. CG is covered with 2Fo-Fc density contoured at 1σ . (C) Schematic view of the Sirt6/CG interactions. (D) Overlay of Sirt6 complexes with CG (cyan) and quercetin (gray), respectively. ADP-ribose (yellow) and His133 at the active site are shown as sticks. (E) Dose-dependent effects of cyanidin on Sirt6 deacetylation activity, red symbols indicate solubility problems at high concentrations. (F) Interaction of cyanidin with Sirt6. Interacting residues are labeled, and polar interactions are indicated by dashed lines. 2Fo-Fc electron density for the ligand is contoured at 1σ . (G) Protein surface of the Sirt6/cyanidin complex colored according to the electrostatic potential. The ligand is shown as cyan sticks and overlaid with quercetin (gray sticks).

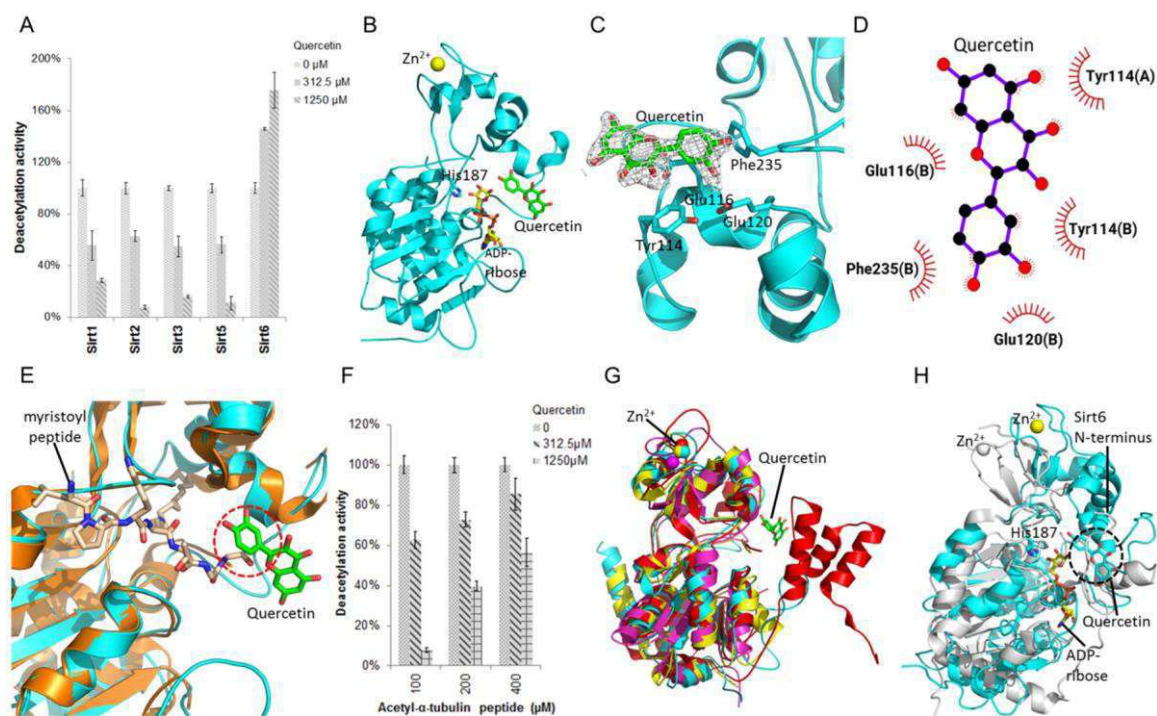


Figure 3: Effect of quercetin on Sirtuin isoforms and structure of Sirt2 in complex with quercetin. (A) Quercetin effects on the deacetylation activities of Sirtuin isoforms. (B) Overall structure of human Sirt2 (cartoon presentation), ADP-ribose (yellow sticks), and quercetin (green sticks); His187 at the active site is represented in sticks. (C) Close view of the Sirt2/quercetin complex, interacting residues are labeled and quercetin (green sticks) is covered with 2Fo-Fc density contoured at 1σ. (D) Schematic view of the Sirt2/quercetin interactions. (E) Overlay of the Sirt2/quercetin complex (cyan cartoon, green ligand) with a Sirt2/myristoyl-peptide complex (gold cartoon, wheat peptide; PDB code 4Y6O). Dotted circle: steric clash between substrate and quercetin. (F) Effects of quercetin on Sirt2 deacetylase activity at various substrate concentrations. (G) Overlay of the Sirt2/quercetin complex (cyan) with Sirt1 (red; PDB code 5BTR), Sirt3 (yellow; PDB code 4HD8) and Sirt5 (magenta; PDB code 4HDA). (H) Overlay of the Sirt2/quercetin complex (cyan/green) with the Sirt6/quercetin complex (gray). Dotted circle: steric clash between Sirt6 N-terminus and quercetin.

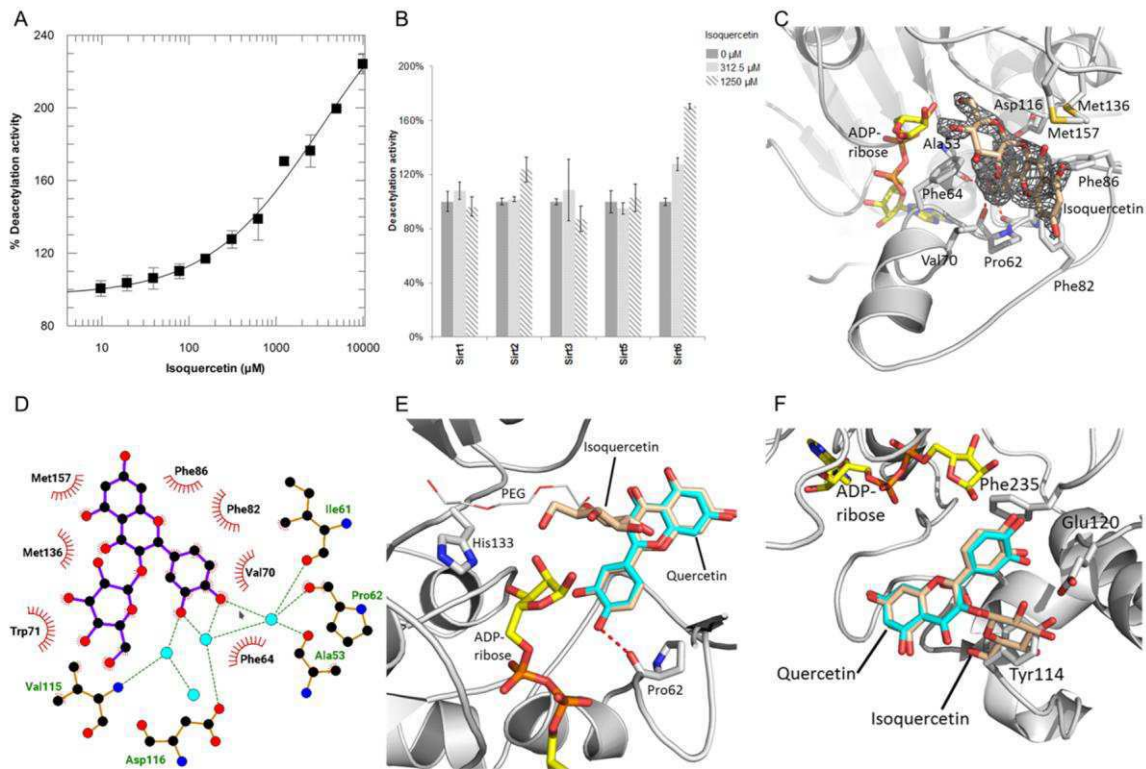
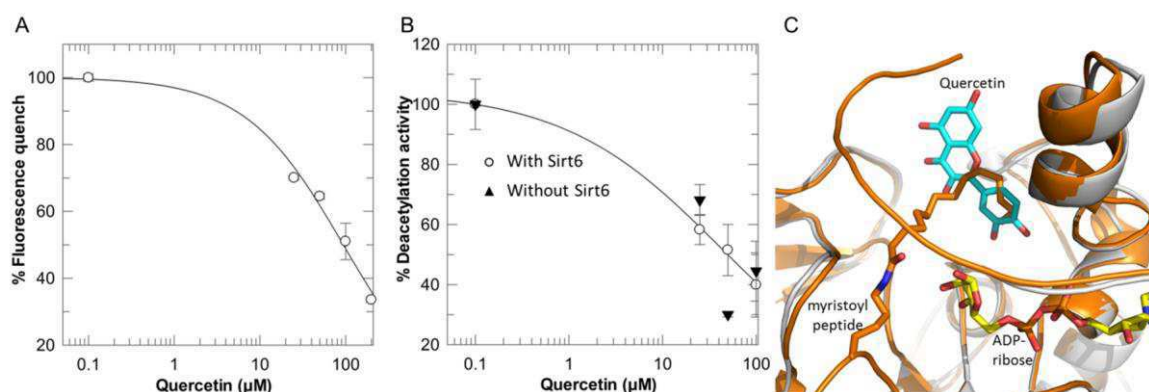
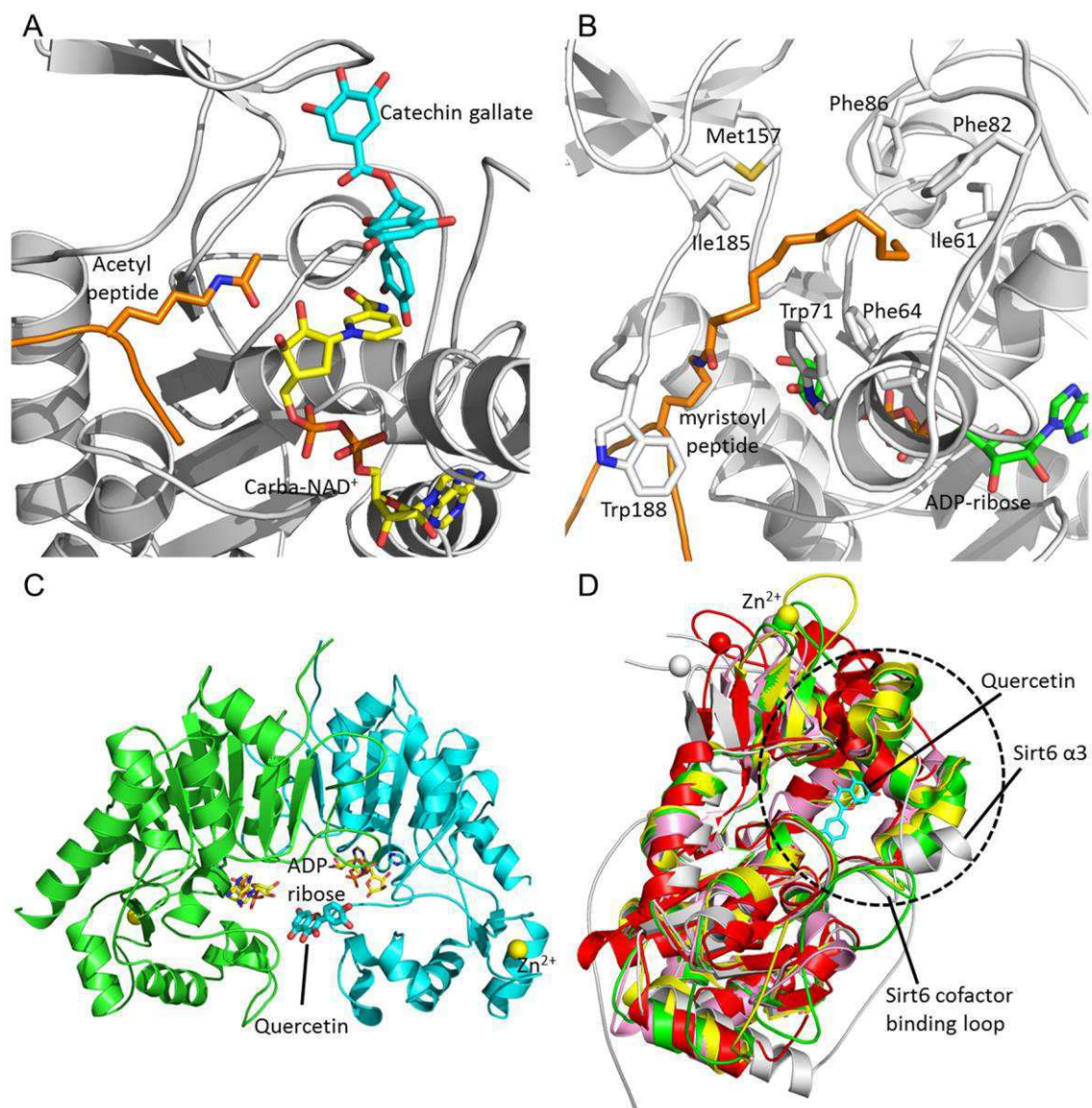


Figure 4: Isoquercetin activates Sirt6 with improved isoform specificity. (A) Dose-dependent effect of isoquercetin on Sirt6 deacetylation activity. **(B)** Effect of isoquercetin on the deacetylation activities of Sirtuin isoforms. **(C)** Close view of the Sirt6/isoquercetin complex. Interacting residues are labeled and isoquercetin (wheat) is covered with 2Fo-Fc density contoured at 1σ . **(D)** Schematic view of the Sirt6/isoquercetin interactions. **(E)** Overlay of the Sirt6 complexes with quercetin (cyan) and isoquercetin (wheat), respectively (protein of isoquercetin complex omitted for clarity). **(F)** Overlay of Sirt2 (grey cartoon) with the Sirt6 complexes with quercetin (cyan) and isoquercetin (wheat), respectively (protein omitted for clarity).

Supplementary Figures



Supplementary Figure 1: (A) Dose-dependent effects of quercetin on the fluorescence signal in control reactions for the FdL assay. (B) Quercetin titration yields concentration dependent inhibitory effects in coupled enzymatic assays in Sirt6 samples (○) but also in control reactions without Sirtuin (▲). (C) Overlay of the Sirt6/quercetin complex (gray cartoon, cyan ligand) with a Sirt6/myristoyl-peptide complex (orange cartoon and peptide, PDB code 3ZG6).



Supplementary Figure 2: (A) Overlay of the Sirt6/ADP-ribose/CG complex (gray cartoon, cyan ligand) with a Sirt3/acetyl-ACS peptide/carba-NAD⁺ complex (PDB ID 4FVT; protein hidden, peptide displayed in orange and carba-NAD⁺ as cyan sticks). (B) Close view of the Sirt6 acyl group binding channel of the Sirt6/ADP-ribose/myristoyl peptide complex structure. Myristoyl group (orange), ADP-ribose (green) and residues that form hydrophobic interactions with the myristoylated lysine are represented as sticks. (C) Overall structure of human Sirt2/ADP-ribose/quercetin complex (cartoon presentation of two symmetry-related monomers in different colors). ADP-ribose (yellow) and quercetin (cyan) are shown as sticks. (D) Overlay of the Sirt6/ADP-ribose/quercetin complex (gray protein, quercetin shown as cyan stick) with Sirt1 (yellow; PDB code 4IF6), Sirt2 (green; PDB code 3ZGV), Sirt3 (pink;

PDB code 4FVT) and Sirt5 (red; PDB code 4G1C). Dotted circle: Cofactor-binding loop and neighboring helix bundle.

(Eidesstattliche) Versicherungen und Erklärungen

(§ 8 Satz 2 Nr. 3 PromO Fakultät)

Hiermit versichere ich eidesstattlich, dass ich die Arbeit selbstständig verfasst und keine anderen als die von mir angegebenen Quellen und Hilfsmittel benutzt habe (vgl. Art. 64 Abs. 1 Satz 6 BayHSchG).

(§ 8 Satz 2 Nr. 3 PromO Fakultät)

Hiermit erkläre ich, dass ich die Dissertation nicht bereits zur Erlangung eines akademischen Grades eingereicht habe und dass ich nicht bereits diese oder eine gleichartige Doktorprüfung endgültig nicht bestanden habe.

(§ 8 Satz 2 Nr. 4 PromO Fakultät)

*Hiermit erkläre ich, dass ich Hilfe von gewerblichen Promotionsberatern bzw. –
vermittlern oder ähnlichen Dienstleistern weder bisher in Anspruch genommen habe
noch künftig in Anspruch nehmen werde.*

(§ 8 Satz 2 Nr. 7 PromO Fakultät)

*Hiermit erkläre ich mein Einverständnis, dass die elektronische Fassung der
Dissertation unter Wahrung meiner Urheberrechte und des Datenschutzes einer
gesonderten Überprüfung unterzogen werden kann.*

(§ 8 Satz 2 Nr. 8 PromO Fakultät)

*Hiermit erkläre ich mein Einverständnis, dass bei Verdacht wissenschaftlichen
Fehlverhaltens Ermittlungen durch universitätsinterne Organe der wissenschaftlichen
Selbstkontrolle stattfinden können.*

.....
Ort, Datum, Unterschrift